THESIS FOR THE DEGREE OF DOCTOR OF PHILOSOPHY

Fabrication and Testing of Doped Uranium Nitride as an Accident Tolerant Fuel Alternative

LUIS G. GONZALEZ F.

Department of Chemistry and Chemical Engineering

CHALMERS UNIVERSITY OF TECHNOLOGY

Gothenburg, Sweden 2023

Fabrication and Testing of Doped Uranium Nitride as an Accident Tolerant Fuel Alternative

LUIS G. GONZALEZ F.

ISBN:978-91-7905-776-3

Doktorsavhandlingar vid Chalmers Teknisk Högskola
Ny serie nr 5242
ISSN 0346-718X

Nuclear Chemistry and Industrial Materials Recycling
Department of Chemistry and Chemical Engineering
Chalmers University of Technology
SE-412 96 Gothenburg
Sweden
Telephone + 46 (0)31-772 1000

Cover: Mechanism of reaction during carbothermic reduction and nitridation of Cr-doped UN microspheres.

Printed by:
Chalmers Digitaltryck
Gothenburg, Sweden 2023

Fabrication and Testing of Doped Uranium Nitride as an Accident Tolerant Fuel Alternative

Luis G. Gonzalez F.
Department of Chemistry and Chemical Engineering
Chalmers University of Technology

Abstract

Nuclear energy is a carbon-free energy source often considered less harmful to the environment than fossil fuels. However, accidents have shown that there are some safety concerns regarding nuclear energy that need to be continuously assessed and further improved. Research into new types of improved fuels, also known as Accident Tolerant Fuels, has therefore become of great importance. Different alternative claddings and fuel materials have been explored in recent years. Amongst these fuels, uranium nitride (UN) has very attractive thermomechanical properties. Nonetheless, UN is easily oxidized in thepresence of air or water, making it undesirable for water-cooled reactors.

In this thesis, UN microspheres were manufactured through a sol-gel method, followed by carbothermic reduction and nitridation. The as-produced microspheres were pressed and sintered into pellets using spark plasma sintering. Thorium, chromium, and aluminum were studied as additives to improve the oxidation resistance of UN. It was observed that Th produced a homogeneous solid solution with UN between 0 % and 20 mol-% thorium metal content. Chromium showed that there was a solubility limit in the UN. Depending on the synthesis conditions, the resulting material can be manufactured to either contain a ternary phase (U_2CrN_3) or metallic chromium. No solubility of aluminum nitride was detected in the UN matrix.

Doping with Th and Cr proved to be efficient in improving the oxidation in air, by increasing the onset oxidation temperatures and decreasing the reaction rates of the pellets. In most cases, the high porosity of the microspheres counterbalanced any protective effect caused by the dopant. Aluminum-containing samples showed the worst oxidation resistance in air due to poor solubility of AlN in the UN. Steam interaction of Cr-doped pellets also showed a delay in the hydrolysis of the UN when Cr is present. The last exposure environment was water, and it was shown that undoped UN pellets can survive at 100 °C and 1 bar pressure with zero mass change. However, at higher temperatures and pressures, 200 °C and 15 bar or 300 °C and 85 bar, pellet disintegration into a UO_2 powder was observed. An incomplete reaction was also observed for the Th-doped pellet in the exposure test at 200 °C, indicating that no improvement in the corrosion resistance of UN in water was achieved by doping with thorium. On the other hand, Cr-doped pellets exposed to water at 200 and 300 °C showed partial crumbling. The resulting material was unreacted UN with some UO_2 byproduct.

Keywords: Uranium nitride, microspheres, doping, sintering, density, internal gelation, ATF, waterproofing.

List of Publications and Manuscripts

This thesis is based on the following papers and manuscript:

Paper I

L.G. Gonzalez Fonseca, M. Hedberg, L. Huan, P. Olsson, T. Retegan Vollmer, Application of SPS in the fabrication of UN and (U,Th)N pellets from microspheres, J. Nucl. Mater. 536 (2020) 152181. doi:10.1016/j.jnucmat.2020.152181

Contribution: Main author and most experimental work.

Paper II

L.G. Gonzalez Fonseca, M. Hedberg, T. Retegan Vollmer, Oxidation and hydrolysis of thorium doped uranium nitride fuel for use in LWR. J. Nucl. Mater. 555 (2021) 153150. https://doi.org/10.1016/j.jnucmat.2021.153150.

Contribution: Main author and all experimental work.

Paper III

L.G. Gonzalez Fonseca, J. Král, M. Hedberg, T. Retegan Vollmer, Preparation of Chromium doped Uranium Nitride via Sol-Gel and Carbothermic Reduction. J. Nucl. Mater. 574. (2023) 154190. https://doi.org/10.1016/j.jnucmat.2022.154190

Contribution: Main author and most of the experimental work.

Paper IV

L.G. Gonzalez Fonseca, M. Hedberg, T. Retegan Vollmer, Effect of chromium doping in the oxidation and hydrolysis of uranium nitride. Manuscript. To be submitted to Journal of Nuclear Materials.

Contribution: Main author and all experimental work.

Conference proceding

L.G. Gonzalez Fonseca, E. Axhage, M. Hedberg, T. Retegan Vollmer, Studies in dual doping of uranium nitride for use as advance technology fuels. Journal of Radioanalytical and Nuclear Chemistry. Resubmitted after revision.

Contribution: Main author and part of the experimental work.

Abbreviations

ATF – Accident Tolerant Fuel

BET – Brunauer-Emmett-Teller

LWR – Light Water Reactor

BWR – Boiling Water Reactors

PWR – Pressurized Water Reactor

EDX – Energy Dispersive X-ray spectroscopy.

FCC – Face Centered Cubic

HMTA – HexaMethyleneTetraAmine

ICP-MS – Inductively Coupled Plasma-Mass Spectrometry

IGP – Internal Gelation Process

LOCA – Loss of Coolant Accident

SBO – Station Black-Out

ORNL – Oak Ridge National Laboratory

SEM – Scanning Electron Microscopy

SPS – Spark Plasma Sintering

TD – Theoretical Density

TGA – Thermo-Gravimetric Analysis

UNH – Uranyl Nitrate Hexahydrate

XRD – X-Ray Diffraction

XRF – X-Ray Fluorescence

PIE – Post Irradiation Examination

TRISO – Tri-Structural isotropic

FCM – Fully Ceramic Microencapsulated

BCC – Body-Centered Cubic

FCC – Face-Centered Cubic

CTR-N – Carbohermic Reduction and Nitridation

Table of contents

1. Introduction 1
2. Background 3
2.1. Uranium nuclear fuels 3
2.2. Fukushima nuclear accident 3
2.3. Accident Tolerant Fuel initiative 4
2.4. Uranium nitride fuel concept 5
2.4.1. UN applications in other reactors 6
2.5. Uranium nitride synthesis 7
2.5.1. Direct nitriding route 7
2.5.2. Hydride-nitride route 7
2.5.3. Ammonolysis route 8
2.5.4. Carbothermic reduction and nitridation 8
3. Theory 9
3.1. Uranium-Nitrogen binary system 9
3.2. Oxidation of UN. 10
3.3. Hydrolysis of UN. 10
3.4. Corrosion prevention 11
3.4.1. Sintering 11
3.4.2. Coating 12
3.4.3. Doping/Alloying 13
3.4.4. U-X-N ternary systems 14
3.5. Synthesis of UN by the sol-gel process and carbothermic reduction. 15
4. Materials and Methods 17
4.1. Chemicals 17
4.2. Instrumentation 17
4.2.1. Gelation system 17
4.2.2. Furnace 18
4.2.3. Scanning electron microscopy (SEM) 18
4.2.4. X-ray diffraction (XRD) 18
4.2.5. Elemental analyzers 18
4.2.6. Inductively coupled plasma-mass spectrometer (ICP-MS) 19
4.2.7. X-Ray Fluorescence (XRF) 19
4.2.8. Spark plasma sintering (SPS) 19

4.2.9. Density, superficial area, and porosity 19
4.2.10. Thermogravimetric analyzer 19
4.2.11. Simultaneous Thermal Analyzer (STA) 19
4.2.12. Autoclave 20
5. Experimental Methods 21
5.1. UN and doped UN microsphere production 21
5.2. Reduction and nitridation process 22
5.2.1. Profile A 22
5.2.2. Profile B 23
5.3. Chromium measurements 24
5.4. Pelletization and sintering 24
5.5. Density measurements 24
5.6. Fuel-oxidant interaction 25
5.6.1. Air interaction 25
5.6.2. Steam interaction 25
5.6.3. Water interaction 25
6. Results and discussion 27
6.1. Thorium doping 27
6.1.1. Microsphere production 27
6.1.2. Pelletization 30
6.1.3. Interaction tests 33
6.2. Chromium doping 38
6.2.1. Microsphere production using heating profile A. 38
6.2.2. Studies on Cr losses and formation of ternary phase 42
6.2.3. Mechanism of reaction for ternary phase formation 45
6.2.4. Microspheres of UN with and without ternary phase 47
6.2.5. Cr-doped UN pellet production 48
6.2.6. Interaction tests 51
6.3. Dual Cr-Al doping 57
6.3.1. Microsphere production 58
6.3.2. Air interaction tests 60
7. Summary and conclusions 62
Future work 64
Acknowledgments 65
References. 66

1. Introduction

Global warming has become an important topic of discussion, as severe weather changes and environmental disasters have surfaced all around the globe. The scientific community has reached the consensus that the emission of greenhouse gases is one of the major contributors to global warming [1]. Around two thirds of the emission of greenhouse gases arise from the combustion of fossil fuels to produce energy [2]. This ratio has not improved in recent years, as the global energy demand has increased steadily across the decades [3]. Greener energy production is necessary to reduce the effects of global warming. However, renewable energy production technologies are still in development. The current energy crisis caused by the shortage of gas from Russia has demonstrated that renewables are not capable of offering a constant and reliable source of electricity thus far [4]. Nuclear energy, on the other hand, is able to supply the constant electricity demands, and it can be adjusted to produce as much energy as required [5]. The European Union declared in 2022 that nuclear energy is to be considered a green energy source, as its carbon dioxide emissions are even lower than some renewables sources [6].

Nuclear energy is a cost effective, carbon-free, and reliable energy source that can play an important role in the decarbonization of electricity production. Nuclear power grew fast from its implementation in the 1950s up until the 1990s, after which its development stagnated until more recent years. Nuclear energy generated 2653 TWh which corresponds to about 10% of the world's electricity supply in 2021 [7]. Further expansion of nuclear power plants has not been extensive due to widespread opposition and public concerns. For example, the current war in Ukraine has shown that nuclear power can still be used to generate panic in the public. Weapon proliferation, radioactive waste, sustainability, and risk of a nuclear accidents are the main arguments used against nuclear energy [8]. Amongst these, the accidents have caused a major distrust in nuclear energy due to the long-lasting and severe consequences.

Not all nuclear accidents end in a catastrophe. Most commonly, fuel inside the reactors can suffer damage due to different events, such as debris fretting, corrosion, and pellet-clad interactions. According to the International Atomic Energy Agency (IAEA), the corrective measurements done by nuclear power plants and nuclear fuel manufacturers have significantly decreased the failure rate in the recent decades [9]. Additionally, reactors have implemented several safety measures to reduce the probability and severity of nuclear accidents. Nonetheless, there are factors that cannot be fully taken into consideration while trying to prevent accidents, such as unpredictably large natural disasters.

The most recent severe nuclear accident occurred in 2011 in Fukushima, Japan. The vast damage produced by a massive earthquake and tsunami caused the loss of the cooling systems in the reactors. This led to an uncontrollable increase in temperature. The fuel cladding reacted with the superheated steam creating a large amounts of hydrogen. The H_2 gas detonated, breaking the containment which allowed the release of radioactive material into the environment [10]. As a consequence, the accident tolerant fuel (ATF) program was started with the aim of finding a safer fuel concept that can withstand accident conditions and prevent the outcomes observed in Fukushima. Currently, UO_2 pellets encapsulated in a zirconium based alloy are the most common fuel design used in power plants. Some of the change suggestions are to modify the cladding, for example, using a SiC or a Cr-doped zircaloy. These changes would normally require an increase in the amount of fissile material to compensate for the

neutronics penalties. Therefore, one option would be to replace the UO_2 by a modified uranium compound, e.g., uranium silicides, carbides, or nitrides. These materials not only have a higher uranium density, but they have also shown better thermal properties.

After ten years since the Fukushima accident, further research into these fuel concepts is still necessary before these can replace the current fuel. In Sweden, an ATF concept has been proposed using uranium nitride pellets encapsulated in a modified Zircaloy cladding. Uranium nitride (UN) is known for its low oxidation and corrosion resistance in oxidizing environments, and therefore it is necessary to modify it for its possible use in light water reactors (LWR). The work presented in this thesis is part of the Superior Accident Tolerant Fuel via Enhanced Technology (SAFETY) project, funded by the Swedish Foundation for Strategic Research (SSF). The project is focused on the fabrication and testing of doped uranium nitride. The process involved the manufacturing of uranium nitride microspheres using a sol-gel method. Studies on the doping effects were done by characterization and interaction of the produced materials with different oxidizing environments, such as air or water.

The main questions raised in this thesis are:

i. Does the addition of dopants affect the sol-gel process and production of UN?
ii. Is doping effective for improving the oxidation resistance of UN?
iii. Are UN microspheres a possible feed material for pellet production?
iv. Can the doped or undoped UN pellets survive the inclusion of water under operation or accident conditions?

2. Background

2.1. Uranium nuclear fuels

Uranium is the 92nd element on the periodic table and has been used for over 50 years in nuclear reactors to produce energy. As such, research involving uranium is quite extensive. Out of all the uranium isotopes, U-233, U-235 and U-238 are the most important in nuclear technologies due to their long half-lives. The first, U-233 is produced in breeder reactors after irradiation of Th-232 as their starting fuel. The other two, U-235 and U-238 are naturally occurring isotopes. Uranium with a natural content of U-235 is used in the Canada Deuterium Uranium (CANDU) reactors. In pressurized water reactors (PWR) and boiling water reactors (BWR) this isotope must be enriched between 2-5% [11].

A multitude of chemical compounds has been produced from uranium; amongst them uranium dioxide (UO_2) has received the greatest attention in fuel fabrication. Its high chemical stability and mechanical properties are the main reasons for its use in light water reactors (LWR), the most common reactor type in the world [12]. Nuclear fuels are normally compacted into high density pellets. Such pellets are then irradiated in the reactor to transform the energy coming from the splitting of the U-235 atoms into thermal and electric energy. This process also produces a large variety of new isotopes of different elements, called fission products. Fuel pellets in the reactor are subjected to a temperature gradient, as the center of the pellet become hotter compared to the edges, which causes severe cracking due to the non-uniform thermal expansion of the fuel [13]. This allows the escape of gaseous fission products from the fuel.

In order to contain the fission products, such as xenon and iodine, the UO_2 is normally encapsulated in a zirconium based cladding (Zircaloy-4). This cladding is widely used in nuclear fuels due to its low neutron absorption, excellent corrosion resistance at operating conditions, and good mechanical stability under neutron irradiation [14].

2.2. Fukushima nuclear accident

The second biggest nuclear accident, although given the highest ranking of the International Nuclear and Radiological Event Scale (INES) category, occurred in the Fukushima Daiichi nuclear power plant in Japan in 2011 [10]. The timeline started by an earthquake in the middle of the Pacific Ocean. The subsequent tsunami far exceeded the designed emergency measures, and the plant lost its connection to the energy grid. Back-up systems in three out of the six units were also disabled during the natural disaster, causing a scenario called station blackout (SBO). The loss of electricity also meant loss of active cooling in the primary circuit, which is also known as a loss of coolant accident (LOCA). Without cooling, the reactors vessel temperature and pressure started to build up. Several security measurements were activated in the reactor units trying to control the coolant injection systems. Nonetheless, more and more liquid coolant turned into steam, leading to the exposure of the cladding to steam. Surface oxidation of the zirconium at temperatures close to 1200 °C resulted in the generation of large amounts of heat

and hydrogen, following Reaction 1. Cladding embrittlement and fuel rod bursting occurred at this point [10], releasing the fission products into the primary circuit.

$$Zr + 2H_2O \rightarrow ZrO_2 + 2H_2 \qquad \Delta H = -590.2\,\frac{KJ}{mol} \qquad (1)$$

Despite all the work from the power plant personnel, unexpected pressure drops indicated venting or breaking of the rector vessels, and subsequently the primary containment. Leakage of radioactive gases and hydrogen was measured in the buildings of Units 1-4. The accumulation of hydrogen in the reactor buildings resulted in explosions of the reactor buildings upper floors, which hindered the efforts to control the temperature in the reactors. Stable conditions were finally reached in 14 days. Nonetheless, radioactive release to the environment was still unavoidable. Noble gases (e.g., ^{133}Xe) and volatile fission products (e.g., ^{131}I, ^{137}Cs, ^{132}Te) were among the first released isotopes to be measured after the nuclear accident.

Currently the Japanese authorities are advancing the decommissioning of the power plant site, a process that will take several decades. The work so far has been centered on the safe retrieval of fuel from the spent fuel pools. More recently, investigation on the removal of fuel debris, also known as corium, is being performed in damaged Units 1-3 [15].

2.3. Accident Tolerant Fuel initiative

After the Fukushima accident, the nuclear industry realized that improvements must be implemented to current fuels in order to further enhance the safety, competitiveness, and economics of commercial nuclear power [16]. Enhanced ATFs are defined as fuel systems that can withstand severe accident conditions in a reactor core for a longer period of time than the UO_2-Zr fuel system. Additionally, the ATFs must also improve or maintain the performance compared to current fuels in the following aspects [17]:

i) Slower reaction kinetics with steam.
ii) Improved fuel properties such as lower operating temperature and increased melting temperature.
iii) Slower hydrogen generation rate.
iv) Improved cladding properties such as thermal shock resistance and limitation of ballooning.
v) Enhanced retention of fission products.

Different ATF concepts have been proposed and researched by countries that rely on nuclear energy. At the beginning of the ATF program, the focus was on cladding alternatives. Some examples of ATF concepts explored are:

- French company AREVA tried investigating an enhanced zirconium alloy cladding in addition to a fuel comprised of UO_2 with up to 10% SiC and diamond additives.
- The CEA was involved in the developing of two potential ATF claddings: Cr coated zirconium alloy and a SiC composite surrounding a thin metallic layer.

- Oak Ridge National Laboratory in the United States of America studied a cladding made of a FeCrAl alloy. This material has been used with success in industries where high temperature oxidation resistance is required. For nuclear cladding applications a Fe-13Cr-(4-5)Al alloy composition was selected for further development.
- US company General Electric was involved in the R&D of claddings to replace the Zr-based alloys. Two concepts were investigated: Advance stainless steels, such as FeCrAl, and Zr coated Mo tubes.
- In India, the Nuclear Fuel Complex (NFC) manufactured a double cladding concept using zircaloy-4 as an inner cladding and modified 9Cr-1Mo steel.
- The Nuclear Power Institute of China (NPIC) was involved in the ATF program in China. They performed a preliminary evaluation of different combinations of cladding and fuel concepts using data collected from the literature.

The consequence of using these modified cladding materials is the neutron penalty caused by the higher neutron capture cross-section compared to the zirconium. To solve this issue, high uranium density fuels are desirable. There have been two main approaches to fuel changes: doping of UO_2 with additives, such as beryllium oxides and silicon carbide, to increase the thermal conductivity; or the use of other uranium compounds with higher uranium density and improved thermal properties. Amongst these compounds, uranium carbides, nitrides and silicides have been studied. Table 2.1 presents the main properties of the different uranium fuel candidates. Higher thermal conductivity and uranium density, lower centerline temperature and similar melting point are the common properties of most fuel candidates when compared to the current UO_2 fuel.

Table 2.1. Comparison of thermal and physical properties of different fuel candidates proposed for the ATF concept.

Fuel	Thermal conductivity (W/mK)	Melting point (°C)	Peak centerline temperature (°C)*	Density (g/cm^3)	Uranium density (g/cm^3)
UO_2	6-2.5 [18]	2875 [19]	2525 [20]	10.96 [19]	9.7[19]
UC	12.6-16 [21]	2495 [22]	700-1300 [21]	13.63 [22]	13.0[19]
UN	19-25 [23]	2630 [19]	930 [20]	14.32 [19]	13.5[19]
U_3Si_2	15-27.5 [24]	1665 [19]	960 [25]	12.2 [24]	11.3[24]

*Peak centerline temperatures depend on the burn up of the fuel.

2.4. Uranium nitride fuel concept

Amongst the fuel alternatives shown in Table 2.1, uranium nitride has received a lot of attention. Uranium nitrides were first researched in the late 1960s. They were developed while looking for a ceramic material better than metallic uranium, however, UO_2 was eventually preferred. Three uranium nitride compounds have been found, uranium mononitride (UN), uranium sesquinitrides (α- and β-U_2N_3), and uranium dinitride (UN_2) [26]. UN is the preferred nitride in nuclear application, as it possesses the highest uranium density. Nitrides have many

advantages compared to UO_2; some examples were defined by Ekberg et al. [27] and can be summarized as:

- Higher fissile density (about 40% more uranium), leading to higher conversion rates.
- Higher thermal conductivity, decreasing the stored energy and the fuel centerline temperature.
- Easily soluble in nitric acid, making it compatible with current purification processes (PUREX).

The relatively high neutron cross section of the N-14 isotope (the most abundant nitrogen isotope in nature) reduces the efficiency of UN in nuclear reactors. The production of the semi longed-lived radioisotope C-14 is undesirable as it increases the radioactivity of the nuclear waste.

$$^{14}N + n \rightarrow p + {}^{14}C \qquad t_{1/2,^{14}C} = 5700\ a \qquad \sigma_{(n,p)} = 1.83 \pm 0.07\ barn \text{ [28]} \quad (2)$$

High uranium enrichment can counter-balance the neutron penalties, however, this can become unrealistic for commercial uses. Researchers have concluded that an enrichment of N-15 is necessary before deployment of UN into LWR is possible. Currently there are no factories with the capability to provide the amount of N-15 necessary to produce the UN required by all reactors in the world. However, the technology exists, and it can be expanded if UN is selected to replace the UO_2. This would nonetheless increase the production cost of nuclear fuel.

Another issue regarding UN fuels is their poor oxidation resistance. Fine powders of rare-earth elements and actinide elements in the nitride form can become pyrophoric, meaning they self-ignite in the presence of oxygen [27]. Therefore, UN production is normally done in oxygen-free atmospheres, which makes it more complicated than their oxide counterparts. Uranium nitrides also react readily with water and steam even at low temperatures. Hence, in the case of fuel failure or clad breaching, the nitride alone would not be able to survive. The fuel would then disintegrate and come into contact with the coolant in the primary circuit, and release of highly radioactive materials would be possible. This makes UN unsuitable for LWRs. The increase of stability of UN towards oxidizing environments has recently become a more popular topic. A widely used method to improve the corrosion of materials is by doping with elements capable of forming a stable passivating oxide layer. In the case of UN, doping with different elements, such as Ni, Al and Zr, was reported prior to this work was started [29,30]. The results were in a preliminary phase and further development on the doping of UN was still needed.

2.4.1. UN applications in other reactors

Use of uranium nitrides in different reactor types has been explored before. For space exploration, the SP-100 reactor program required a high density, high thermal conductivity fuel [31]. Therefore, UN and UO_2 were tested, and the post irradiation experiments (PIE) showed that the UN was the best available fuel at that time [32].

Tri-structural isotropic fuels (TRISO), which are particles of uranium oxide or oxi-carbide, are commercially used in gas cooled reactors. The fully ceramic microencapsulated fuel concept

(FCM) refers to TRISO particles encased in SiC [33]. In 2010, the idea that FCM fuels could replace the UO_2 pellets in LWRs as an ATF alternative was conceived. Nonetheless, the new structure did not contain enough uranium, and the solution was to change the fuel to UN in addition to increasing the particle size. Early irradiation tests on UN-TRISO showed no evidence of fission gas release from the set of four particles.

Uranium nitride is also currently being studied for use in metal cooled reactors of Gen IV [31]. It was successfully tested in the sodium cooled reactor BR-10 in Russia and in the EBR-II test reactor [34]. Additionally, most lead and lead-bismuth cooled reactors concepts are being developed with UN as their fuel [35].

2.5. Uranium nitride synthesis

Uranium nitride has been synthesized using different uranium sources and experimental conditions. Some relevant methods are presented, and the advantages and disadvantages of each are discussed.

2.5.1. Direct nitriding route

During the direct nitriding, the uranium metal used as starting material reacts in a nitrogen atmosphere to form the overstoichiometric uranium nitrides, as seen in Reaction 3. Excess nitrogen is removed by reaction at high temperatures in argon or vacuum [25], according to Reaction 4. The resulting products are high purity UN; however the intermediate product's large grain size complicates the denitridation process.

$$U\ (s) + N_2(g) \leftrightarrow\ UN_{1.5-1.75}\ (s) \qquad \text{T > 850 °C} \quad (3)$$

$$UN_{1.5-1.75}\ (s) \leftrightarrow\ UN(s) \qquad \text{900-1300 °C} \quad (4)$$

2.5.2. Hydride-nitride route

Another method that uses metallic uranium is hydride-nitride synthesis. Uranium reacts with hydrogen to form uranium trihydride (UH_3), which falls off the surface of the metal and produces a fine powder. The UH_3 is able to react with nitrogen at lower temperatures than the metallic uranium. This method has the advantage of avoiding carbon and oxygen impurities and has been used in the preparation of other actinide nitrides, such as PuN or ThN [36]. However, only small volumes are able to be nitrided at the same time. The chemical reactions occurring during the Hydride-nitride route are written in Reactions 5-7.

$$2U\ (s) + 3H_2(g) \leftrightarrow\ 2UH_3(g) \qquad \text{200-250 °C} \quad (5)$$

$$4UH_3\ (s) + 3N_2(g) \leftrightarrow\ 2U_2N_3(s) + 6H_2(g) \qquad \text{300 °C} \quad (6)$$

$$2U_2N_3(s) \leftrightarrow 4UN(s) +\ N_2(g) \qquad \text{1150 °C} \quad (7)$$

2.5.3. Ammonolysis route

Two ammonolysis routes can be used depending on the starting material. Reaction 8 and 9 show the reaction of UO_2 with ammonium bifluoride (NH_4HF_2) producing ammonium uranium fluoride, $(NH_4)_4UF_8$. Sequentially, this compounds reacts with NH_3 to produce UN_2 which can be denitrided according to Reaction 10.

$$UO_2\ (s) + 4NH_4HF_2\ (s) \leftrightarrow (NH_4)_4UF_8(s) + 2H_2O \quad (8)$$

$$(NH_4)_4UF_8(s) + 6NH_3(g) \leftrightarrow\ UN_2(s) + 8NH_4F(s) + H_2(g) \quad (9)$$

$$UN_2(s) \leftrightarrow \frac{1}{2}U_2N_3(s) + \frac{1}{4}N_2(g) \quad (10)$$

Alternatively, uranium tetrafluoride (UF_4) can also be used as a staring material to react directly with NH_3 to produce the UN_2.

$$UF_4(s) + 2NH_3(g) \leftrightarrow\ UN_2(s) + 4HF(g) +\ H_2(g) \quad (11)$$

2.5.4. Carbothermic reduction and nitridation

The most likely route to reach industrial scale production of UN is the carbothermic reduction [37]. In this method, the oxide material to be reacted is mixed with carbon and heated in an inert or N_2 atmosphere to produce the carbide or nitride, respectively. The chemistry of the carbothermic reduction and nitridation of uranium can be summarized in Reaction 12.

$$UO_2(s) + 2C(s) + \frac{1}{2}N_2(g)\ \leftrightarrow\ UN(s) + 2CO(g) \quad (12)$$

The nuclear industry has used the carbothermic reduction to transform UO_2 into UC and UN. The previously mentioned TRISO particles are made from spheres treated with the carbothermic reduction to produce carbides. An in-depth chemistry analysis of this process will be further discussed in the theory section.

3. Theory

In this section the most important concepts for the understanding and discussion of the experiments will be provided.

3.1. Uranium-Nitrogen binary system

The uranium-nitrogen binary system has been studied extensively since the late 1960s. Different phase diagrams have been calculated and presented in previous studies [32,38,39]. An example of such a diagram is shown in Figure 3.1.

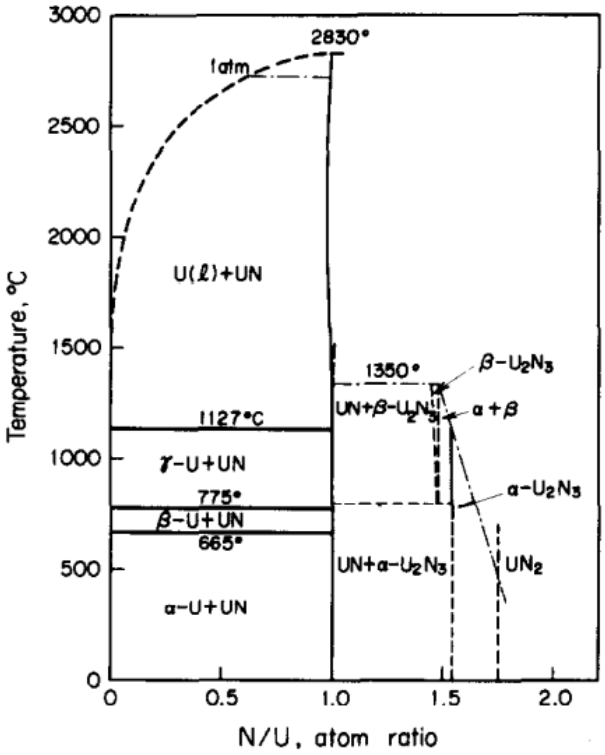

Figure 3.1. U-N binary phase diagram showing the most stable uranium nitride phases at specific temperature and nitrogen/uranium ratios [39].

All phase diagrams show the presence of the three main compounds identified for uranium-nitrogen system. Uranium mononitride is the lowest stoichiometric nitride. It exists as a Face-Centered Cubic (FCC) structure (NaCl) with lattice parameter of 4.890 Å and belongs to the F*m3m* space group. The uranium dinitride is found on the opposite side of the spectrum, showing the highest N/U ratio. It has an FCC structure (CaF_2) with a lattice parameter of 5.310 Å and also belongs to the F*m3m* space group. In between these two compounds there is one more, uranium sesquinitride. This compound can be found in two phases, the more common alpha (α-U_2N_3) and the less common beta (β-U_2N_3). The α-U_2N_3 has a Body-Centered Cubic (BCC) Mn_2O_3-like structure, belonging to the *Ia3* space group with a lattice parameter of 10.699 Å. The β-U_2N_3 is indexed as a trigonal structure with lattice parameters a/b=3.693 and c= 5.770 Å.

During reaction of U and N_2, the synthesis of higher nitrides occurs at lower temperatures than the mononitride. Pure UN_2 materials are reported only during synthesis at high N_2 pressure [40]. Therefore, it is more common to observe a solid solution of UN_2 and α-U_2N_3 at all intermediate compositions above $UN_{1.54}$ [38,41]. The name UN_2 is given to solutions with N/U ratios above 1.75, while U_2N_3 is for solutions between 1.5 and 1.75 [38]. U_2N_3 has been thought to derive from the UN_2 structure by systematic removal of nitrogen resulting in an ordered crystal structure. Therefore, during decomposing of UN_2 into UN, the U_2N_3 is formed as an intermediary phase. This behavior becomes important during synthesis of pure UN materials.

3.2. Oxidation of UN

The mechanism for UN oxidation was proposed by Dell et al. [42]. In oxygen environments, the reactions start on the surface where the oxygen is chemisorbed. At lower temperatures, about 200 °C, UO_2 is the only observed oxidation product. At higher temperatures, U_3O_8 is the final oxidation product obtained in this process.

Reactions for the production of higher oxides have been discussed by Rao et al. [43] and is shown in Reaction 13. They suggest that there can be two nucleation mechanisms that guide the reaction, and that they are differentiated only by the presence of a separate UO_2 phase in the bulk material. In both cases, the transport of oxygen atoms in a solid material is what causes further oxidation.

$$UN\ (s) + \frac{2+x}{2}\ O_2(g)\ \rightarrow UO_{2+x}(s) + N \quad (13)$$

The nitrogen released from the reaction tends to react with the UN to form the U_2N_3 species. Additionally, it can react with another N atom and form molecular nitrogen. This is represented by Reactions 14 and 15.

$$2UN(s) + N\ \rightarrow U_2N_3(s) \quad (14)$$

$$N + N\ \rightarrow N_2\ (g) \quad (15)$$

The U_2N_3 is considered an intermediate product instead of a side reaction as it reacts further with O_2 to form more oxides, as presented in Reaction 16.

$$U_2N_3(s) + 2O_2\ (g) \rightarrow 2UO_2(s) + \frac{3}{2}N_2(g) \quad (16)$$

3.3. Hydrolysis of UN

Research on the water oxidation mechanism was performed by Dell et al. [44]. Reaction 17 shows the reaction between UN and water produces UO_2, with NH_3 and H_2 as gaseous by-products.

$$UN\ (s) + 2\,H_2O\ \rightarrow UO_2(s) + NH_3(g) + \frac{1}{2}\ H_2(g) \quad (17)$$

Moreover, U_2N_3 was also observed during some of their partial oxidation experiments. Thus, Reaction 18 was proposed to occur as a secondary reaction. U_2N_3 can also be further oxidized to UO_2 releasing NH_3 and N_2 as by-products, as seen in Reaction 19.

$$3\,UN\,(s) + 2\,H_2O \rightarrow UO_2(s) + U_2N_3(s) + 2\,H_2(g) \quad (18)$$

$$U_2N_3(s) + 4\,H_2O \rightarrow 2UO_2(s) + \frac{8}{3}NH_3(g) + \frac{1}{6}\,N_2(g) \quad (19)$$

UN interaction with water and steam shows a slightly different behavior than with oxygen. It is currently known that the reaction product after the reaction of UN with water is UO_2, as mentioned by Rao et al. [43]. The absence of higher oxide phases, such as UO_3 or U_3O_8, in the hydrolysis products was explained by the lower oxidation potential in addition to the larger size of water molecules compared to oxygen. Additionally, the gaseous byproducts (H_2 and NH_3) of the hydrolysis reaction are undesirable from a nuclear application standpoint due to their combustible properties. Additionally, ammonia will change the water chemistry in the primary circuit in the case of fuel deterioration due to water inclusion.

3.4. Corrosion prevention

In order to control and improve the corrosion weakness of UN different approaches were suggested: decrease the available surface of reaction, coating with corrosion resistance substance and doping with materials capable of forming a passivating layer.

3.4.1. Sintering

Sintering is described as a process that uses high temperatures to convert loose fine particles into a solid coherent body without fully melting the particles [45]. The driving force of sintering is the reduction of interfacial energy [46]. This reduction occurs via densification and grain growth. The mechanism can be explained using a two particle model. During sintering, the atoms move across boundaries of the particles, causing the fusion to form the solid piece. Highly porous materials allow for more active places for oxidation reactions to occur. To limit this, surface reduction can be achieved by sintering the materials.

In nuclear materials sintering is an important process during fuel fabrication. UO_2 is normally pressed into pellets and then sintered to increase the density of the materials. The sintering is done in a reducing atmosphere at temperatures between 1500 and 1800 °C [47,48].

It was reported in the literature [49] that early attempts to sinter uranium nitride pellets proved to be more challenging than the oxides or the carbides. For example, sintering at 1700 °C in a vacuum showed no densification of the UN. Moreover, increasing the temperature in an inert atmosphere resulted in decomposition of the UN into metallic uranium and nitrogen, which is expected by the phase diagram [50]. The sintering of UN must therefore be performed under a nitrogen atmosphere. It has been suggested that sintering at 2200 °C for a couple of hours is necessary to achieve densities higher than 90% theoretical density (TD) [51]. The temperature could be lowered to 2000 °C if longer sintering times are used [25].

Lower sintering temperatures for UN materials were achieved by spark plasma sintering (SPS). A schematic representation of the assembly used in SPS can be seen in Figure 3.2, where the

sample is located inside a graphite die between graphite punchers. This type of sintering uses an electrical current to reach high heating rates of up to 1000 °C/min [52–54]. Simultaneously, pressure is applied to aid in the compaction of the particles inside the die. Sintering of uranium nitride powders using SPS has been studied before by several authors [55–57]. UN pellets with densities of about 90% TD were fabricated by Muta et al. [56] using temperatures as low as 1400 °C. Similar results were observed by Malkki et al. [55]. However, sintering was performed at 1650 °C for only 3 minutes. Higher densities have also been reported by Johnson et al [57].

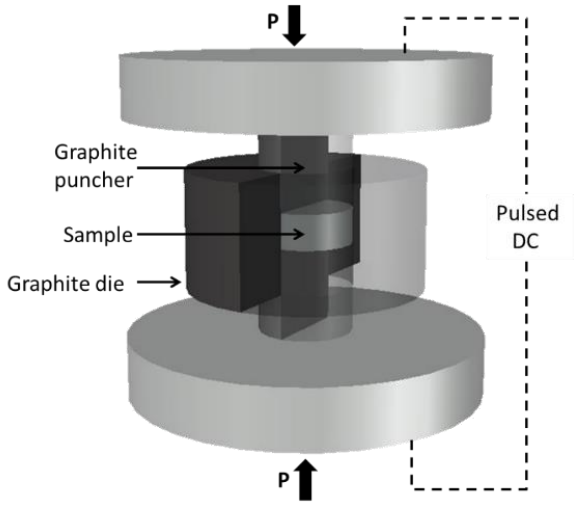

Figure 3.2. Graphical representation of the graphite die used for SPS, where the pellet is packed between two graphite punchers. P represents the direction of applied pressure [58].

3.4.2. Coating

Coating is a method of corrosion protection where the material is covered with a thin film of an inert substance. Some examples of coating material are zinc for iron, chromium on steel parts, organic polymers such as paints, and inorganic materials such as enamel. Coating substance selection depends on the corrosive medium where the bulk material is not stable. Coated materials have an improvement of the corrosion resistance via three mechanisms: prevention of interaction of the bulk material with the oxidizing environment (barrier), sacrifice of the coating (cathodic protection), and passivation. The coating material is therefore required to be able to limit the transport of oxidizing agents through its layer [59]. Several different coating methods exist today. Some examples are electrolytic plating, hot dipping, cold and thermal spraying, and chemical vapor deposition (CVD).

Coating is currently being studied to prevent the oxidation of claddings. For example, new ATF cladding concepts are based on the coating of the Zircaloy-4 with, for example, chromium. On the other hand, coating of fuel pellets is not possible due to cracking of pellets during irradiation. In this case, the bulk of the pellet will be exposed to the environment, which makes the coating useless. Nonetheless, coating has been used in the production of fuel in a different geometry. The TRISO particles fuels are an example of coating of nuclear fuels. These particles are spheres of uranium oxycarbides, which have been covered with a multilayer barrier composed of two graphite layers and a SiC layer in between.

3.4.3. Doping/Alloying

Doping is the intentional introduction of impurities into a material for the purpose of modifying the structural properties, whereas alloying is the mixture of two phases of which one is a metal. Corrosion of alloys follows different principles than a pure phase. The dissolution of one of the components occurs sooner and an intermediate region of different composition can develop. The most stable phase is then found in the surface of the material, acting as a barrier.

A variety of systems have been proposed for the corrosion improvement of UN. The material can be mixed with two types of materials: uranium oxides (UO_2) or silicides (U_3Si_2) to form composites, and additives (Al, Cr, Ni) for doping. Composite formation has been studied previously [18,49,60]. In these studies, the methods used powder metallurgy to produce the composite materials. The main conclusion was that the composites formed showed slower degradation compared to the pure UN.

Additives available for mixing are required to form a stable layer that would act as a barrier and protect the UN. Chromium, aluminum, yttrium, titanium are commonly used additives in the steel and metals industry. Chromium is known to form a stable chromia scale (Cr_2O_3) at the surface of the steel if the Cr composition in the alloy is higher than 5% [61]. Moreover, chromia is stable over a wide range of pH. However, it is been reported that substantial vaporization occurs at temperatures as low as 600 °C [62]. In a PWR reactor, the coolant temperature is maintained between 275 and 315 °C, the dissolved oxygen levels are kept low and the electrochemical potential was measured between -100 and -150 mV [63] while the pH can vary from 6-9 [63]. After examination of the Pourbaix diagram in Figure 3.3, it is feasible that chromia should be stable at the mentioned conditions and could therefore be considered a good candidate for UN waterproofing.

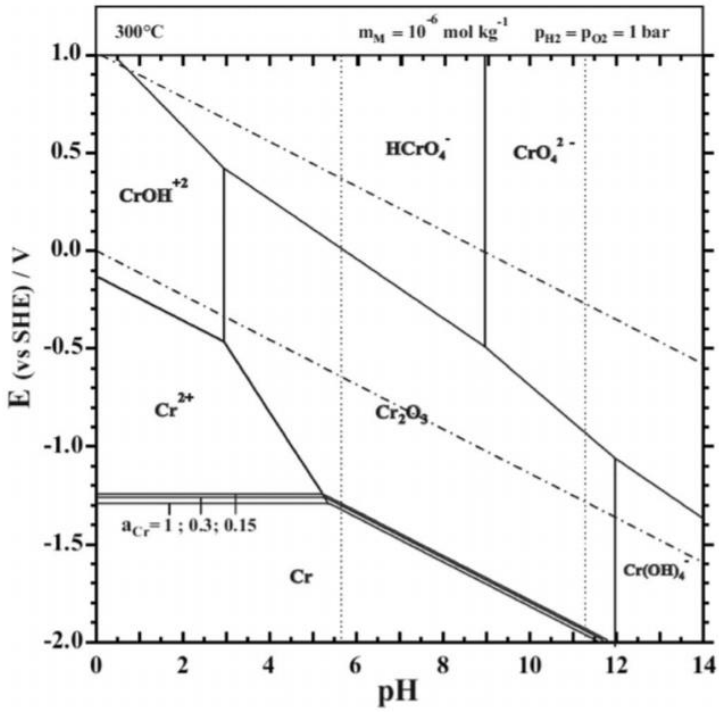

Figure 3.3. Pourbaix diagram of chromium at 300 °C. The vertical dotted lines indicates the neutral pH (below pH 6) and the basic pH limit (above pH 11) [64].

Previously, a screening for possible additives to improve corrosion resistance of UN was done by Herman et al. [29]. It was shown that Cr-doped UN pellets survived for longer periods of time in boiling water compared to an undoped pellet. The data was not extensive and further development was still necessary to understand the behavior and reactions occurring during oxidation of these type of materials. Other additives proposed for UN waterproofing are Al, Ni, and Th. The last of these has not been proven to form a protective scale. However, studies have reported that ThN oxidizes faster than UN and that ThO_2 is less soluble in water than UO_2 [65]. Thorium could therefore be investigated as a candidate additive for protection of UN.

3.4.4. U-X-N ternary systems

The interaction between the UN and the dopant can become complicated depending on the synthesis method. For example, the results from Herman [29] did not present much information regarding the chromium reactions during the carbothermic reduction at high temperatures.

In the case of alloying with metallic additives, the formation of solid solutions can be defined by the Hume-Rothery rules [66]. This method compares the atomic radius, electronegativity and crystal structure of two components of a material to determine if a solid solution is likely to form. Uranium and additives properties regarding Hume-Rothery Rules are listed in Table 3.1. All showed the same crystal structure in the nitride form, with the exception of AlN. Aluminum properties suggested that the formation of a solid solution between UN and AlN is not achievable. On the other hand, the similar properties of Th to uranium suggests that a solid solution in the nitride system is highly probable.

Table 3.1. Elemental properties of additive candidates with regard to the Hume-Rothery rules.

Element	Atomic radius (Å) [67]	Atomic radius difference with uranium (%)	Electronegativity (Pauling scale) [67]	Crystal structure as mononitride (space group)
Cr	2.06	14	1.66	FCC (NaCl) [68]
Al	1.84	23	1.61	Hexagonal (wurtzite) [69]
Y	2.32	3.7	1.22	FCC (NaCl) [70]
Ti	2.11	12	1.54	FCC (NaCl) [71]
Th	2.45	1.7	1.90	FCC (NaCl) [72]
U	2.41	0	1.83	FCC (NaCl) [73]

The interaction between UN and TiN, YN, NdN, or CeN was experimentally studied by Holleck et Al. [74–76]. In that study, composite materials made using arc melting resulted in a complete miscibility of the UN-XN systems, except for the TiN, where it was shown to be soluble between 1 and 4 mol%. Phase diagrams of the actinide-transition metal-nitrogen systems were published by Holleck [77]. The phase diagrams showed that most elements formed solid solutions with UN, however, the formation of ternary phases was also possible. In the case of Cr as an additive, a ternary phase with the U_2CrN_3 composition is expected to form at 1200 °C (Figure 3.4). This phase is present in an orthorhombic crystal structure and belongs to the space group *Immm* [78]. Theoretical calculations made by Mishchenko et al., [79] have shown that the solubility of CrN in UN crystal is thermodynamically favorable and expected.

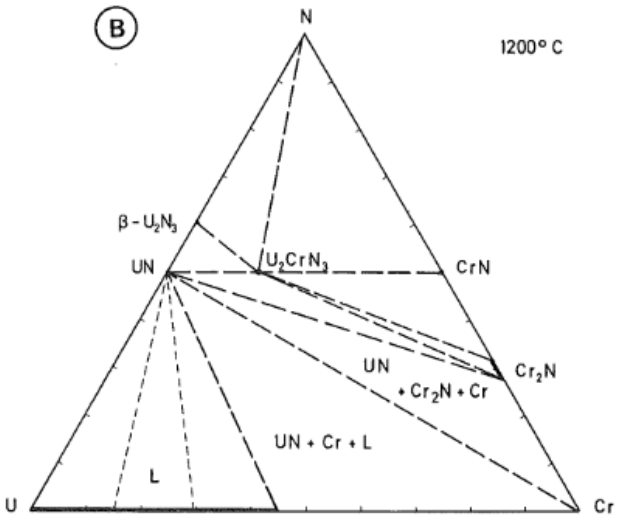

Figure 3.4. Ternary phase diagram of the U-Cr-N system at 1200 °C reported by Holleck [77]. *Multiple phases were mentioned; however, special attention is drawn to the formation of a ternary phase U_2CrN_3.*

3.5. Synthesis of UN by the sol-gel process and carbothermic reduction.

Gelation methods have been developed to provide advantages over powder methods. For example, more homogeneous distribution of elements mixtures can be achieved, and the use of liquid starting materials, which are simpler to transport and transfer, and facilitates remote operation. There are different types of sol-gel methods, such as the external gelation, the ORNL process, and the internal gelation process. Each have their own benefits and disadvantages. These processes are based on the precipitation of metal solutions as oxides or hydroxides, usually in the shape of spheres. The sol-gel processes have been used in the nuclear industry to produce uranium dioxide [80–82], uranium carbide, and uranium nitride microspheres (spheres with diameter smaller than 1000 μm). The main advantage of using this method is the possibility to add doping elements to the liquid mixture, in which case it can form a completely homogeneous mixture of the dopants in the bulk.

The internal gelation process used in this work is based in the hydrolysis and precipitation of uranium cations in solution due to the increase in pH when the solution is heated. The starting uranyl nitrate solution is mixed with a complexation agent (urea) and a gelation agent (HMTA) to produce a sol. Temperature is kept low (0 to 5 °C) while mixing to prevent the decomplexation and decomposition of the gelation agent [83].

$$UO_2^{+2}(aq) + 2[CO(NH_2)_2](aq) \leftrightarrow [UO_2 \cdot 2(CO(NH_2)_2)]^{+2}(aq) \quad (20)$$

The sol is then dripped into an immiscible heat-carrying media to start the gelation. Once the temperature increases, the uranyl-urea complex is broken, and the cation is hydrolyzed and precipitated as uranyl hydroxide.

$$[UO_2 \cdot 2(CO(NH_2)_2)]^{+2}{}_{(aq)} + 2H_2O \leftrightarrow UO_2(OH)_{2(s)} + 2[CO(NH_2)_2]_{(aq)} + 2H^+{}_{(aq)} \quad (21)$$

HMTA consumes the protons released and decomposes into ammonium and formaldehyde. The equilibrium is thereby shifted towards the products side by the Le Chatelier's principle.

$$(CH_2)_6N_4\ (aq) + H^+(aq) \leftrightarrow\ [(CH_2)_6N_4H]^+(aq) \tag{22}$$

$$[(CH_2)_6N_4H]^+(aq) + 3H^+(aq) + 6H_2O\ \leftrightarrow\ 4{NH_4}^+(aq) + 6\,CH_2O(aq) \tag{23}$$

The next step in the synthesis is nitridation. In this work, carbothermic reduction and nitridation (CTR-N) was used. The general reaction was mentioned beforehand in Reaction 12. According to Sooby et. Al. [37] the process can be divided in three segments: the oxygen removal (Eq. 24), nitrogen introduction (Eq. 24-25), and excess carbon removal (Eq. 25-26). The reactions taking place during the CTR-N can be written as:

$$UO_2(s) + (2+x)C(s) + \frac{(1-x)}{2}N_2(g)\ \leftrightarrow\ UN_{1-x}C_x(s) + 2CO(g) \tag{24}$$

$$UN_{1-x}C_x(s) + \frac{x}{2}N_2(g) \leftrightarrow\ UN(s) + xC(s) \tag{25}$$

The carbon contaminations must be removed, as carbides can cause embrittlement of the zircaloy claddings [84]. This is accomplished using the same reaction atmosphere and higher temperatures, where the production of HCN is the expected method of carbon elimination.

$$2C(s) + H_2(g) + N_2(g) \leftrightarrow\ 2HCN(g) \tag{26}$$

Moreover, the final product of the sol-gel process can be written as $UO_3{\cdot}H_2O$, which must be reduced to UO_2. This is done either by reacting in a H_2 containing atmosphere, or increasing the carbon to uranium ratio in the feed material. This has repercussions in the amount of carbon in the UN, which is the main disadvantage of using CTR-N over other methods.

$$UO_3(s) + H_2(g)\ \leftrightarrow\ 2UO_2(s) + H_2O(g) \tag{27}$$

$$UO_3(s) + C(s)\ \leftrightarrow\ UO_2(s) + CO(g) \tag{28}$$

Other metals used as dopants are also expected to follow a similar mechanism of precipitation using the sol-gel method. Additionally, CTR-N has been used for other metal nitrides [85–89], and as such it is expected to be able to produce nitride mixture between the doping elements and the uranium nitride.

4. Materials and Methods

The materials and instruments used for the experiments conducted in this work are presented in the following section.

4.1. Chemicals

All uranium solutions were made in-house by dissolving a metallic bar of natural uranium in concentrated HNO_3 (67%, Merck). The resulting uranyl nitrate hexahydrate (UNH) $[UO_2(NO_3)_2{\cdot}6H_2O]$ crystals were filtered and left to air dry. To prepare the solutions, a known amount of UNH was dissolved in MQ water (18.2 MΩ·cm).

The chemicals used during the gelation were:

- Thorium nitrate $[Th(NO_3)_4{\cdot}5H_2O]$, received as a solid prepared in-house.
- Chromium nitrate $[Cr(NO_3)_3{\cdot}9H_2O]$, 99% purity, purchased from Sigma Aldrich.
- Aluminum nitrate $[Al(NO_3)_3{\cdot}9H_2O]$, 98% purity, purchased from Sigma-Aldrich.
- Urea in solid form, >99% purity, purchased from Sigma Aldrich.
- Hexamethylenetetramine (HMTA), >99% purity, purchased from Sigma Aldrich.
- Carbon black (MOGUL-L), provided by CABOT.
- Triton X-100, laboratory grade purity, purchased from Sigma Aldrich.
- Silicone oil v-1000, purchased from Rhodorsil.
- Petroleum ether, purchased from Alfa-Aesar.
- Ammonium hydroxide (NH_4OH) solution, 28-30%, purchased by Sigma-Aldrich.

Gases used during the experiments were:

- 5% H_2/N_2, 99,99% purity, from AGA, used for the synthesis of microspheres.
- Argon, 99.998% purity, from Air Liquide, used in the synthesis of microspheres.
- Synthetic air (21% O_2/79% N_2), 99.99% purity, from AGA, used for oxidation experiments.
- Helium, 99.999% purity, from AGA, used for density measurements.
- Nitrogen (N_2), 99.98% purity, In-house, used for porosity measurements.

4.2. Instrumentation

This section will present the instruments used to perform the experiments in this thesis.

4.2.1. Gelation system

A double jacketed 50 mL glass beaker was used to mix the solutions of metals and gelation chemicals at low temperatures (4 °C). A 30 cm-tall 5 cm-inner-diameter jacketed glass column connected to a temperature-controlled water bath was used during the gelation of the microspheres. Part of the gelation system can be seen in Figure 5.2.

4.2.2. Furnace

A horizontal electrical tube furnace (ETF 30-50/18-S) from ENTECH with a maximum operating temperature of 1800 °C was used for the nitridation of uranium microspheres. Alumina tubes (1.1 m long and 4.2 cm inner diameter) and alumina boats (10 x 3 x 1.7 cm) were obtained from KYOCERA Fineceramics Nordics AB.

4.2.3. Scanning electron microscopy (SEM)

Two microscopes were used during the study. A Hitachi TM 3000 tabletop scanning electron microscope coupled with an energy-dispersive X-ray (EDX) was used for the surface analysis of microspheres. The Hitachi SEM was positioned in a glovebox with argon atmosphere. A Leo Ultra 55 SEM equipped with an EDX detector for chemical analysis was used for SEM analysis of the pellets surface. Both measurements were carried out in high vacuum with a high voltage ranging from 10-30 kV.

4.2.4. X-ray diffraction (XRD)

X-ray diffraction measurements were done in a BRUKER D2 PHASER XRD, which includes a Cu (λ = 1.54184 Å) radiation source in a 2θ range of 20˚ - 144˚, and a lynxeye detector. The operating voltage and current used were 30 kV and 10 mA, respectively.

The lattice parameters of the materials can be calculated using the diffractograms. Eq. 29 relates the lattice parameter (a) to the Miller index of the crystallographic plane causing the diffraction peak (hkl), the wavelength of the X-rays used (λ), and the interference diffraction angle (θ).

$$a^2 = \frac{(h^2 + k^2 + l^2)\lambda^2}{4sin^2(\theta)} \quad (29)$$

Diffrac.Topas (V6.0) software provided by Bruker, in addition to the open access JEdit software were used to determine the lattice parameter and phase composition of complex compounds and mixtures by means of a Rietveld refinement.

An X'Pert^3 Powder X-ray diffraction system, which includes a monochromatic Cu (λ = 1.54184 Å) radiation source, was used to analyze the reaction products after the steam interaction experiments.

4.2.5. Elemental analyzers

Two different elemental analyzers were used depending on the target element. The carbon content in the samples was measured using a LECO CS744 carbon analyzer. Approximately 50 mg of sample was weighed out in an alumina vial and introduced into the instrument to be oxidized to CO_2, which is then measured by an infrared detector. Nitrogen and oxygen were measured in a LECO TC-436DR analyzer. Approximately 50 mg of the sample was weighed out in a Sn thin foil boat, closed, and put in a Ni basket. The basket was then introduced into the furnace, where it was placed in a graphite crucible and heated to temperatures high enough to melt the samples. Nitrogen is released as N_2 and quantified by measuring the change in thermal conductivity of the He carrier gas. Oxygen reacts with the crucible to form CO_2,which was measured with non-dispersive infrared cells. Measurements in both instruments were made in triplicate to estimate the measurement uncertainties in the instruments.

4.2.6. Inductively coupled plasma-mass spectrometer (ICP-MS)

Uranium, thorium, and chromium composition ratios were measured with an inductively coupled plasma-mass spectrometer (ICP-MS) iCAP Q from Thermo Scientific. Samples were dissolved in aqua regia (1:3 HNO_3: HCl), filtered, and then diluted with 0.5M HNO_3 in the range of calibration (1-50 ppb). An approximate 0.1 ppb detection limit was estimated for the method used. The calibration was prepared by dilution of the standards in 0.5M HNO_3.

4.2.7. X-Ray Fluorescence (XRF)

To determine the Cr content in microspheres and pellets, a portable Delta-50 XRF instrument (Innov-X, Olympus) was used. It contains a Ta anode X-ray tube, which provides a beam of up to 50 kV with a diameter of 10 mm. Samples were loaded into a sample holder that had a 23 μm-thick Mylar® film at the opening of the cell facing the X-ray source. The instrument was mounted in its test stand, with the analyzer window facing upwards. The sample was then placed on top of the analyzer window and measured for 1 minute in triplicates.

4.2.8. Spark plasma sintering (SPS)

A modified DrSinter SPS-530ET instrument, contained within a glovebox under an inert argon atmosphere, was used to press and sinter the pellets. The maximum pressure allowed for sintering is 250 MPa and temperatures lower than 2500 °C can be used. A graphite die with an internal and external diameter of 8.4 and 25 mm, respectively, and a height of 5 cm was used during sintering. Two graphite puncher with 8 mm diameter and 20 mm in length were used to contain the sample and to press it afterwards. Graphite paper with a thickness of 0.2 mm was used to prevent the sample from sticking to the graphite die and punchers. Sintering was performed under high vacuum (<10 Pa) to avoid damage to the instrument. The temperature was measured on the surface of the graphite die by an optical pyrometer.

4.2.9. Density, superficial area, and porosity

A gas pycnometer (Accupyc II 1340, Micromeritics) was used to measure the density of the fuel pellets. The instrument works by measuring the amount of helium gas that is displaced after introduction of the material into the chamber. Surface area and open porosity were studied with an ASAP 2020 instrument from Micromeritics, using the BET principle of adsorption and desorption of nitrogen in the pores at low temperatures (-196 °C).

4.2.10. Thermogravimetric analyzer

A thermogravimetric analyzer (TGA) Q-500 from TA Instruments was used for the study of oxidation of samples in air. Samples are placed in an alumina basket held by a Pt wire in the furnace, and the mass change is measured with a precision balance. The thermogravimetric data collected was analyzed using the Universal Analysis software provided by TA Instruments. Mass change was measured with an accuracy of ± 10 μg.

4.2.11. Simultaneous Thermal Analyzer (STA)

A Customized Linseis STA PT1600 Simultaneous Thermal Analyzer coupled with OmniStar ThermoStar GSD320 Gas Analysis System was used during the steam interaction experiments.

The reaction progress was tracked using the high precision Linseis balance, with a resolution of 0.025 μg. An S-type thermocouple was used to measure the temperature of the sample holder and reference sample holder. Sample crucibles were made of alumina.

4.2.12. Autoclave

A stainless-steel autoclave (Parr Instruments Co., USA) was used for the water interaction test. The reported maximum temperature and pressure of 350 °C and 200 bar, respectively, limited the temperature and pressure range that could be used in the experiments. The autoclave is equipped with a pressure gauge, two gas valves, and a thermocouple, the latter of which is connected to a temperature control. The autoclave was placed in a heating mantle, also connected to the temperature control unit. The mantle had no cooling system, thus only air cooling could be used. A schematic representation of the autoclave can be seen in Figure 4.1.

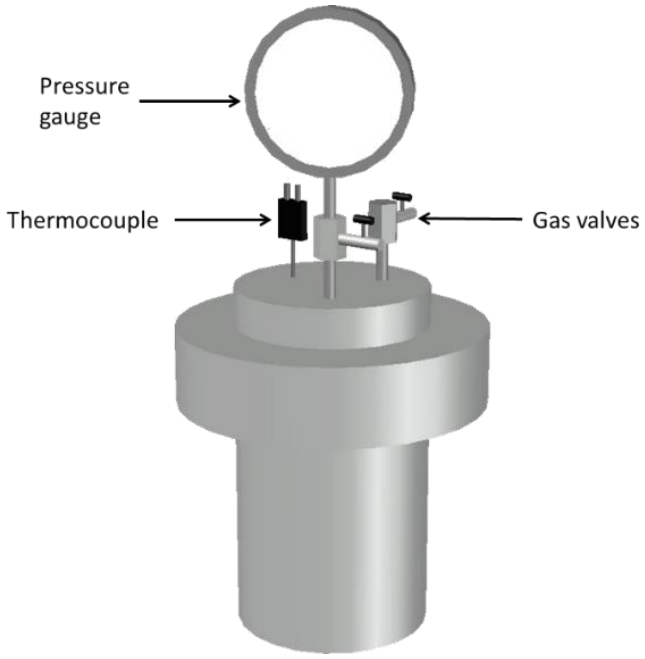

Figure 4.1. Graphical representation of the stainless-steel autoclave used in the water/steam interaction experiments [90].

5. Experimental Methods

Details of the methods used during the production and testing of the UN and doped UN microspheres and pellets will be presented in this section. A summary of the whole process for each additive can be seen in Figure 5.1. Sample nomenclature was dependent on the original metal molar content. For example, a material with thorium content of 20 mol-% was named U80Th20N-X. A dual doping sample containing 5 mol-% Al and 15 mol-% Cr was named U80Cr15Al5N-X. The X denotes the batch number if there were multiple batches with the same composition.

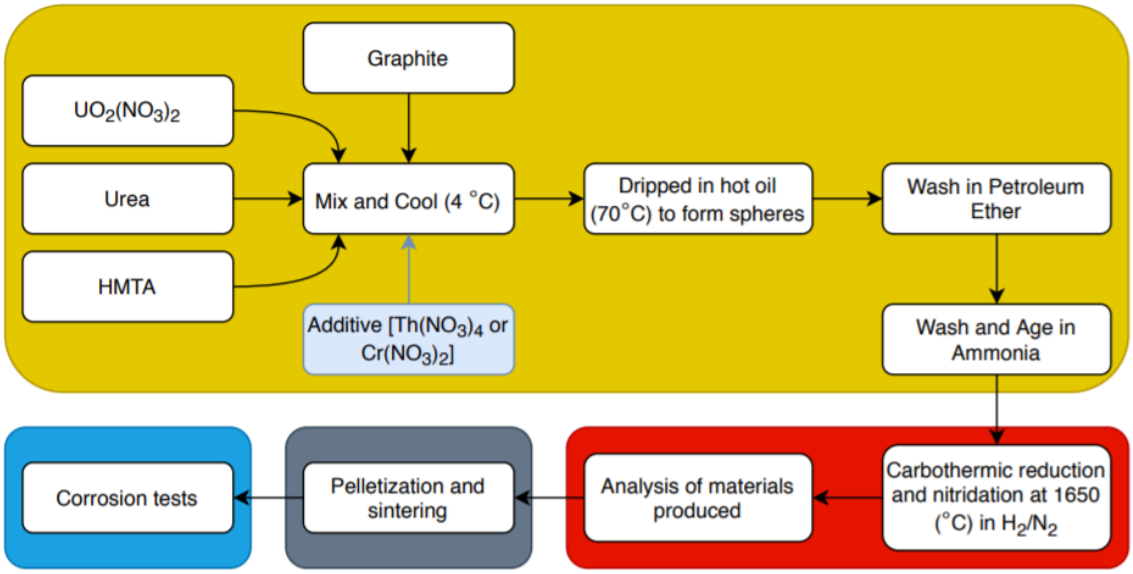

Figure 5.1. Workflow scheme for the proposed work showing the division of the four main areas: microsphere production, nitride production, pellet manufacturing, and corrosion tests.

5.1. UN and doped UN microsphere production

The sol-gel method was followed in the production of microspheres for two main reasons: to avoid the handling of radioactive powders and to be able to produce a homogeneous mixture of metals as the starting materials.

The synthesis started by cooling solution of $UO_2(NO_3)_2$ to 4 °C under magnetic stirring. Dopant metals were added as a solid and allowed to dissolve in the cooled uranyl solution. Urea was added to obtain a urea/metal molar ratio of 1.3. Once the urea was completely dissolved, the HMTA was gradually added, allowing it dissolve before more was added. The final HMTA/metal molar ratio was 1.7 for undoped and Th-doped microspheres, and 1.8 for Al- and Cr-doped microspheres. After all the HMTA was dissolved, Triton X-100 was dropped into the solution to reach a concentration of 0.02 g/mL. Afterwards, carbon black was added to reach a C/metal molar ratio of 2.5. The solution was then allowed to mix for 10-15 minutes before the gelation.

The solutions were manually dripped using a plastic pipette into the gelation column filled with silicone oil. The oil temperature was maintained at 70 °C for undoped and Th-doped

microspheres, and 90 °C for Al- and Cr-doped microspheres. An average dripping rate of 2 min per mL of solution was employed during the gelation of microspheres. After all the solution was dropped, the microspheres were collected in a sieve, and washed twice in petroleum ether to remove the remaining oil. The final washing of the spheres was performed in ammonium hydroxide solution followed by a wash in water to age the microspheres and remove the unreacted chemicals. The microspheres were then left to air dry at room temperature for 24 - 48 hours.

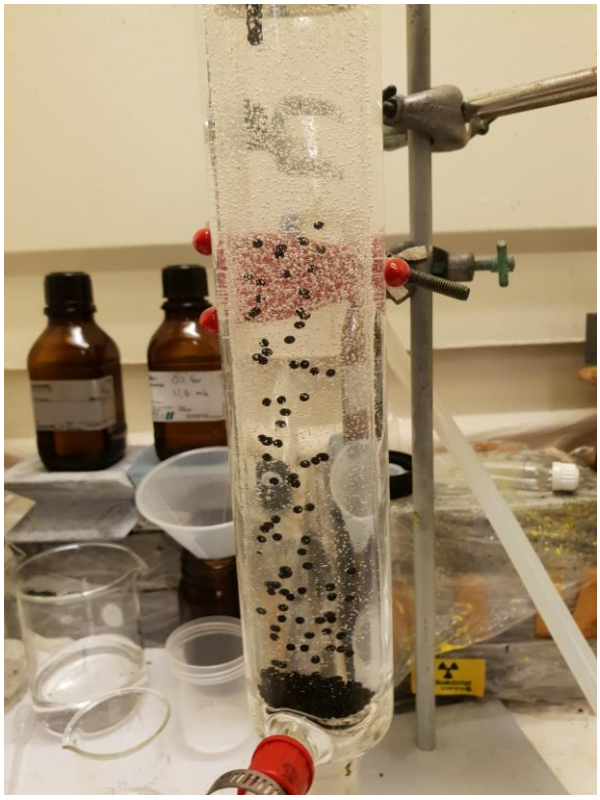

Figure 5.2. Example of the experimental setup for the internal gelation process, where the forming of the microspheres in the oil column is shown.

5.2. Reduction and nitridation process

In order to produce nitrides, the samples were heated in the furnace to temperatures above 1500 °C in a H_2/N_2 atmosphere. Two different heating profiles were used for the experiments.

5.2.1. Profile A

The first heating process was divided in two sections:

- A mild heating process to reduce the cracking of the microspheres: the materials were heated at a rate of 3 °C/min to reach 350 °C, which was held for 1 hour. Afterwards the temperature was raised to 800 °C with a 10 °C/min heating rate. After 1 hour of reaction at 800 °C, the materials were cooled at a rate of 10 °C/min.
- Nitridation and decarburization: This section involved the heating of the samples to 1550 and 1650 °C, respectively. Heating rates of 10 °C/min were used. The temperature was

held for 4 hours at 1550 °C and for 1 hour at 1650 °C. At 30 minutes before the cooling started, the gas was changed to Ar to avoid the formation of higher nitrides. Cooling was carried out at a rate of 10 °C/min.

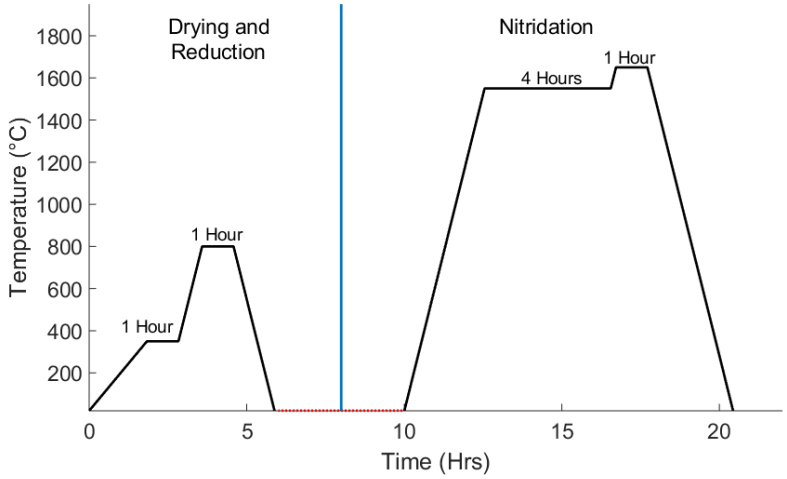

Figure 5.3. Temperature profile A for the carbothermic reduction and nitridation process. Heating and cooling rates of 10 °C/min were used for the nitridation. Heating and dwelling were performed under 5% H_2/N_2 while the cooldown was performed under an inert atmosphere (Argon).

5.2.2. Profile B

Profile B is a simplified version of Profile A and was applied to some samples containing chromium in order to prevent the suspected chromium loss. The reduction at 800 °C was included in the overall heating process, and the temperature of reaction was lowered to 1500 °C. The temperature was first increased at a rate of 5 °C/min until 600 °C, after which it was increased to 1500 °C at a rate of 10 °C/min, where it was kept constant for 4 hours. The cooling gas was changed from Ar to H_2/N_2 to study its effect on the synthesis of Cr-doped UN.

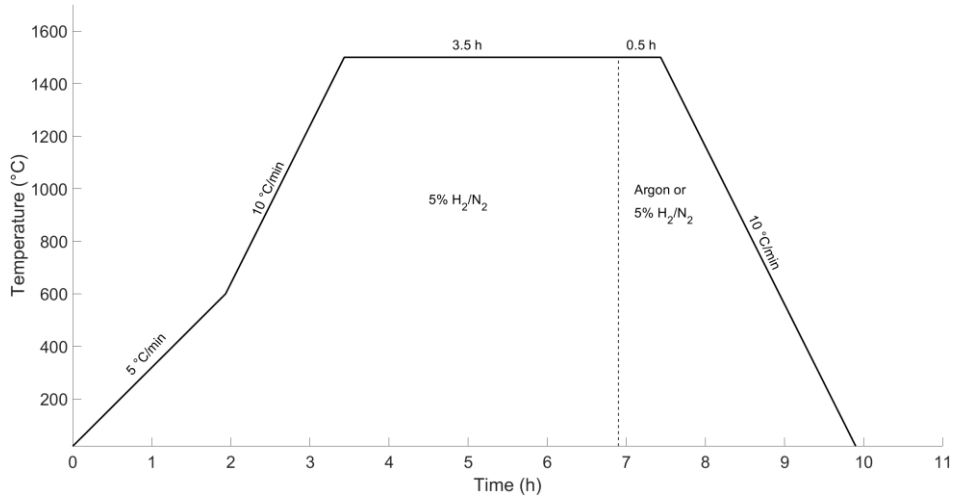

Figure 5.4. Temperature profile for the carbothermic reduction and nitridation process. Heating and dwelling at 1500 °C were performed under 5% H_2/N_2 while the cooldown gas was either Ar gas or the same reaction gas, 5% H_2/N_2.

If the cooling gas is H_2/N_2, a denitridation is necessary to convert the higher nitrides into the mononitride. This is achieved by heating the samples at 1200 °C for 2 hours in an inert atmosphere (Ar). Heating and cooling rate was set to 10 °C/min.

5.3. Chromium measurements

Chromium content was measured using two methods ICP-MS and XRF. For the ICP-MS, about 15mg of the material was dissolved in 20 mL aqua regia (1:3 HNO_3:HCl) for up to 24 hours. The solution was then filtered and diluted to be able to measure the Cr/U ratios.

For the XRF measurements, the samples were positioned in a sample holder with a Mylar® film and measured using two of the three beams available; 15KV and 40 KV where necessary to measure the Cr and U, respectively. The results were analyzed separately from the instrument by peak area integration.

5.4. Pelletization and sintering

The materials were pressed and sintered into the shape of a pellet by SPS. Approximately 2 grams of the microspheres were packed in the graphite die in a glove box with controlled atmosphere (PO_2 < 1ppm). The material was transported to the SPS facilities and placed into the SPS instrument. The temperature was raised at a rate of 100 °C/min until it reached the sintering temperature, where it was held for 5 or 10 min. Pressure was slowly increased after the temperature reached 400 °C. During cooling, once the temperature was below 400 °C, the SPS was opened, and the samples were retrieved.

Three different pellet batches were fabricated in this work: Th-doped UN, Cr-doped UN, and pellets containing the ternary phase U_2CrN_3. For all batches the same procedure was followed, except for the sintering conditions. For the Cr containing pellets the sintering was done at 1550 or 1650 °C, with 75 MPa pressure for 5 min. The sintering conditions for the pure UN and Th-doped UN pellets are listed in Table 5.1.

Table 5.1. Sintering parameters used during the pelletization of UN and Th-doped UN microspheres.

Sample name	Sintering temperature (°C)	Sintering pressure (MPa)	Sintering time (min)
UN-1	1450	75	10
UN-2	1550	75	10
UN-3	1650	50	10
UN-4	1650	75	5
UN-5	1650	75	10
UN-6	1650	100	10
UN-7	1750	75	10
(U95Th5)N	1650	75	10
(U90Th10)N-1	1650	75	10
(U90Th10)N-2	1750	100	10
(U80Th20)N-1	1650	40	10
(U80Th20)N-2	1650	75	10

5.5. Density measurements

The density of microspheres was estimated geometrically by measuring the average weight of the spheres and using an optical microscope to determine the diameter.

Density of pellets was measured with a gas pycnometer and corrected by deducting the open porosity measured using a BET instrument. The density will be given as a percentage of theoretical density (%TD) due to the density (ρ) difference between phases of pure UN and doped UN. This was calculated using the following equation:

$$\%TD = 100 \times \frac{\rho}{TD} \qquad (30)$$

The theoretical density (TD) was calculated using the density of the phases, the material composition, and the rule of mixtures [91].

5.6. Fuel-oxidant interaction

Microspheres and pellets were exposed to different atmospheres (air, steam, and water) to study their interaction with oxidizing environments.

5.6.1. Air interaction

The interaction of all materials with air was studied with TGA. Approximately 20 mg of samples were placed in the holder and introduced into the instrument. Temperature was raised at a rate of 5 °C/min up to 900 °C, where it was held for 5 min. The samples were then cooled at a rate of 20 °C/min. A mixture flow of 90 mL/min synthetic air and 10 mL/min pure N_2 was used during the process.

5.6.2. Steam interaction

Steam experiments were performed at Studsvik AB in the STA system. Approximately 50 mg of the pellets were placed in the holders and introduced into the STA, where the mass change during interaction with steam was measured. The materials were first heated to 200 °C under an inert atmosphere (Ar) with a flow rate of 100 mL/min, after which the steam was introduced at a flow rate of 160 mL/min (0.1 mL/min of water). Temperature was raised at a rate of 10 °C/min up until 1000 °C. Thereafter, the samples were cooled down in Ar at a rate of 10 °C/min. The final products were analyzed by XRD.

5.6.3. Water interaction

Pellet interaction with ultra-pure water was studied in the autoclave presented in Figure 4.1. Pellets were placed in a stainless steel basket designed to maximize the available area for interaction. A volume of 30 mL of MQ water was used to ensure that the pellets were submerged in the water during the entirety of the experiment, regardless of temperature and pressure. Oxygen in the chamber was purged with argon, which was adjusted to atmospheric pressure before heating. Temperature was increased at an average rate of 5 °C/min to 100, 200 or 300 °C where it was maintained for 2 hours. Afterwards, the heating was turned off, and the autoclave was left to cool overnight before opening. The samples were retrieved, and if pellet

disintegration occurred, samples were filtered and dried. The reaction products were analyzed with XRD and elemental analyzers.

6. Results and discussion

In the following sections the effect of dopant addition to the production and oxidation resistance of UN fuel will be presented. The results were divided depending on the dopants used.

6.1. Thorium doping

Results presented in this section are based on those published in Paper I and Paper II

Thorium was used as a dopant due to previous studies [65] [92], where thoria (ThO_2) showed higher stability and lower solubility in water than the urania (UO_2). All thorium materials were synthesized using heating profile A (Figure 5.3).

6.1.1. Microsphere production

The first step in the analysis was a visual analysis of the materials fabricated. The products of the synthesis were microspheres with diameters between 700 and 1000 μm. The sol-gel process was optimized for pure UN spheres, therefore, by adding thorium, the HMTA/metal molar ratios had to be increased for the gelation to happen. This as thorium in aqueous solutions is found in a +4 oxidation state, while the uranyl is +2, and therefore, more HMTA is needed to react with the higher amount of H^+ produced. Figure 6.1 shows the shape of UN microspheres with different levels of thorium content. It was evident that more cracking occurred in spheres with higher thorium content. This was attributed to the increase of unreacted chemicals, which decompose into gases, increasing the pressure inside the microsphere.

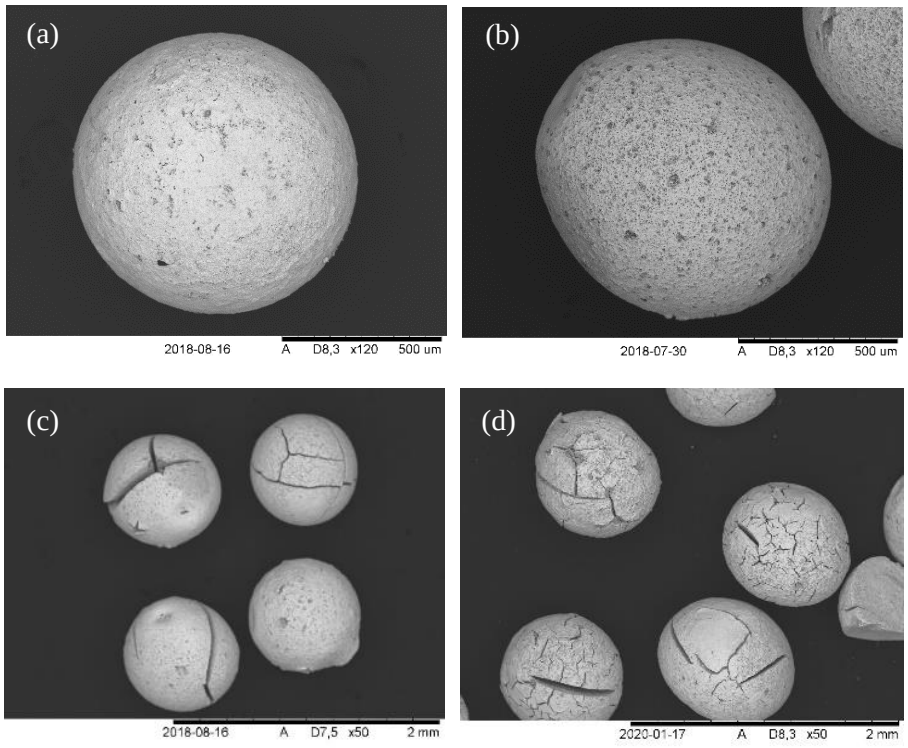

Figure 6.1. Scanning electron microscopy of uranium nitride and thorium-doped uranium nitride microspheres synthesized using the internal gelation process followed by carbothermic reduction. In order: a) UN, b) (U95Th5)N, c) (U90Th10)N, d) (U80Th20)N.

The elemental distribution analyzed by EDX (Figure 6.2) showed a complete homogeneity between U and Th in the nitride microsphere. Elemental composition by EDX was not completely reliable because the signals for these two elements are very close and the instrument is not able to properly differentiate between the elements. Carbon, nitrogen, and oxygen have the same issues with each other and therefore, the elemental composition had to be analyzed using other methods.

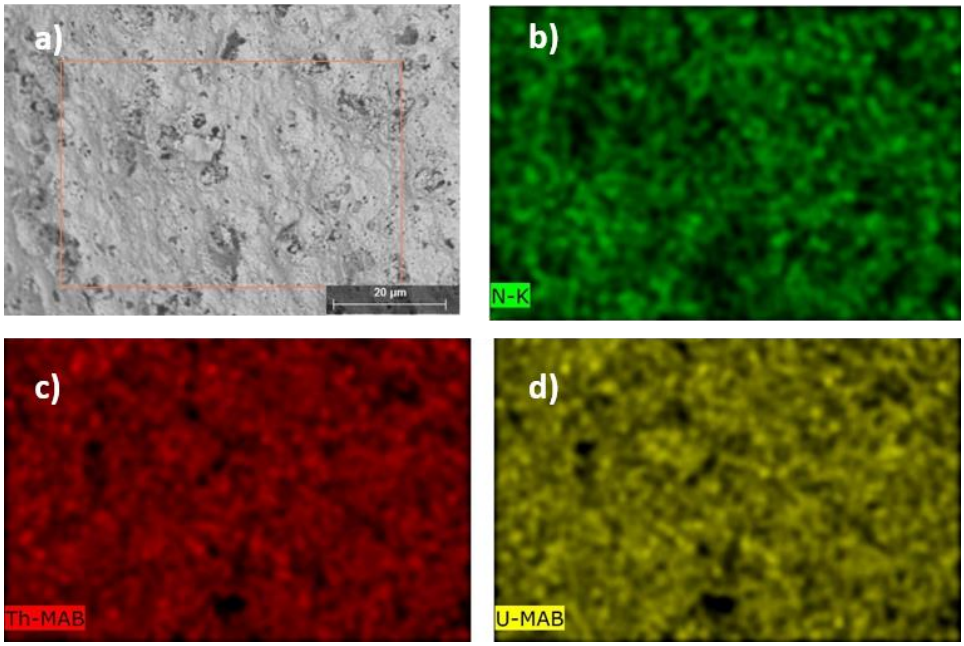

Figure 6.2. Elemental distribution on the microsphere surface for a (U90Th10)N sample synthesized by carbothermic reduction. In order: a) surface SEM (gray), b) nitrogen (green), c) thorium (red), d) uranium (yellow). Black zones are caused by imperfections on the surface, such as pores.

For the quantification of thorium, the spheres were dissolved before and after nitridation. The resulting solutions were analyzed in the ICP-MS to measure the the U and Th content. Table 6.1 shows the results after nitridation, where the Th content was similar to the amount added during production. This also shows a similarity in the solubility of both UN and ThN and their solid solution. Carbon, nitrogen, and oxygen were measured using their respective analyzer. The theoretical nitrogen content for a pure UN sample is around 5.56 wt-%, however, nitrogen content in the samples varied between 3.5 and 5.6 wt-%. Carbon and oxygen contamination varied significantly between all batches, although the same synthesis method was used. Samples UN-4, UN-6, and (U80Th20)N-2 could have had a variation in the amount of graphite and gelation chemicals, which could lead to a higher carbon content. Due to the elemental analysis of these samples, it is possible to conclude that the carbon residue is most likely found as the carbonitride (UC_xN_{1-x}) that did not complete the synthesis. Moreover, higher levels of carbon were balanced by (generally) lower oxygen residues, meaning that the nitridation completion was highly dependent on the amount of carbon accessible for reaction. The oxygen could have also been reintroduced to the samples during transport to the glove box.

*Table 6.1. Elemental composition of thorium-doped uranium nitride microspheres produced through carbothermic reduction. The lattice parameter was estimated using the XRD spectra measured. The n.d. indicates the value was not determined. The confidence level for the uncertainties is 2σ. *Th in samples with 20% was not measured. n.d. stands for not determined.*

Sample name	Thorium molar metal fraction (%)	Nitrogen content (wt.-%)	Carbon content (wt.-%)	Oxygen content (wt.-%)	Lattice parameters (Å)
UN-1	0	5.2 ± 0.1	0.27 ± 0.01	0.574 ± 0.002	4.896 ± 0.004
UN-2	0	5.0 ± 0.1	0.6 ± 0.1	0.23 ± 0.02	4.896 ± 0.002
UN-3	0	5.4 ± 0.3	0.011 ± 0.004	0.3 ± 0.2	4.891 ± 0.002
UN-4	0	n.d.	2.0 ± 0.1	n.d.	n.d.
UN-5	0	5.3 ± 0.2	0.2 ± 0.1	0.08 ± 0.02	4.894 ± 0.002
UN-6	0	4.02 ± 0.04	2.3 ± 0.4	0.24 ± 0.06	4.92 ± 0.02
UN-7	0	5.3 ± 0.2	0.01 ± 0.03	0.09 ± 0.02	4.892 ± 0.002
(U95Th5)N	5.2 ± 0.1	5.6 ± 0.4	0.010 ± 0.002	0.26 ± 0.02	4.913 ± 0.006
(U90Th10)N-1	10.2 ± 0.1	4.7 ± 0.8	1.1 ± 0.2	0.3 ± 0.1	4.931 ± 0.004
(U90Th10)N-2	10.40 ± 0.04	5.3 ± 0.4	0.3 ± 0.1	0.4 ± 0.1	4.924 ± 0.002
(U80Th20)N-1	20*	5.1 ± 0.1	0.5 ± 0.1	0.6 ± 0.1	n.d.
(U80Th20)N-2	20*	3.5 ± 0.2	2.4 ± 0.1	0.37 ± 0.02	4.99 ± 0.01

The phase composition was investigated with XRD, and the main results are presented in Figure 6.3. The calculated lattice parameters are listed in Table 6.1. The displacement of the UN peaks towards lower angles indicates an increase in the lattice parameter of the UN according to Vergard's law [93]. This effect can be explained by the presence of the carbonitride phase suggested by the elemental composition. The substitution of nitrogen atoms by carbon atoms in the crystal structure will cause an increase in the crystal lattice, as carbon is bigger than nitrogen. Small peaks corresponding to UO_2 can sometimes be seen in the XRDs, which is expected from the elemental composition. As no other reflection peaks can be observed in the diffractograms of Th-doped UN, it is possible to assume a complete solid solution of these phases. Theoretically, the replacement of U atoms by Th in the UN system will cause an expansion of the crystal lattice, displacing the reflection peaks towards lower angles. As both carbon and thorium are present in the samples, the effect on the peak shifting will be combined. Moreover, determination of composition by measuring the lattice parameters as previously done by Hedberg et al., [94] will become rather difficult.

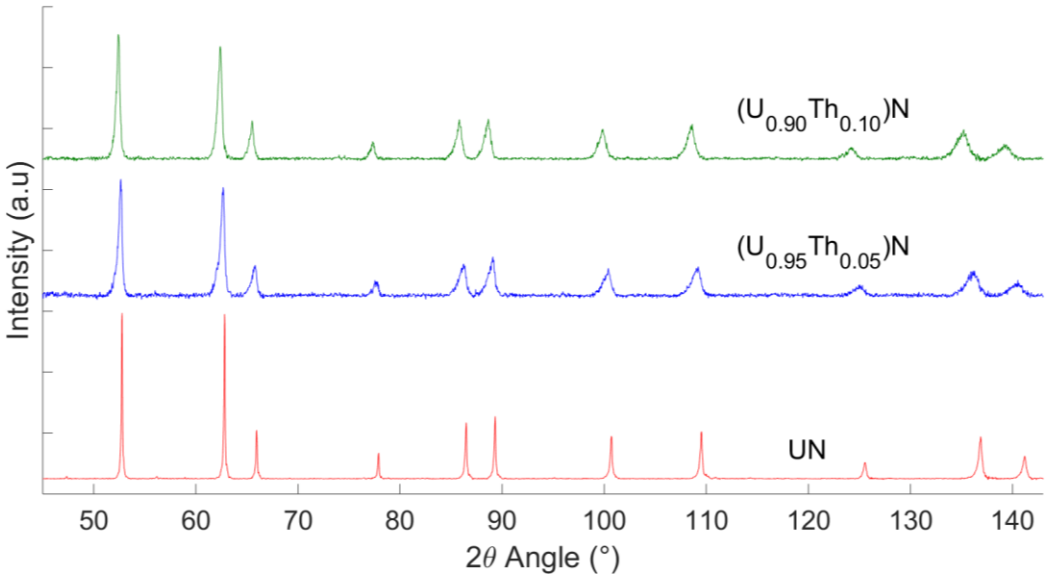

Figure 6.3. Effect of thorium composition on the XRD pattern for crushed microspheres. From top to bottom: (U90Th10)N with an estimated lattice parameter of 4.924Å, (U95Th5)N with a lattice parameter of 4.913Å and UN with a lattice parameter of 4.894Å.

6.1.2. Pelletization

Current UO_2 pellets are sintered to approx. 95% of their theoretical density to accommodate fission gas products, and therefore is an acceptable density target. UN pellets made from powders and SPS were reported in literature [56,57] with densities between 90 and 100%. Conventional sintering of UN microspheres done by Herman et al., [29] proved inefficient, reaching densities below 80%. In this work, SPS was used to press and sinter UN and Th-doped UN microspheres in order to achieve higher densities than conventional sintering.

During sintering a behavior was observed where the sintering onset temperature increased with increased dopant level. The behavior can be more clearly seen in Figure 6.4. It is common for materials with higher melting temperatures to sinter at higher temperatures. Therefore, it can be possible that the melting point of the solid solution is higher than the pure UN phase. On the other hand, the sintering can be explained by the rearrangement of atoms and defects in the crystal structure. If thorium is introduced as a substitutional atom, the expansion of the crystal lattice will increase the energy necessary for defect migration. Theoretical modelling describing this theory is explained in Paper 1.

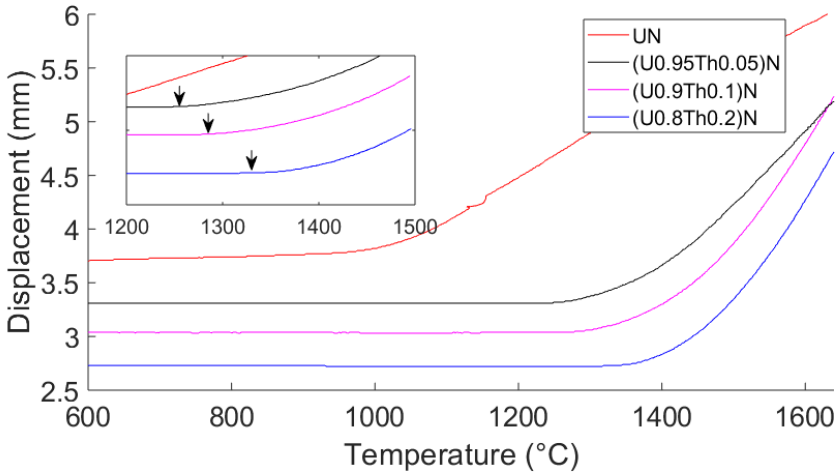

Figure 6.4. Sintering profile for different materials when temperature is increased. From top to bottom: UN, (U95Th5)N, (U90Th10)N and (U80Th20)N. Arrows indicate the onset temperature identified graphically, showing the temperature range where the pellet starts to shrink.

After first polishing of the pellets, the surface showed a blackberry-like structure, which was lacking in the bulk. Looking at its SEM (Figure 6.5) it was possible to determine that graphite paper was trapped in between the spheres during sintering. This causes the observed structure. In addition, it is possible to observe the fusing of spheres in the absence of graphite paper. The bulk of the material did not have the same macrostructure. The cross section showed that the carbon penetration depth reached up to 0.3 mm into the bulk. Deeper polishing must be done to completely remove the carbon, which will increase the amount of fuel lost during manufacturing. Otherwise, the selection of a more appropriate material can be done during the scaling up of the process.

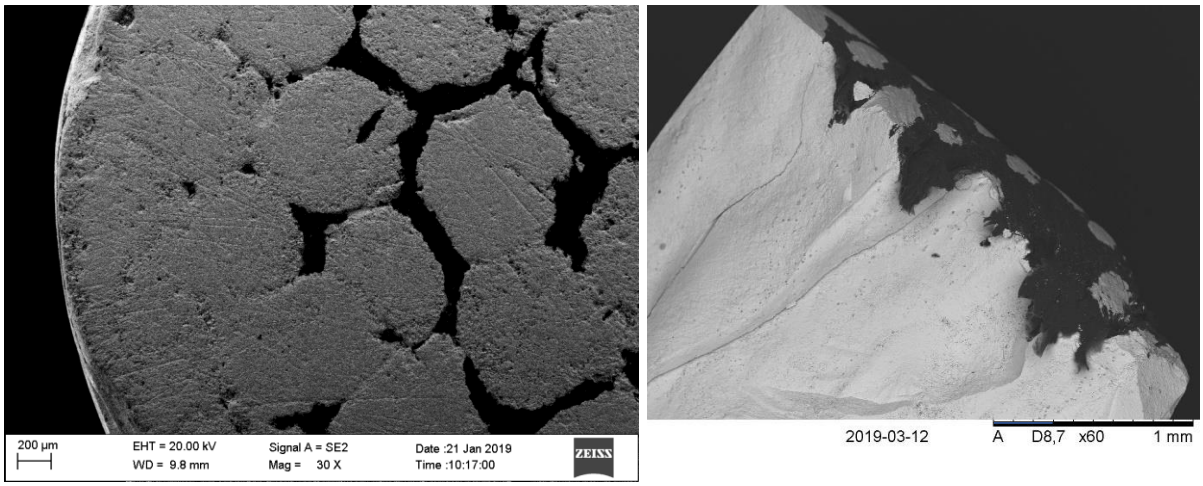

Figure 6.5. SEM of a Th-doped pellet surface showing the presence of carbon after polishing that marks the shape of the microspheres that could not fuse due to the insertion of graphite paper.

The aforementioned blackberry structure was lost on the surface after deeper polishing. Closer examination of the pellets surface showed a single phase present. This further confirms the ability of Th to form a solid solution in the UN. Different degrees of porosity were observed in the pellets, which generally decreased with higher sintering temperature, pressure, and time. In Figure 6.6, the porosity can be explained by the low pressure used in the manufacturing of this pellet (40 MPa).

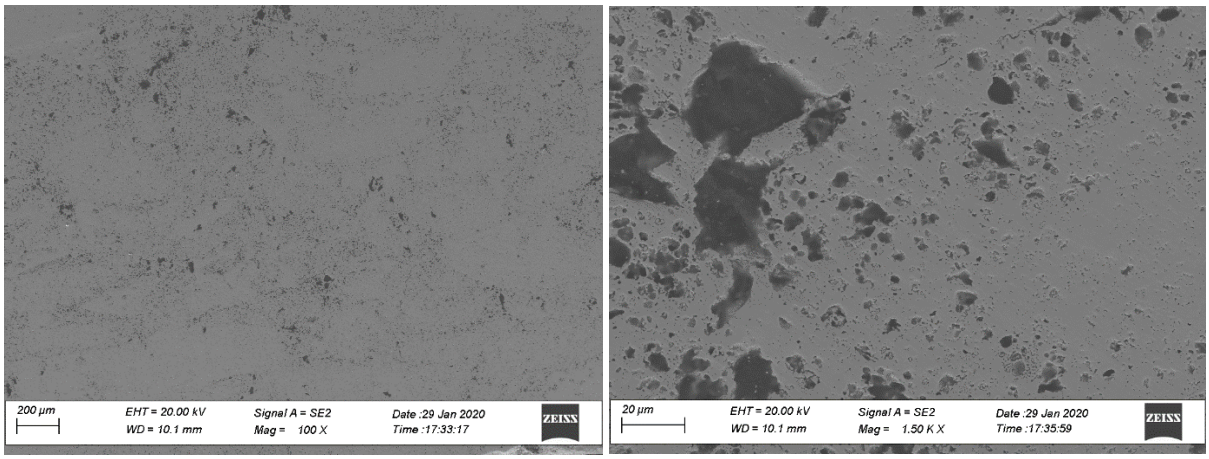

Figure 6.6. Higher magnification of the SEM of Th-doped UN pellet, showing the porosity present on the surface, and the existence of a single phase system.

The density of UN and Th-doped UN pellets made directly from microspheres is listed in Table 6.2. As can be seen, the method used in these experiments was capable of manufacturing pellets with comparable density (90-100 %TD) to pellets made from UN powders [56,57]. The density is related to the porosity, and therefore, the sintering parameters can be tailored to achieve the desired density. Further investigation on the effect of the sintering parameters on the pellet density can be found in Paper 1.

Table 6.2. Density of UN and Th-doped UN pellets compared to their theoretical density. Theoretical densities were calculated using the lattice parameters determined experimentally with the XRD pattern.

Pellet name	Theoretical density (g/cm^3)	Measured density (g/cm^3)	%TD
UN-1	14.26 ± 0.04	12.91 ± 0.06	90.5 ± 0.5
UN-2	14.26 ± 0.02	13.45 ± 0.06	94.3 ± 0.4
UN-3	14.31 ± 0.02	12.72 ± 0.02	88.9 ± 0.2
UN-4	14.32*	13.3 ± 0.1	92.5 ± 0.8
UN-5	14.28 ± 0.02	13.30 ± 0.05	93.1 ± 0.4
UN-6	14.0 ± 0.2	12.67 ± 0.05	90 ± 1
UN-7	14.30 ± 0.02	14.05 ± 0.06	98.2 ± 0.4
(U95Th5)N	14.10 ± 0.06	13.42 ± 0.06	95.2 ± 0.6
(U90Th10)N-1	13.93 ± 0.04	13.10 ± 0.06	94.1 ± 0.5
(U90Th10)N-2	13.99 ± 0.02	13.66 ± 0.08	97.7 ± 0.6
(U80Th20)N-1	13.79*	12.46 ± 0.04	90.4 ± 0.3
(U80Th20)N-2	13.4 ± 0.1	12.75 ± 0.04	95.0 ± 0.9

6.1.3. Interaction tests

The materials produced were tested in different oxidizing environments to investigate if Th-doping has any effect on the corrosion and oxidation resistance of UN.

6.1.3.1. Air

Materials in the shape of spheres and pellets were exposed to synthetic air (21% oxygen mixed with nitrogen) and heated to 900 °C in a TGA. The mass change was recorded, and typical TGA curves can be seen in Figure 6.7. Multiple measurements were made for each sample, however, only one is shown for simplicity as the results were very similar. The curves can be divided in three zones. The first is a very slow mass gain, the second is a fast increase in mass gain, and the last is a plateau at high temperatures once the material oxidation has finished. For some materials, between 300 and 500 °C, higher than the expected 11.4% mass gain is seen. This increase was explained by the entrapment of gases, mostly N_2, produced during the oxidation reaction (Eq. 13-14). The mass increase in samples (U90Th10)N-2 and UN-1 was even higher than for the other samples, and this could be attributed to the formation of UO_3 according to the expected weight change, 13.5% for pure UN and 12.9% for (U90Th10)N.

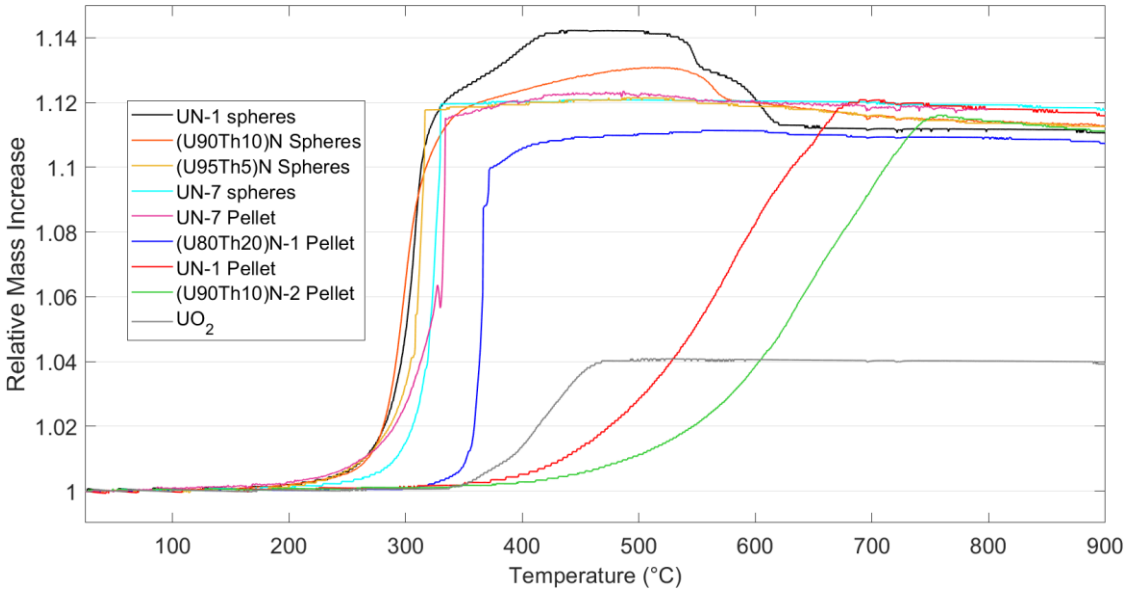

Figure 6.7. Average TGA curves for oxidation in synthetic air of uranium nitride and thorium-doped uranium nitride microspheres and pellets compared to a UO_2 pellet.

For the TGA curves, the onset reaction temperature was defined as the temperature where the material had increased to 5% of its maximal mass gain. The maximal reaction rate temperature is obtained from the maximal point in the derivative of the TGA curve. The results for the doped and undoped UN spheres and pellets are compared in Table 6.3. From the data collected it was clearly seen that pellets had a tendency to oxidize at higher temperatures than the microspheres. The onset temperature for microspheres varied between 125 and 250 °C, while for pellets it was always above 300 °C.

Table 6.3. Porosity and reaction temperatures of UN and Th-doped UN spheres and pellets exposed to air in the TGA.

Sample	Total Porosity (% volume)	Onset temperature (°C)	Maximal reaction rate temperature (°C)
UN-1 Spheres	71	216	305
(U90Th10)N-2 Spheres	n.d.	125	300
(U95Th5)N Spheres	66	217	310
UN-7 Spheres	58	244	325
UN-1 Pellet	9.5	122	330
UN-7 Pellet	1.8	315	580-600
(U80Th20)N-1 Pellet	9.6	326	360
(U90Th10)N-2 Pellet	2.3	416	630-650
UO_2	7.6	305	365

Two set of pellets were selected for the analysis; either they had higher or lower than 5% porosity. For each set, one pellet was doped with thorium. Results showed that pellets with lower porosity had higher onset temperature than their lower porosity counterparts. Additionally, the derivative of the TGA curves for low porosity pellets did not show a sharp peak, but a broad signal, indicating that the oxidation kinetics were slowed down significantly. Moreover, materials with similar density but with thorium doping showed an increase in their reaction temperatures suggesting a favorable effect of thorium on the oxidation resistance of UN in air. For comparison, one UO_2 pellet was used as a benchmark for the new UN pellets. Similar onset temperature was observed for a Th-doped UN pellet with similar density, while low density UN pellet showed more than 100 °C increase in onset temperature.

According to the literature, the final products of the oxidation of UN and ThN in a pure oxygen atmosphere should be U_3O_8 [42] and ThO_2 [95], respectively. Therefore, a theoretical mass increase of 11.4% and 7.3% is expected for pure samples. As the thorium content in some of the samples was 10% or 20 mol-%, the final mass increase was expected to be 11.0% and 10.6%, respectively. The final mass gain of all UN samples was measured to be 11.9%, which is higher than the expected value. Th-doped materials also showed slightly higher maximal mass increase. This behavior is most likely caused by the development and entrapment of nitrogen gas during the reaction of UN with O_2 [42,96,97]. Nonetheless, this weight shift should not affect the trends observed for the reaction onset temperatures and maximal reaction rates temperatures.

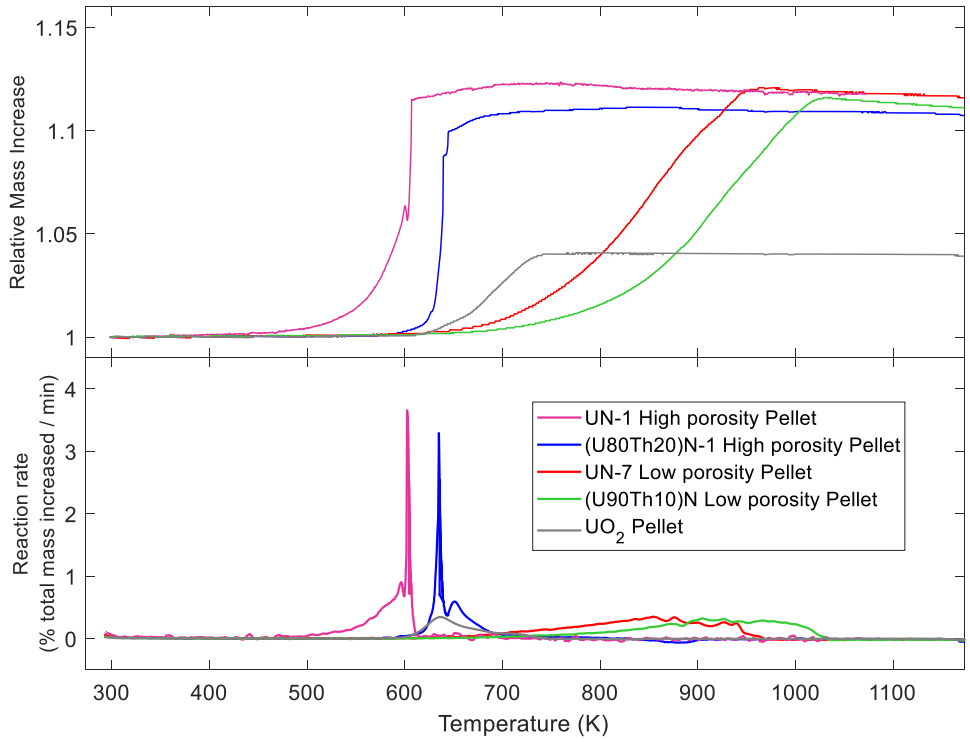

Figure 6.8. Upper panel: TGAs for oxidation of UN and (U,Th)N pellets with high and low porosity compared to the standard UO_2. Lower panel: Derivative of the TGAs showing the reaction rate as mass increase per unit of time

6.1.3.2. Water

The water exposure experiments were designed to test the sintered and doped pellets in conditions resembling the operation parameters in a BWR. Preliminary results by Herman et al., [29] showed that Cr-doped pellets made with cold pressing could survive boiling water for a few hours, while undoped pellets survived for up to 2 hours. Hence, this was an acceptable starting point. Additionally, the autoclave is able to withstand up to 325 °C, therefore, 300 °C was the highest temperature used in the experiments. Pressure was dependent on the temperature because the vessel was sealed during experiments. Specific conditions and main results can be found in Table 6.4.

Table 6.4. Summary of the results obtained after the water exposure experiments of UN and Th-doped UN pellets at different temperatures. Nitrogen and oxygen were measured only in the powder collected after reaction. n.m. indicates not measured.

Pellet Name	Dwelling Temp. (°C)	Pressure (bar)	Pellet disintegration	U conc. (mM)	Th conc. (mM)	N content (wt-%)	O content (wt-%)
UN-5	100 (air)	1	No	n.m.	-	-	-
UN-2	100	2	No	n.m.	-	-	-
UN-6	200	15	Yes	8.0	-	0.71 ± 0.04	12.9 ± 0.2
UN-4	300	85	Yes	16.8	-	0.04 ± 0.01	11.59 ± 0.04
(U80Th20)N-2	200	15	Yes	27.7	3.9	0.29 ± 0.01	14.87 ± 0.05

Pellets of pure UN were able to survive the exposure for several hours at 100 °C, both in the autoclave and in open air. These pellets have a lower porosity, which allowed them to survive for longer periods than previously reported in Herman's work [29]. Mass change was not evident after exposure, suggesting absence of corrosion. SEM/EDX of the pellet cross-section (Figure 6.9) showed that the distribution of nitrogen and oxygen was still homogeneous after exposure. These observations could change if the surface is looked at with a greater magnification, however, this was not possible with the equipment available.

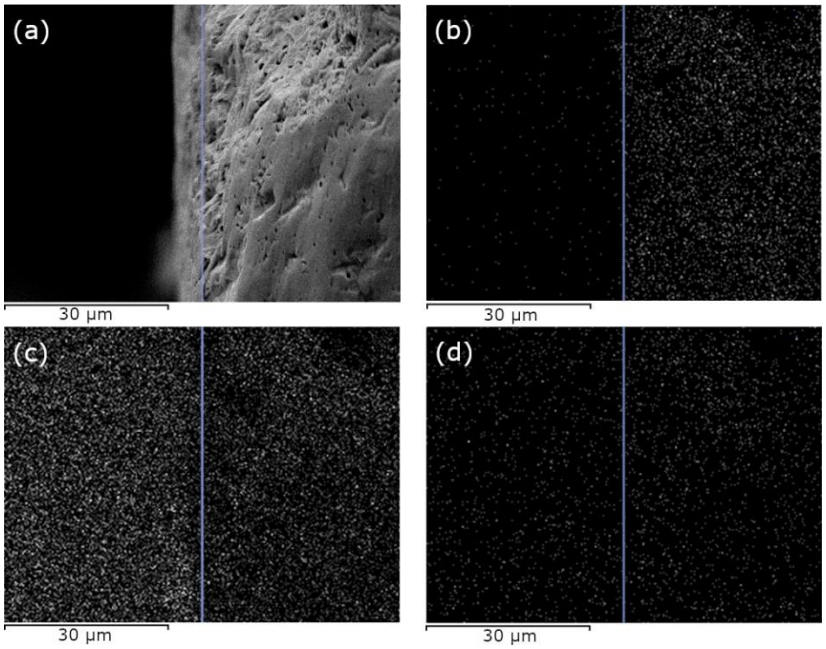

Figure 6.9. SEM image of the UN-2 pellet (a) after interaction with water at 100 °C for six hours showing the nitrogen (b), carbon (c) and oxygen (d) distribution on the edge of the pellet. The blue line indicates the edge of the pellet as seen by the EDX.

Pellets exposed to water at higher temperatures lost their physically cohesive structure also known as loss of integrity, regardless of density or composition. The resulting liquid was filtered and the solid collected for further analysis. A small amount of both uranium and thorium was measured in the filtered liquid, although the solubility on UO_2 and ThO_2 in water has been reported to be negligible [92]. This could also suggest that small particles were not filtered and therefore measured in the ICP-MS. Figure 6.10 shows the degradation of pellet UN-6 after water exposure at 200 C. Table 6.4 shows that some of the nitrogen remained in the sample after experiments at 200 °C, while at 300 °C all nitrogen had disappeared.

Figure 6.10. Picture of pellet UN-6 before and after water interaction. The powder was filtered from the remaining liquid and left to dry in a glovebox with <1 ppm O_2.

As expected from the elemental analysis, some of the UN phase should still be present in the collected powder after interaction at 200 °C. XRD patterns in Figure 6.11 showed a mixture of UN and UO_2, while a pure UO_2 phase was observed after exposure at 300 °C. The higher than expected oxygen content in all of the residual powders was attributed to the presence of water, which was later corroborated using TGA measurement in an inert atmosphere. The presence of a U_2N_3 phase has been reported in literature [44] to be present during hydrolysis of UN with steam. However, this phase was not observed in this work. This is attributed to the higher pressure used in the experiments presented here.

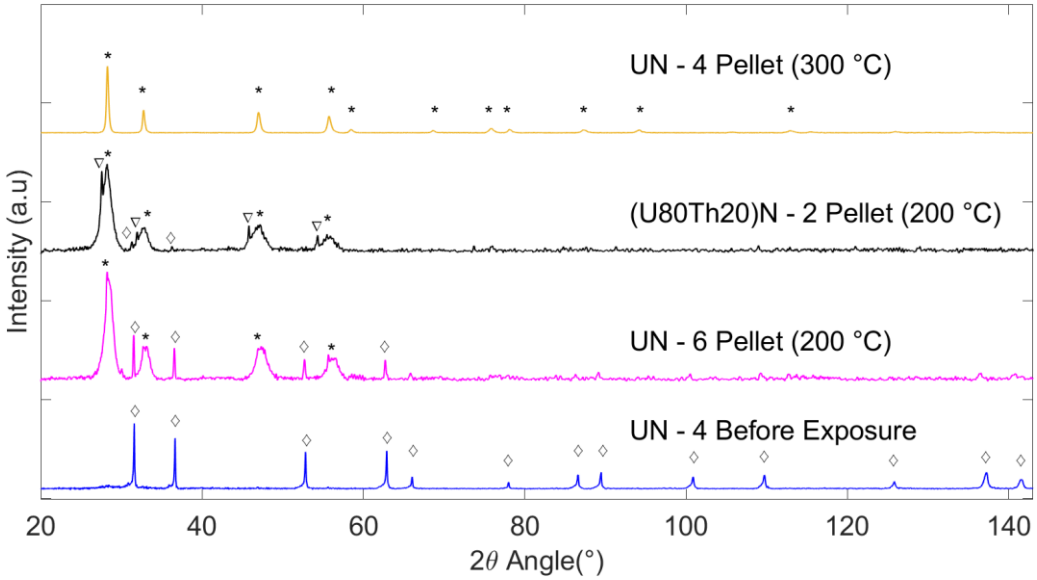

Figure 6.11. X-Ray diffractograms for powders collected after pellet disintegration in the corrosion testing compared to the UN pellet before interaction, where UN(◊), UO_2 (*), or ThO_2 (▽) peaks were identified.

The thorium doped pellet subjected to the interaction experiment showed similar behavior to the undoped UN. However, ThO_2 signals were observed in the XRD patterns. This suggests that the solid solution was unstable during the hydrolysis, probably due to the higher reactivity of the ThN than the UN. The mechanism leading to the phase separation is yet unclear and further investigation is required. However, it is possible to conclude that the thoria layer was either not formed or was not protective at the conditions of the experiments.

6.2. Chromium doping

Results presented here are based on those published in Paper III and Paper IV

Cr was chosen as it has been vastly used in other industries to aid in the corrosion protection, mostly in the steel industry, and due to previous preliminary studies in our group regarding Cr-doped UN. In the same manner as for thorium, the chromium content was varied between 5 and 20 mol-%. The Cr-doping experiments were divided into two parts, with the designations Batch A and Batch B, where the name is related to the heating profile used (see Figures 5.3 and 5.4).

6.2.1. Microsphere production using heating profile A

The first experiments followed the same synthesis path as for Th-doped UN microspheres. The synthesis was performed at a maximum temperature of 1650 °C, according to Figure 5.3, and the results presented in this subsection are referred to as Batch A. The effect of Cr-doping in the shape and surface of the microspheres can be seen in the micrographs in Figure 6.12. Severe cracking of the spheres was observed when chromium was added as a doping element. When the doping level was increased above 10 mol-%, the molar ratio of HMTA/metal had to be increased to 1.9 to be able to form the spheres during the gelation. Although the shape was stabilized, the cracking severely increased with chromium content. This behavior was very similar to the one observed for the thorium doping and can be explained by the same reasons mentioned before, i.e., higher amount of gases increasing the inner pressure.

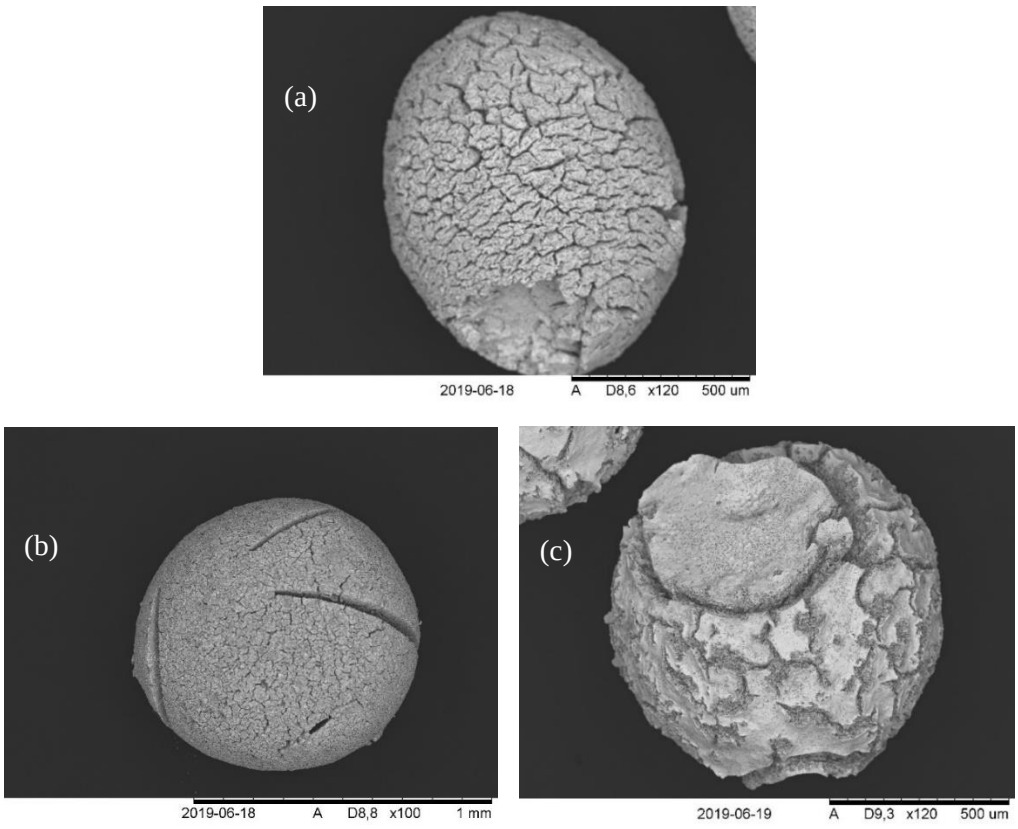

Figure 6.12. Scanning electron microscopy of chromium-doped uranium nitride microspheres synthesized using the internal gelation process followed by carbothermic reduction. In order: a) (U95Cr5)N, b) (U90Cr10)N, c) (U80Cr20)N.

The elemental analysis of the Batch A Cr-doped UN microspheres is listed in Table 6.5. Oxygen content was measured below 0.3 wt-%, and was similar between samples, which indicates an almost complete reduction of the materials. This oxygen is most likely reintroduced during transport. On the other hand, carbon content varied between 0.01 and 1.7 wt.-%. However, higher average carbon contents were measured for these materials than for the Th doped UN. This was due to the lower C/Metal molar ratio (Eq. 31) [98] required in the carbothermic reduction of chromium compared to thorium or uranium (Eq. 23). Samples with the lowest C content were usually synthesized in smaller volumes, and it is possible that the nitridation of larger volumes required a larger sample holder or longer nitridation times. The microsphere density was also dependent on the Cr content, where higher Cr ratios led to higher densities. This can occur if the Cr is decreasing the lattice parameter of the UN, increasing the theoretical density. It was also seen in Figure 6.12 that the sphere surface seems to have a higher amount of microfractures at low Cr content.

$$Cr_2O_3(s) + 3C(s) + N_2(g) \leftrightarrow 2CrN(s) + 3CO(g) \quad (31)$$

Table 6.5. Elemental analysis and density of synthesized Cr-doped UN microspheres (Batch A) using heating profile A. Uncertainties calculated by measuring in triplicates.

Sample name	Carbon content (wt-%)	Nitrogen content (wt-%)	Oxygen content (wt-%)	Microsphere density (g/cm^3)
UN-1	0.011 ± 0.004	5.4 ± 0.3	0.3 ± 0.2	4.16 ± 0.06
U95Cr5N-1	1.1 ± 0.1	4.4 ± 0.1	0.16 ± 0.02	3.26 ± 0.09
U95Cr5N-2	1.2 ± 0.4	3.92 ± 0.02	0.15 ± 0.01	3.6 ± 0.1
U95Cr5N-3	0.01 ± 0.01	5.55 ± 0.04	0.54 ± 0.03	3.4 ± 0.1
U90Cr10N-1	1.0 ± 0.4	4.31 ± 0.01	0.13 ± 0.01	3.7 ± 0.2
U90Cr10N-2	1.7 ± 0.2	4.5 ± 0.2	0.21 ± 0.02	3.83 ± 0.07
U80Cr20N-1	0.66 ± 0.04	4.77 ± 0.07	0.17 ± 0.02	4.55 ± 0.05
U80Cr20N-2	1.11 ± 0.03	4.65	0.14	5.00 ± 0.06
U80Cr20N-3	0.79 ± 0.04	4.65 ± 0.02	0.23 ± 0.01	3.96 ± 0.04

The effect of the carbon residues can be clearly seen in the XRD patterns (Figure 6.13). As with thorium, the reflection signals are shifted towards lower angles due to the bigger atomic size of carbon compared to nitrogen. Unlike thorium, if chromium was in solid solution with the UN lattice, the lattice should theoretically decrease, and increase the angles of reflection. The combined effect of both elements is observed in the refined lattice parameters. Regardless of Cr content, all lattice parameters were higher than the pure UN, however, their values decreased with higher Cr doping. Moreover, the presence of other phases besides UN and UO_2 were not observed in the XRD. This could mean the existence of a solid solution; however, the expected ternary phase (U_2CrN_3) was not identified in the patterns. These results are comparable to those previously seen from preliminary results by Herman [29]. In their work, they reported the presence of several phases, however, not enough data was provided to support their findings.

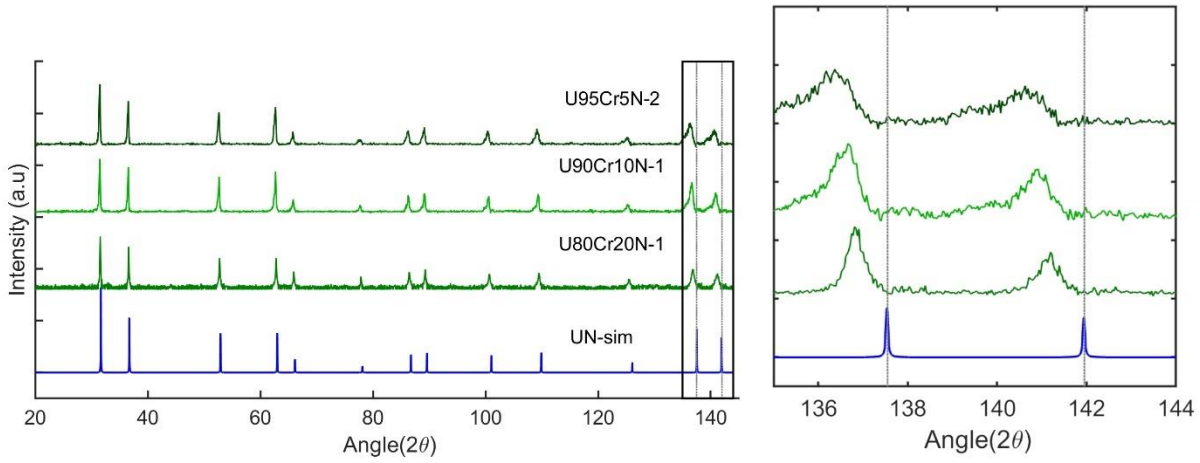

Figure 6.13. Effect of chromium composition on the XRD pattern for crushed microspheres (Batch A) compared to a simulated XRD pattern for UN with a lattice parameter of 4.889 Å. The lattice parameter for the 5%, 10% and 20% Cr mol-% were measured to be 4.916 Å, 4.909 Å, and 4.901 Å, respectively. The lattice parameter used for the simulated UN was 4.890nm.

Doping with chromium below 10 mol-% showed a homogenous distribution of the chromium and the uranium after nitridation. However, closer inspection of the microsphere's surface with 20 mol-% Cr-doping showed the presence of a Cr-rich phase precipitation. EDX analysis was not able to identify the phase. Absence of uranium in the spots in addition to the low nitrogen and oxygen content in Table 6.5 suggest that the phase could be either a chromium carbide or metallic chromium. Neither phase was seen in the XRD. This can happen if the unidentified Cr phase content is below 5 wt-%.

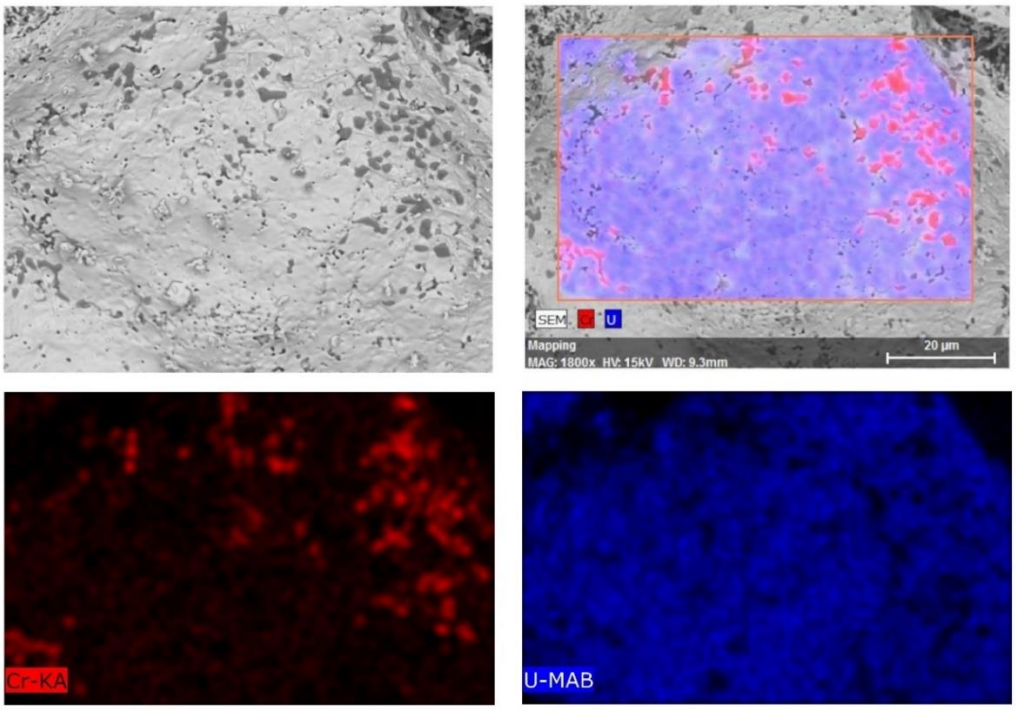

Figure 6.14. SEM image of the surface of a U80Cr20N-1 microsphere after synthesis using profile A. The Cr (red) and U (blue) mapping is presented to show the precipitation of a chromium-rich phase.

Additionally, chromium reaction with the crucible was noted in the form of a pink coloration on the alumina boats after reaction, see Figure 6.15. The color is attributed to the formation of a chromium-aluminum-oxide phase ($AlCrO_3$) due to partial vaporization of Cr. It has been reported in the literature [62,99] that chromium evaporation can occur between 500 and 800 °C in the form of the volatile compound chromium oxy-hydroxide [CrO(OH)]. The formation of a Pure CrN is unstable at temperatures above 1400 °C, where it decomposes into Cr_2N and metallic chromium [100,101]. Chromium low vapor pressure [102] allows for the volatilization and subsequent interaction with the alumina crucible.

Figure 6.15. Alumina crucibles used as sample holders after carbothermic reduction and nitridation of the Cr-doped microspheres. Pink coloration was observed on the edge, suggesting a possible reaction with Cr.

To determine how much chromium was being lost during synthesis, the samples were dissolved in aqua regia in the same way as the thorium doped UN materials. The ratio of Cr/metal was measured by ICP-MS, and results at three stages during the synthesis are listed in Table 6.6. As can be seen, the Cr content decreased to levels below 5 mol-% after nitridation at 1650 °C. Partial reduction of Cr was observed occasionally after reduction at 800 °C. It was concluded that the synthesis at high temperatures needed to form and purify the UN cannot be reached if Cr is added as a dopant.

Table 6.6. Chromium molar metal ratio measured in the as-produced Cr-doped UN microspheres, after reduction at 800 °C, and after nitridation at 1650 °C. The n.d. indicates the value was not determined.

Sample name	Expected Cr content (mol-%)	Cr content as-produced (mol-%)	Cr content after reduction (mol-%)	Cr content after nitridation (mol-%)
U95Cr5N-1	5	5.8 ± 0.6	7.8 ± 0.7	1.0 ± 0.4
U95Cr5N-2	5	5.5 ± 0.5	5.5 ± 0.7	1.0 ± 0.4
U95Cr5N-3	5	n.d.	6.1 ± 0.9	2.5 ± 0.3
U90Cr10N-1	10	11.2 ± 0.9	7.0 ± 0.7	4.1 ± 0.4
U90Cr10N-2	10	15 ± 1	9.6 ± 0.6	2.5 ±0.4
U80Cr20N-1	20	22 ± 1	20 ± 1	4.9 ± 0.7
U80Cr20N-2	20	26 ± 1	19 ± 1	n.d.
U80Cr20N-3	20	18.4 ± 0.8	12 ± 1	± 0.6

6.2.2. Studies on Cr losses and formation of ternary phase

In an attempt to understand the chromium loss mechanism, the as-produced spheres with 20 mol-% Cr doping were heated to a different temperature using heating profile B (Figure 5.4) and the cooling was done in the same gas atmosphere to simplify the synthesis. The products after reaction were analyzed to follow the reaction progress. Elemental analysis is presented in Table 6.7, where it can be seen that uranium nitridation was first observed after reaction at 1200 °C. At 1400 °C, the signals for uranium oxide disappear and the nitrides reflection peaks in the XRD pattern are shifted towards lower angles, which indicates a higher UN_2/U_2N_3 ratio or carbon impurities in the crystal structure. The nitridation was not completed until the dwelling temperature was raised to 1500 °C, as both the carbon and oxygen levels were reduced to 0.04 and 0.25 wt-%, respectively. The C and O impurities measured in these samples were lower than those measured for Batch A. This was attributed to the smaller volume that was synthesized, as the aim was to investigate the products of reaction and not the pelletization of this material.

The nitrogen content was expected to be higher than 5.6%, as superstoichiometric compounds, namely U_2N_3 and UN_2, would form under the synthesis conditions. The XRD patterns in Figure 6.16 showed that these phases were found after synthesis. It can be seen that after reaction at 1500 °C, the phases present are the ternary phase (U_2CrN_3), and a solid solution of U_2N_3 and UN_2. The measured nitrogen content after reaction at 1500 °C was about 8.3 wt-%, which can be calculated if all Cr is found in the ternary phase and the uranium nitride phase is a U_2N_3/UN_2 solid solution with a 50-50 wt-% composition. This was confirmed after refinement of the diffractogram, where the lattice parameter was calculated to be 10.64 Å, which according to the literature corresponds to a N/U ratio of 1.75 [38].

Table 6.7. Elemental analysis and density of synthesized Cr-doped UN microspheres using heating profile B at different dwelling temperatures. The Cr content was measured using ICP-MS and the lattice parameter was determined from the Rietveld refinements. Uncertainties in parenthesis were calculated by measuring in triplicates.

Dwelling Temp. (°C)	Carbon content (wt-%)	Nitrogen content (wt-%)	Oxygen content (wt-%)	Cr content after reaction (mol-%)	Microsphere density (g/cm^3)	Lattice parameter of $UN_{1.5+x}$ (nm)
As-produced	14.1(5)	n.d.	n.d.	20(2)	1.78(6)	-
400	11.4(1)	0.89(2)	10.7(3)	19(1)	n.d.	-
800	10.2(3)	0.110(4)	10.1(3)	10(1)	n.d.	-
1000	10.0(2)	0.10(1)	8.8(9)	9(1)	2.55(2)	-
1200	7.7(1)	2.34(1)	6.2(1)	4.9(3)	4.41(1)	1.061
1400	1.1(1)	8.11(4)	0.42(1)	19(1)	5.57(5)	1.065
1500	0.036(1)	8.277(4)	0.25(1)	19(2)	5.42(1)	1.064
1500 (Ar)	1.36	4.42	0.29	2(2)	n.d.	-

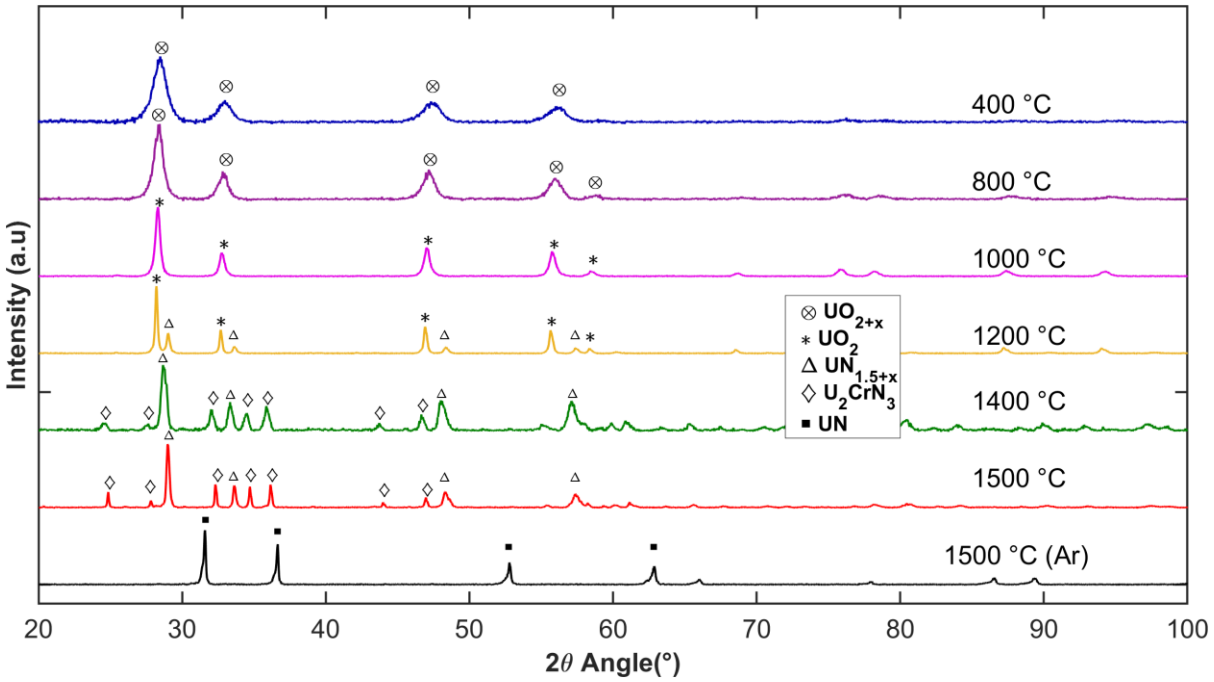

Figure 6.16. XRD patterns measured for the materials heated to different temperatures and cooled in the synthesis gas (H_2/N_2). Phases present were: UO_{2+x} (⊗), UO_2 (∗), $UN_{1.5+x}$ (Δ), U_2CrN_3 (◊),UN(▪).

SEM analysis of these microspheres is presented in Figure 6.17. It was observed that the shape of the microspheres was maintained during the heating treatment. However, cracking became more predominant at 1500 °C, due to the change in density during the transition from UO_2 into UN and escape of CO alongside other gas products. Examination of the surface did not show the same Cr-rich precipitates observed previously in Batch A (Figure 6.14). This shows the

complete integration of the Cr into the UN structure, forming the ternary phase identified in the XRD patterns. Moreover, chromium showed an interesting behavior during the experiments, as can be seen in Table 6.7. As temperature started to increase, up to 1200 °C, the chromium was decreasing, reaching the low levels observed in Batch A (Table 6.6). However, at 1400 and 1500 °C the content increased again to values similar to the initial amount of chromium. This led to the hypothesis that Cr was not completely being evaporated below 1500 °C, and it was likely forming a compound that was insoluble in the aqua regia. The hypothesis was later confirmed by XRF measurements, where the Cr can be measured independently of the phase that the element is found in the material.

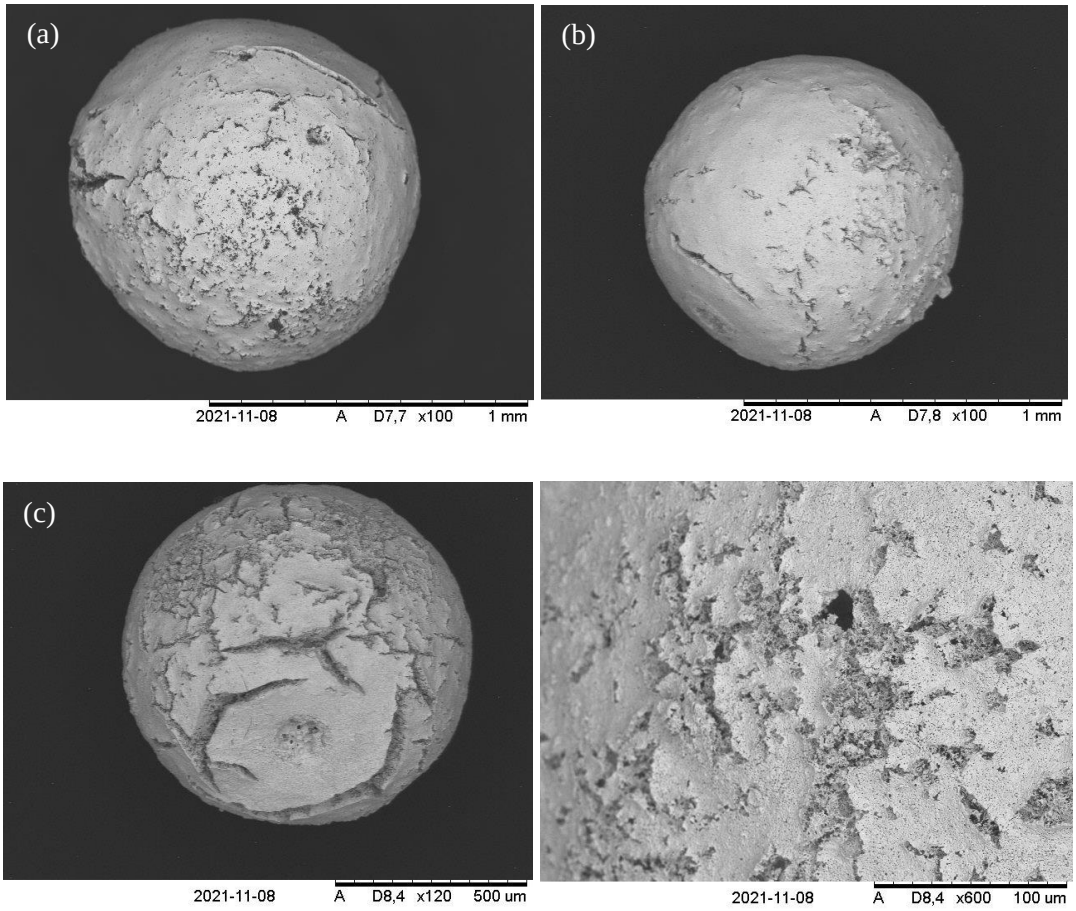

Figure 6.17. Scanning electron microscopy of the produced chromium-doped uranium microspheres after heating to 1000 (a), 1200 (b) and 1500 (c) °C and using H_2/N_2 as the reaction and cooling gas. A closer magnification of the surface showed the absence of Cr precipitates.

Samples were also synthesized using heating profile B, but the cooling gas was changed to Ar to prevent the formation of higher nitrides. The material produced was very similar to that obtained in Batch A, although at lower temperatures. XRD data (Figure 6.16) showed the absence of the ternary phase. Therefore, the interaction of Cr and UN did not happen in materials cooled in Ar. The surface was covered with Cr-rich precipitates (Figure 6.18), which was assumed to be metallic chromium, as the elemental analysis (Table 6.7) showed low nitrogen content. Additionally, ICP-MS data showed again a decrease in Cr content, while XRF measurements showed that the Cr content was not decreasing (see Paper 3). This means that

the Cr in the as-produced spheres and in the ternary phase is completely soluble in aqua regia. In contrast, chromium is insoluble in the other Cr phases, such as metallic chromium, carbides, or nitrides, which are formed between 800 and 1200 °C [103–105]. This behavior can be attributed to the formation of a protective layer around the Cr precipitates, which might not be formed on the ternary phase.

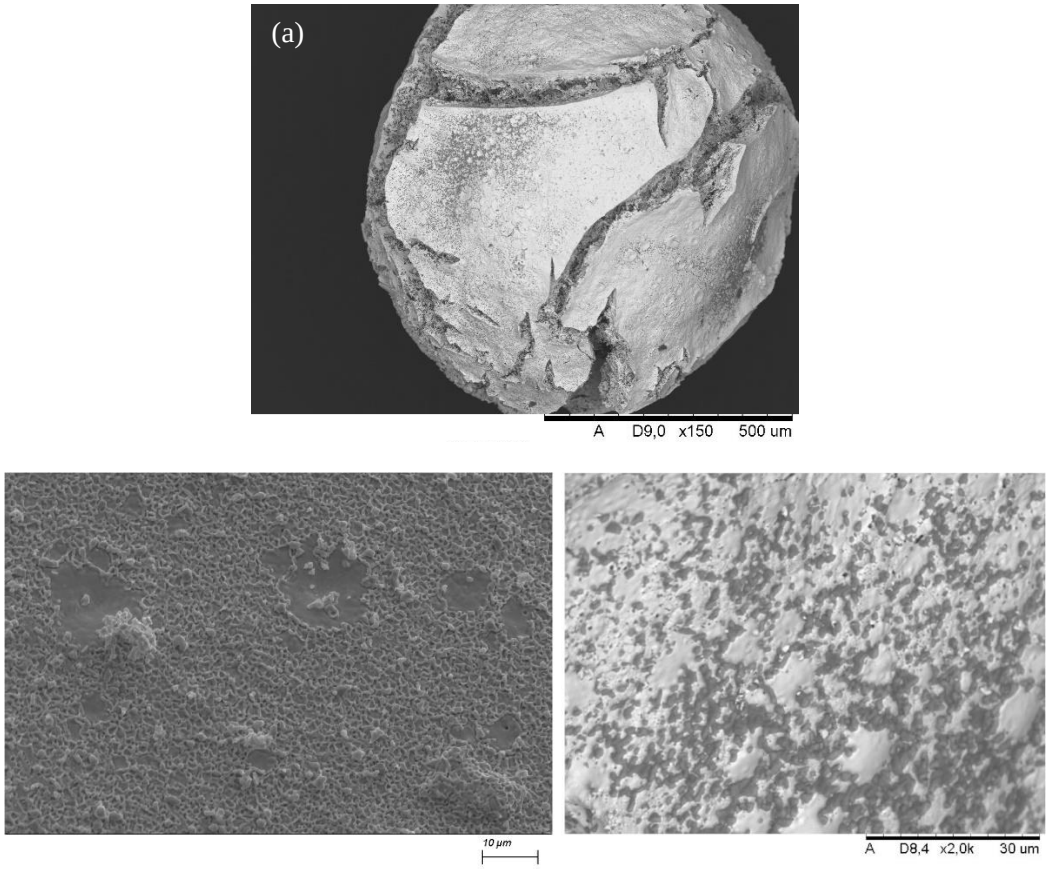

Figure 6.18. Scanning electron microscopy of the produced chromium-doped uranium microspheres after heating to 1500 (a) °C and using H_2/N_2 as the reaction and Ar as cooling gas. A closer magnification of the surface showed the presence of the Cr precipitates covering a large portion of the surface.

6.2.3. Mechanism of reaction for ternary phase formation

With the data collected, a mechanism of reaction was proposed to explain the products of reaction after synthesis of Cr-doped UN microspheres. A graphical summary is displayed in Figure 6.19. The first reactions occur at temperatures below 1000 °C. The hyperstoichiometric UO_{2+x} is reduced to UO_2 in the synthesis atmosphere H_2/N_2. Carbothermal reduction and nitridation of Cr_2O_3 also happens around this temperature.

$$UO_{2+x} + xC \rightarrow UO_2 + xCO \qquad (32)$$

$$Cr_2O_3 + 3C + N_2 \rightarrow CrN + 3CO \qquad (33)$$

Once temperature increases above 1000 °C, uranium oxide starts to form uranium nitrides, which turn into the mononitride (UN) while dwelling at 1500 °C. Additionally, CrN is not stable at such high temperatures and decomposes into metallic chromium.

$$2\,CrN \rightarrow 2\,Cr + N_2 \quad (34)$$

$$2UO_2 + 4\,C + N_2 \rightarrow 2UN + 4\,CO \quad (35)$$

If the temperature is lowered while the reaction gas is left unchanged, the excess of nitrogen allows the formation of U_2N_3 or CrN. These compounds are able to react with Cr and UN, respectively, and the ternary phase (U_2CrN_3) is created. On the other hand, if the atmosphere is changed to an inert gas, such as argon, the higher nitrides are not formed. Reaction of UN and metallic Cr is not possible due to stoichiometry.

$$U_2N_3 + Cr \rightarrow U_2CrN_3 \quad (36)$$

$$2UN + CrN \rightarrow U_2CrN_3 \quad (37)$$

$$2UN + Cr \not\rightarrow U_2CrN_3 \quad (38)$$

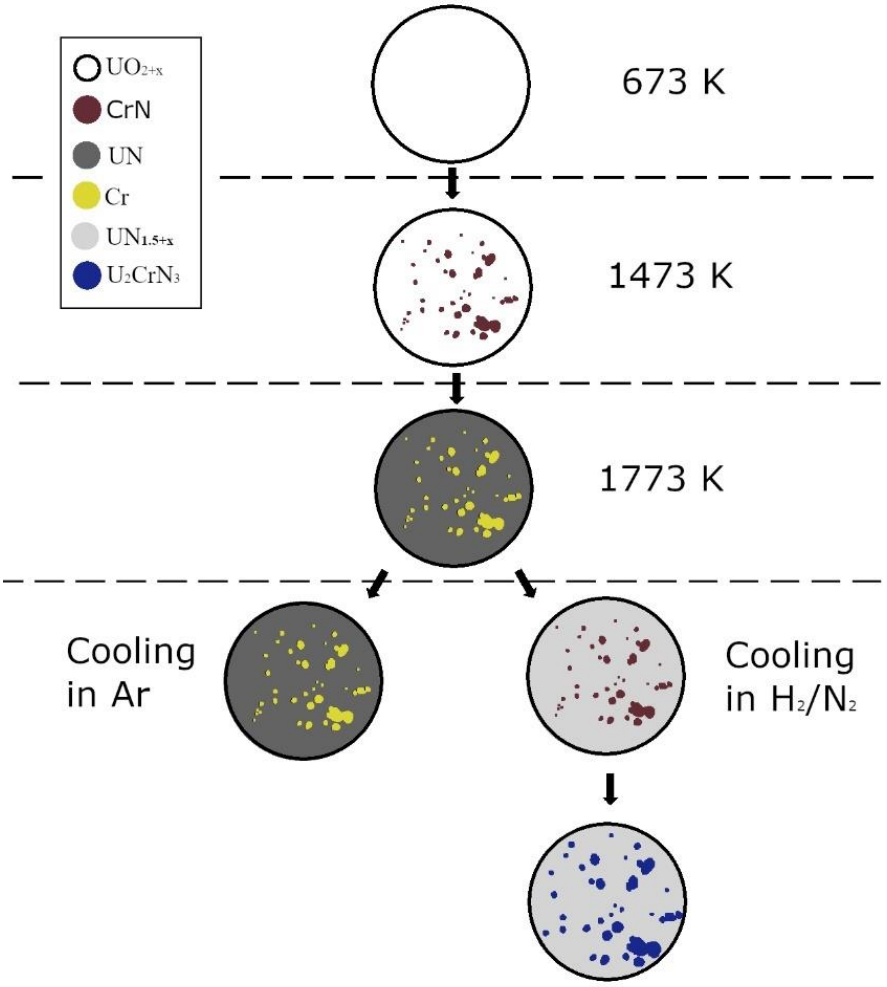

Figure 6.19. Graphical of the mechanism of reaction during the production of Cr-doped uranium nitrides. The main difference occurs during cooling, where special conditions are necessary for the created phases to interact and form the ternary phase.

6.2.4. Microspheres of UN with and without ternary phase

The ternary phase was only identified when synthesis also led to the formation of higher nitrides of uranium. The ATF concept studied here has been specifically designed with uranium mononitride doped with chromium. Samples with 20 mol-% of Cr were synthesized using heating profile B and therefore are denoted as Batch B. The cooling gas was either unaltered or changed to argon and, as expected, the spheres were composed of $UN_{1.5+x}$ and U_2CrN_3 when the gas was unchanged. These samples had to be denitrided in an argon atmosphere at 1200 °C. The XRD patterns showed that it was possible to obtain the UN mixed with the ternary phase. According to the pattern refinement (Figure 6.20), the ternary phase composition was unchanged during denitridation. Additionally, it was stable up to this temperature, which is expected from calculations made by other authors [77,79].

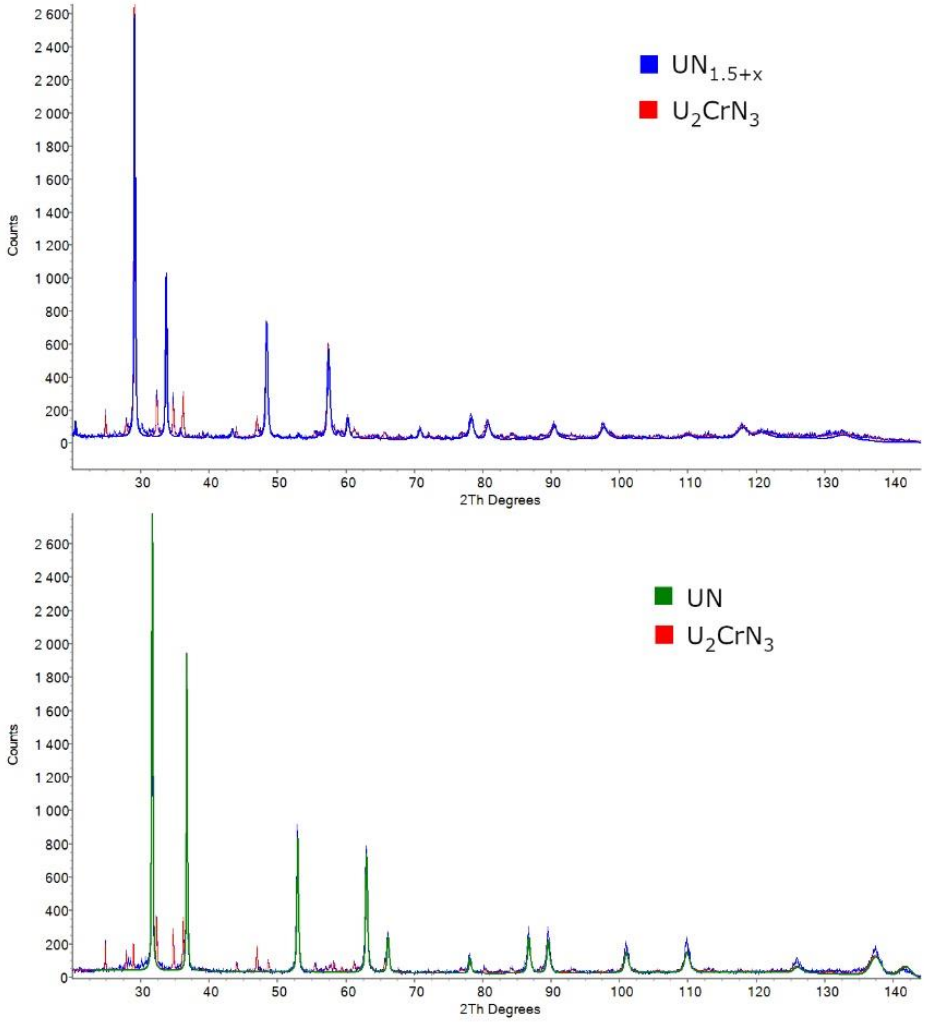

Figure 6.20. Diffraction patters of sample U80CR20N-23 before (upper) and after (lower) denitridation at 1200 °C showing the transformation of the $UN_{1.5+x}$ into UN while the ternary phase remained intact.

Composition of samples in Batch B is listed in Table 6.8. Multiple batches were made to corroborate the replicability of both the XRF and the synthesis method. Samples showed that ternary phase only accounts for 20% of the weight, while the expected content if all Cr was

involved in the ternary phase should reach about 50%. This was attributed to the larger volumes used during the synthesis, which decreases the formation of nitrides. This also caused the large variation of carbon residues in the spheres. Table 6.8 also presents the chromium content measured using XRF, and as can be seen, the content is similar regardless of the phase the Cr is found in the spheres.

*Table 6.8. Elemental analysis and phase composition of samples in Batch B. Chromium content was measured with XRF. Samples were tailored to contain or not contain the ternary phase. The ternary phase composition was calculated using Rietveld refinement of the XRD patterns. The n.d. indicates the value was not determined. * Elemental analysis of these samples has not been made yet.*

Sample name	Carbon content (wt-%)	Nitrogen content (wt-%)	Oxygen content (wt-%)	Chromium Content (mol-%)	Ternary phase present
UN-11	0.02 ± 0.01	5.50 ± 0.05	0.33 ± 0.05	-	-
U80Cr20N-13	0.00 ± 0.02	*	*	18.8 ± 0.1	-
U80Cr20N -23	0.58 ± 0.13	*	*	n.d.	Yes
U80Cr20N -14	1.69 ± 0.14	4.65 ± 0.02	0.24 ± 0.01	21.3 ± 0.3	-
U80Cr20N -24	0.10 ± 0.02	*	*	20.0 ± 0.1	Yes
U80Cr20N -15	2.00 ± 0.20	3.78 ± 0.05	0.20 ± 0.01	23.7 ± 0.2	-
U80Cr20N -25	1.90 ± 0.07	*	*	22 ± 1	Yes
U80Cr20N -16	1.28 ± 0.04	4.53 ± 0.17	0.17 ± 0.01	19.2 ± 0.5	-
U80Cr20N -26	0.50 ± 0.06	5.32 ± 0.01	0.20 ± 0.01	17.5 ± 0.1	Yes

6.2.5. Cr-doped UN pellet production

The pelletization and sintering of UN and Cr-doped UN was also done by SPS, as this proved to be able to produce high density pellets in the previous Th-doped UN samples. The microspheres were loaded directly in the dice without any previous pretreatment or addition of sintering additives. Two different batches of pellets were prepared: one with the microspheres produced in Batch A and one with the Batch B. Therefore, the pellets were also denominated A or B, according to their starting materials.

6.2.5.1. Batch A

Pellets made from the spheres in Batch A were made from materials with different chromium content to observe the effect of Cr content in the manufacturing of UN fuels. Sintering temperature was selected to be 1650 °C, as it was the best parameter observed for pellets in the Th-doping section. SPS should be able to sinter Cr-containing materials and the short sintering time (5min) was expected to reduce any Cr evaporation. The main results obtained for density and Cr content of the pellets of Batch A is found in Table 6.9. These pellets had the highest densities amongst all pellets sintered during this work. However, the Cr contents were lower than the original value. Evaporation was the main cause for the decrease in Cr due to the high temperatures (1650 °C) used, even at low sintering times. SEM of the (U80Cr20)N-1 pellet's surface can be seen in Figure 6.21 where very low porosity can be observed. The black spots

on the surface were identified as a chromium phase and were formed in what looks like the void or pores. This can explain the high density of these materials, as there is very little open porosity left. The black chromium spots were not seen in pellets with lower Cr-content.

Table 6.9. Chromium content and density of Cr-doped UN pellets from Batch A compared to their theoretical density. Theoretical densities were calculated using the lattice parameters determined experimentally with the XRD pattern. Cr content was measured with XRF.

Pellet name	Cr-Content (mol-%)	Theoretical density (g/cm^3)	Pycnometer density (g/cm^3)	%TD
(U95Cr5)N-1	1	14.28	13.86 ± 0.03	97.0 ± 0.2
(U95Cr5)N-2	1	14.29	13.72 ± 0.04	96.0 ± 0.3
(U95Cr5)N-3	0*	14.22	13.44 ± 0.06	94.5 ± 0.4
(U90Cr10)N-1	0*	14.14	13.87 ± 0.09	98.0 ± 0.6
(U90Cr10)N-2	3	14.22	13.2$^+$ ± 0.2	93$^+$ ± 1
(U90Cr10)N-3	5	14.11	13.1$^+$ ± 0.3	92$^+$ ± 2
(U80Cr20)N-1	0*	14.10	14.06 ± 0.02	99.7 ± 0.1
(U80Cr20)N-2	3.7*	14.06	12.7$^+$ ± 0.3	90$^+$ ± 2
(U80Cr20)N-3	6	14.06	13.80 ± 0.04	98.2 ± 0.3
(U80Cr20)N-4	14.3	14.12	13.92 ± 0.09	98.6 ± 0.6

** Cr-content measured using ICP-MS. $^+$ density calculated by measuring the pellet volume with calipers.*

The ternary phase observed by other authors [79,106] was not clearly seen in these pellets either. The starting materials were spheres of UN with metallic chromium, as stated in the previous sections. However, it has been reported [79] that the reaction of UN powders with metallic chromium can produce the ternary phase. This was not clearly observed, however, in the results from pellets of Batch A.

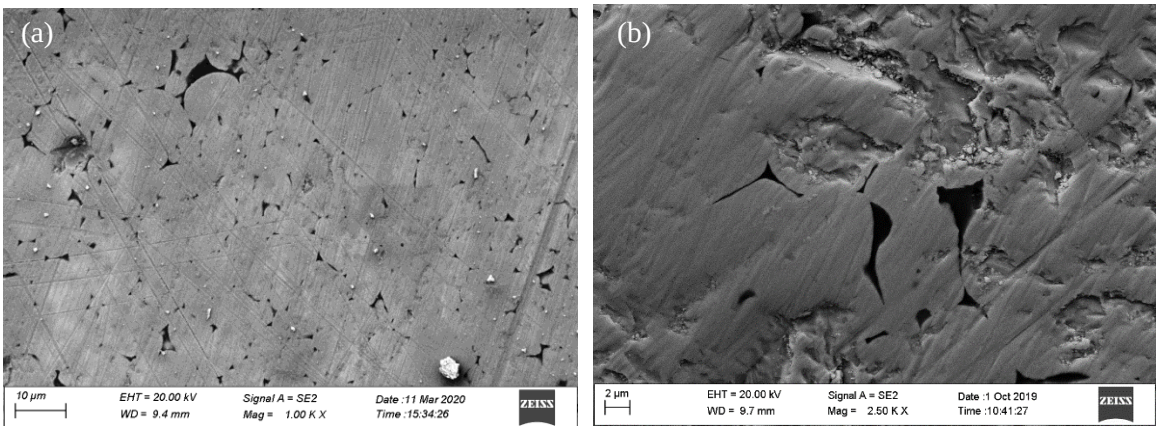

Figure 6.21. SEM of (a) the surface of the (U80Cr20)N-1 pellet and (b) the surface of the (U80Cr20)N-2 pellet after polishing, showing the presence of Cr precipitates instead of porosity.

6.2.5.2. Batch B

Pellets from microspheres in Batch B were manufactured to investigate the effect of having the ternary phase in the starting material. The sintering was also performed at lower sintering temperatures (1550 °C), as from previous experience, sintering at 1650 °C caused chromium evaporations. The main results are summarized in Table 6.10. The densities obtained varied between 90 and 95%, which are considerably lower than for pellets in Batch A. This was expected as the sintering temperature was lower. XRF measurements also showed that the Cr-content was not altered, unless the sintering was done at 1650 °C, as seen for the pellet U80Cr20N-26.

Table 6.10. Sintering temperature and summary of the properties of the Cr-doped UN pellets from Batch B. The chromium content was determined with the XRF. The theoretical density was calculated with the expected content of ternary phase.

Pellet name	Sintering temperature (°C)	Cr Content after sintering (mol-%)	Pycnometer density (g/cm3)	%TD
UN-11	1550	0	12.87 ± 0.01	90.0 ± 0.1
U80Cr20N-13	1550	17.9	13.3 ± 0.1	98.5 ± 0.7
U80Cr20N-23	1550	27.8	12.99 ± 0.03	96.2± 0.2
U80Cr20N-14	1550	23.1	12.90 ± 0.02	95.5± 0.2
U80Cr20N-24	1550	25.3	12.81 ± 0.01	94.9± 0.1
U80Cr20N-26	1650	11.8	13.39 ± 0.02	95.6± 0.2

The polished surface of the pellets sintered at 1550 °C can be seen in Figure 6.22. The main outcome was the presence of the ternary phase (dark gray) in pellets made from materials with or without the ternary phase. It was also seen that a metallic chromium phase was created in materials that started from spheres containing the ternary phase. On the other hand, the spheres where Cr was found in a metallic form was able to interact with the uranium nitride and form the ternary phase. The interaction could have been possible at the high pressure and fast heating rates used during sintering.

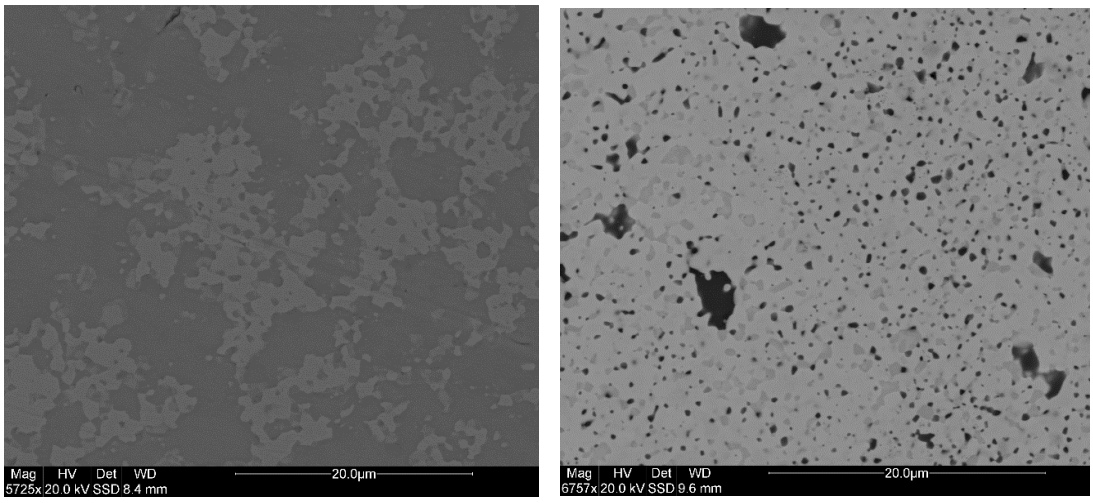

Figure 6.22. SEM of the surface of the U80Cr20N-23 pellet (left) made from spheres containing the ternary phase and the U80Cr20N-13 pellet (right) made from spheres that did not contain the ternary

phase. The ternary phase (U_2CrN_3) in dark gray was observed in both materials. UN phase is seen in light gray while metallic chromium is seen as black spots.

A singular pellet was also made from UN microspheres and CrN powders to observe if the results observed by other authors with UN powders were able to be recreated using the spheres. The pellet (Figure 6.23) showed that chromium was not homogeneously distributed from the start, and the CrN powder was located at the bottom of the material before sintering. Nonetheless, the side of the pellet that had the CrN powder showed the exact same results observed by Mishchenko [79], where the ternary phase is formed between the Cr and the UN phases.

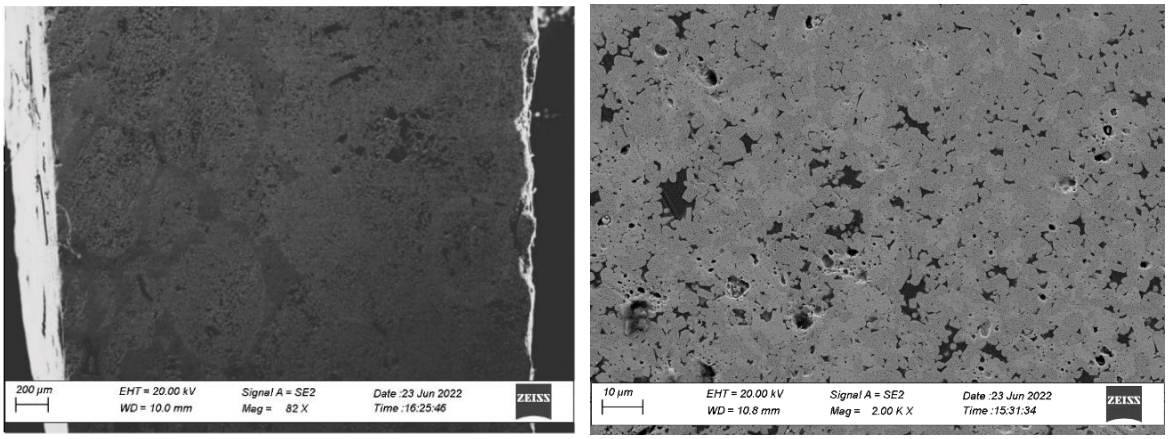

Figure 6.23. SEM (left)of the surface of the pellet made from UN spheres and CrN powders, where CrN powder was located towards the bottom of the pellet. Higher magnification (right) was helpful to identify metallic Cr and UN phases surrounded by the ternary phase (U_2CrN_3).

6.2.6. Interaction tests

As with thorium, Cr-doped microspheres and pellets were subjected to interaction with oxidizing environments. The reaction with air, steam and water was investigated to determine if Cr doping was effectively improving the corrosion resistance of UN.

6.2.6.1. Air

Air corrosion would be more dominant during fuel fabrication and transport. The interaction of oxygen and Cr-doped UN materials were analyzed in the TGA (Figure 6.24). The Batch A of Cr-doped UN showed an improvement in the oxidation resistance of the spheres, by increase in the onset and maximal reaction rate temperatures, as seen in Table 6.11. The improvement was observed regardless of doping levels. However, the extent of the improvement was not proportional to the doping level. This variation exists due to the porosity of the spheres outperforming the Cr-doping effect. For the doped pellets of Batch A, it was observed that the pellet (U90Cr10)N-1 and (U95Cr5)N-1 had an increase in the oxidation temperatures. However, the pellet (U80Cr20)N-1, which had the highest level of doping, showed very similar results to an undoped UN pellet. This pellet also had the metallic Cr precipitations, which can swell during heating, cracking the pellet, and revealing more of the bulk material to react, decreasing the oxidation resistance of this sample. In lower Cr-containing samples, the Cr

seems to be incorporated in the UN, and this increases the temperature required to start the oxidation.

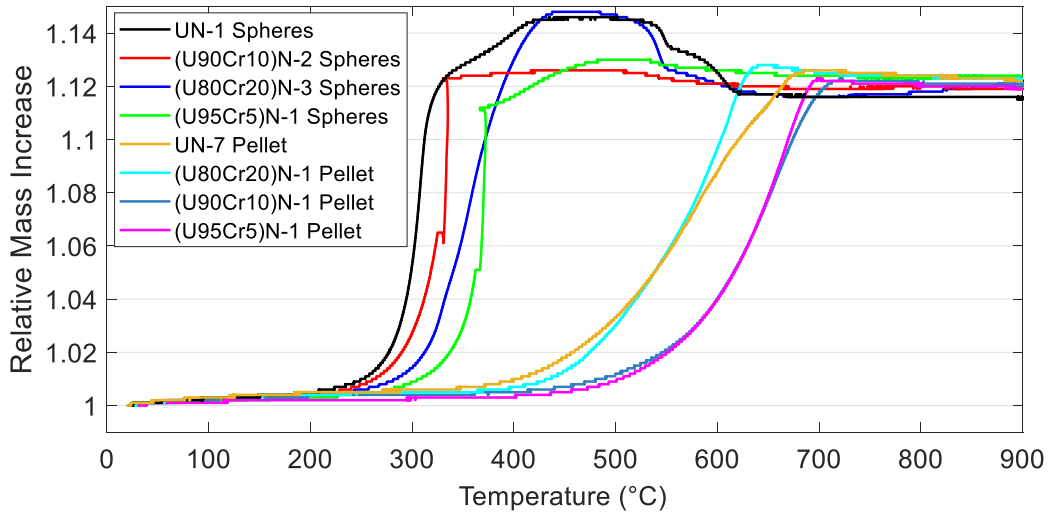

Figure 6.24. Average TGA curves for oxidation of uranium nitride and chromium-doped uranium nitride microspheres and pellets from Batch A using synthetic air.

Materials in Batch B had higher Cr-doping levels after the modifications to the synthesis parameters. Half of the spheres were synthesized to contain the ternary phase, while the others had the Cr precipitates. The TGA graphs (Figure 6.25) from the air exposure showed very similar results to those observed for the Th-doping. The mass first increases above the expected maximal increase, and then slowly reduces until it reaches a steady plateau. As previously explained, this occurs probably due to the nitrogen gas not being able to escape the sphere until higher temperatures are reached. No significant difference was measured for the onset temperature between the two types of doping. However, the onset of the reaction was lower than for the undoped spheres, which can be attributed to the higher porosity and cracking of Cr-doped UN spheres.

Table 6.11. Porosity and reaction temperatures of UN and Cr-doped UN spheres and pellets made from Batch A and B. The n.d. indicates the value was not determined.

Sample	Total porosity (% volume)	Onset temperature (°C)	Maximum reaction rate temperature (°C)
(U95Cr5)N-1 spheres	77	277	365
(U90Cr10)N-2 spheres	73	234	330
(U80Cr20)N-3 spheres	71	250	355
U80Cr20N-23 spheres	n.d.	242	292
U80Cr20N-14 spheres	n.d.	224	294
UN-11 spheres	n.d.	264	311
(U95Cr5)N-1 pellet	2.9	464	665
(U90Cr10)N-1 pellet	2.0	426	660
(U80Cr20)N-1 pellet	0.3	380	610
UN-11 pellet	10	397	411
U80Cr20N-24 pellet	3.8	411	421
U80Cr20N-14 pellet	4.5	422	492

Differences in behavior between the two type of materials was mainly observed at temperatures above 600 °C. Spheres with the ternary phase reached the plateau at this temperature. On the other hand, the spheres without the ternary phase showed an additional increase in mass starting at 650 °C before reaching the plateau. The increase was attributed to the oxidation of the Cr precipitates, which have been reported to oxidize at temperatures above 600 °C [107]. This also means that Cr in the ternary phase is being completely oxidized during the oxidation of the UN below 600 °C.

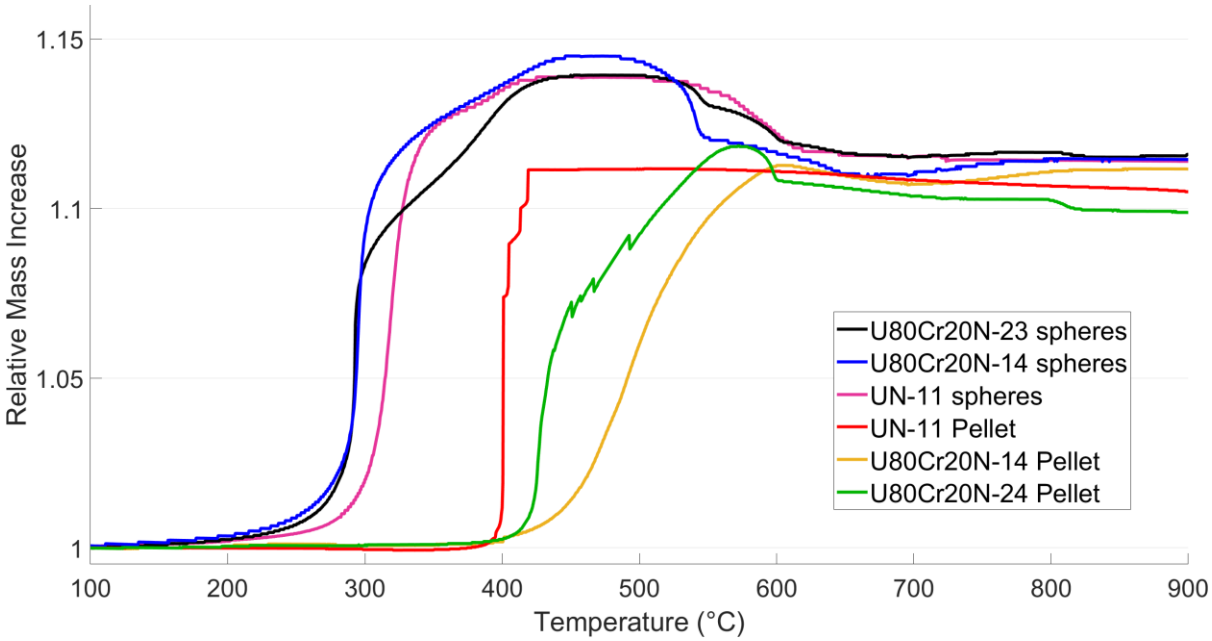

Figure 6.25. TGA curves for oxidation of uranium nitride and chromium-doped uranium nitride microspheres and pellets from Batch B using synthetic air, showing the difference between materials with and without the ternary phase.

Pellet oxidation happens at higher temperatures than spheres, as expected by the higher density. Cr-doped pellets showed higher reaction onset than the undoped counterparts, contrarily to the trend observed in spheres. This indicates that the porosity had a bigger impact that could not be counterbalanced with the Cr additions. Moreover, pellet U80Cr20N-14, which was made from materials that did not have the ternary phase, showed a higher onset temperature than pellet U80Cr20N-24, which can be attributed to the difference in the microstructure. Pellet U80Cr20N-14 also had the same late mass increase above 650 °C observed in spheres without the ternary phase, which indicates the presence of metallic chromium still present in the pellet.

6.2.6.2. Steam

In case of accident or cladding failure, if water comes in contact with the fuel, it would be instantaneously flashed into steam. It is therefore important to investigate the behavior of the Cr-doped UN pellets in a steam atmosphere. The experiments were conducted at Studsvik AB, and only Cr-doped pellets from Batch B were able to be analyzed in a single experiment per sample. Figure 6.26 shows the steam TGA mass change as temperature was increased. It was clearly seen that the onset temperatures for Cr-doped pellets were higher compared to the undoped pellet. Nonetheless, the pure UN pellet showed a similar mass gain curve than pellets produced from powder that had higher densities [108]. Moreover, pellet U80Cr20N-26, which

was sintered at 1650 °C, was also analyzed. Its Cr-content was lower, and its density higher compared to pellets U80Cr20N-14 and U80Cr20N-24. This pellet showed a very similar behavior in the TGA to pellets with high Cr-content, indicating that the improvement in corrosion provided by the Cr-doping can be balanced by the increase in density. The final mass gain for the pure UN pellet was 7.5%, which corresponds to the oxidation into UO_2, as expected by previous reports [109]. Doped pellet had a higher mass gain due to the oxidation of Cr. There is no explanation as to what caused the behavior observed in pellet U80Cr20N-24 between 700 and 800 °C besides errors in the weighing balance.

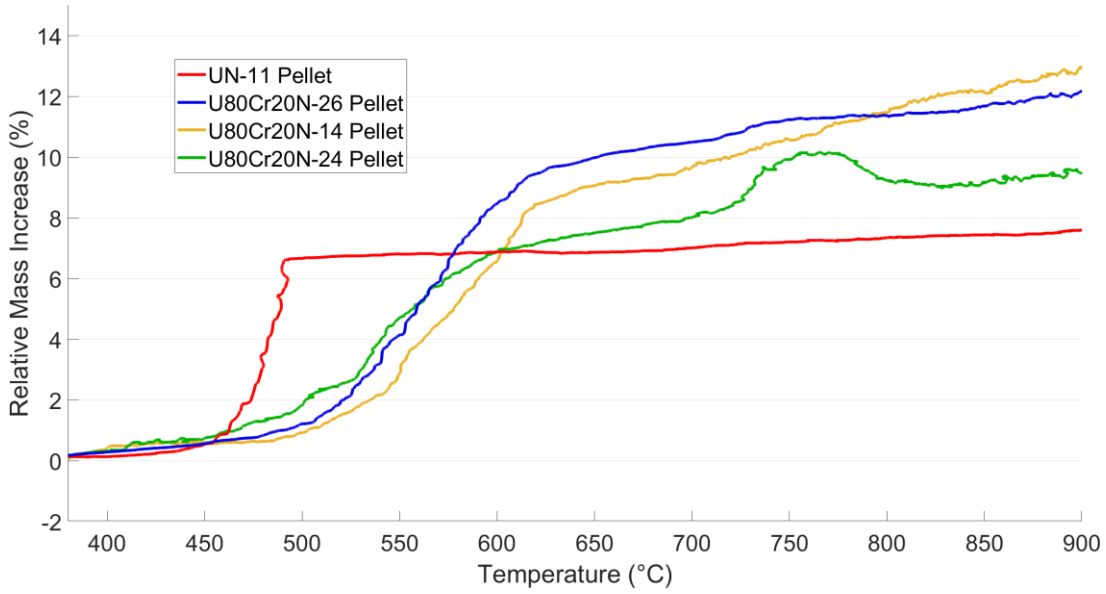

Figure 6.26. Steam TGA curves for hydrolysis of uranium nitride and chromium-doped uranium nitride pellets from Batch B.

The final product of the reaction was UO_2 as observed in the XRD patterns in Figure 6.27. Chromium phases were absent in all diffractograms, which is attributed to the lower weight of these phases compared to the uranium bulk phases. The formation of U_3O_8 was confirmed from the refinement of the XRD patterns. This phase is not expected to form in the reaction with water, and therefore was attributed to a small air leakage into the STA system.

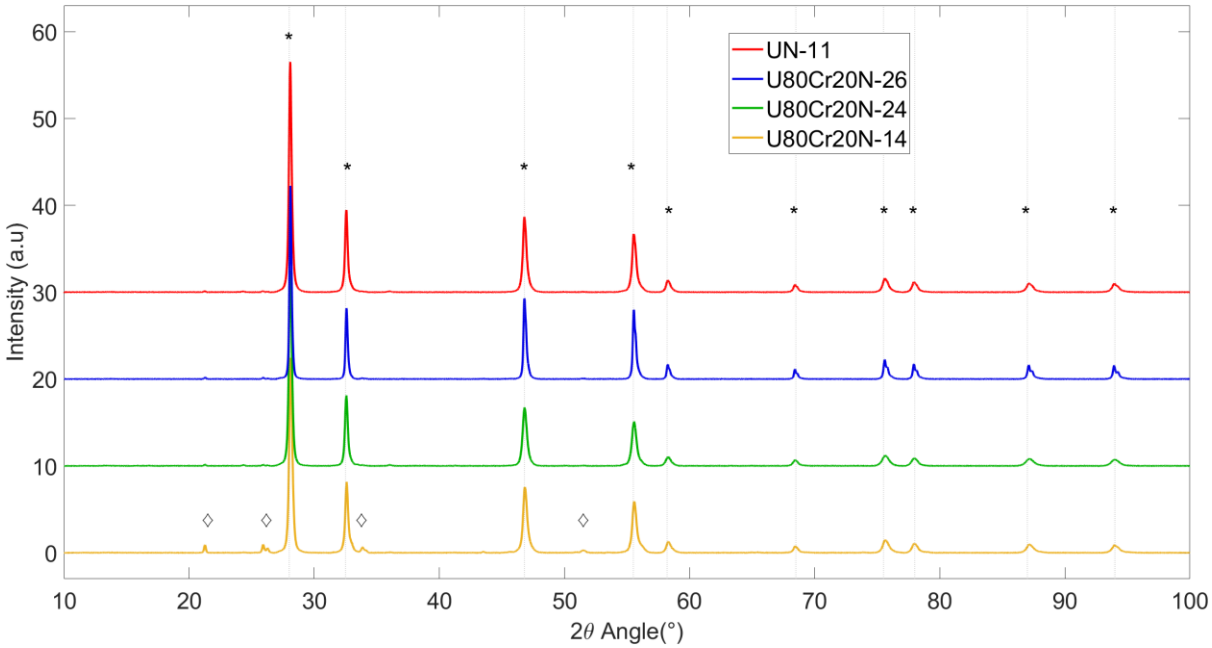

Figure 6.27. X-Ray diffractograms for powders collected after pellet disintegration in the steam interaction experiments, where UO_2 (*) and U_3O_8 (◊) signals were identified.

6.2.6.3. Water

The interaction with water was studied in an autoclave, and temperatures were increased to 200 or 300 °C. Visual examination of the pellets after exposure can be seen in Figure 6.28 and were compared to the hydrolysis of a pure UN pellet previously presented in this work (Figure 6.10). The pure UN pellet lost its integrity after exposure to water at 200 °C. On the other hand, UN pellets doped with Cr are able to survive the exposure to water at 200 and 300 °C for 2 hours, however, some damage to the pellets was still taking place. Pellet U80Cr20N-23 was reintroduced into the autoclave to extend the exposure time for an extra 3 hours. After a total of 5 hours of interaction, the pellet finally lost its integrity. It was also observed that samples with higher Cr-content and lower C-contaminants were less affected by the integration with water and were able to withstand experiments at 300 °C with minimal damage.

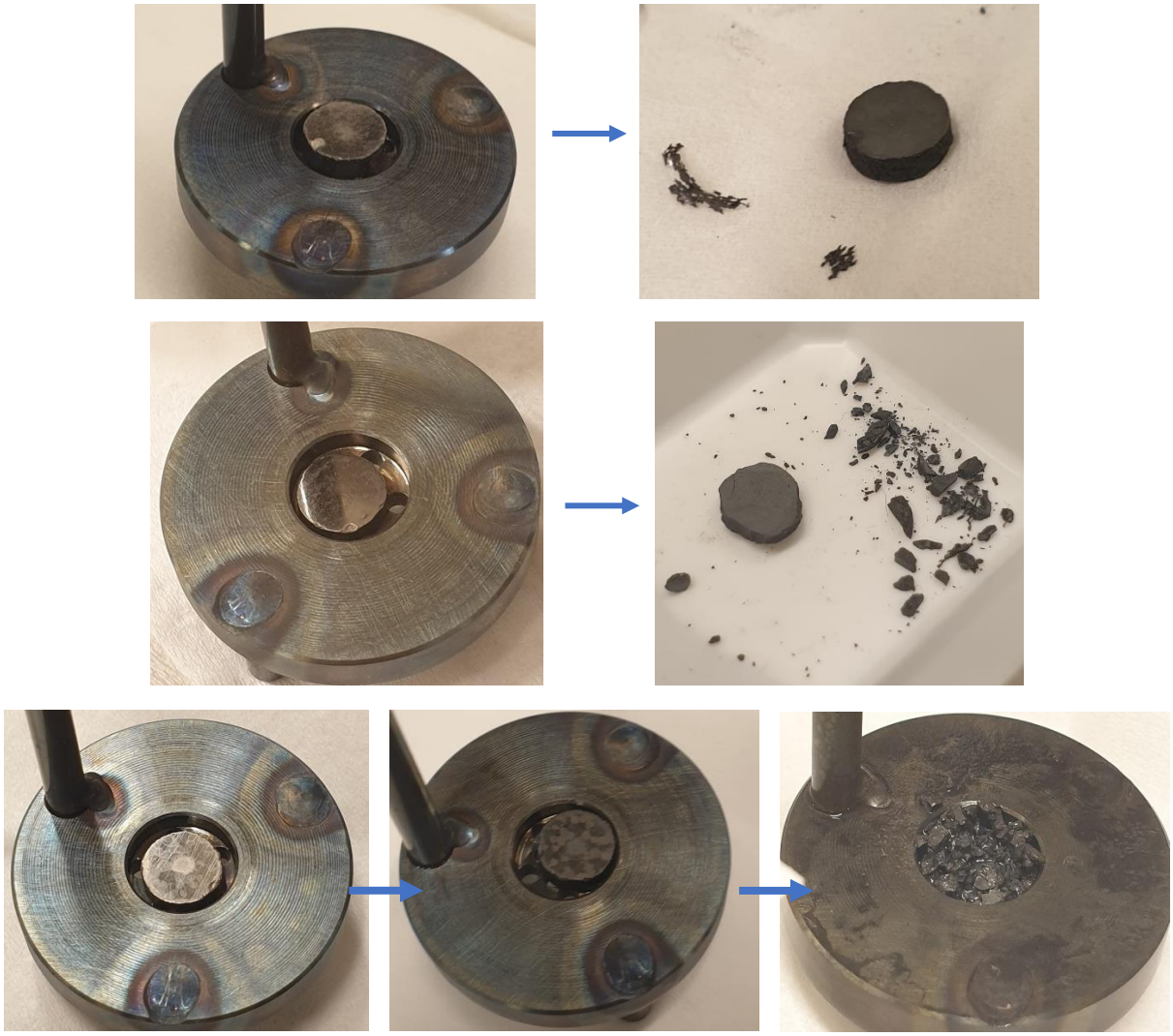

Figure 6.28. Photographs of (U80Cr20)N-3 (top), U80Cr20N-13 (middle), and U80Cr20N-23 (bottom) Cr-doped UN pellets from Batch A and B before and after exposure to water at 300 °C. The U80Cr20N-23 pellet was exposed for 3 extra hours, after which crumbling occurred.

The elemental composition of the powders or pellet pieces collected after the interaction with water were measured for comparison purposes and are summarized in Table 6.12. Although the Cr-doped pellets lost their integrity, the measured nitrogen content was still high enough, indicating a partial oxidation of the materials, unlike the results observed previously. The XRD patterns of the material after interaction of Pellets from batch B have not been measured due to the malfunctioning of the XRD instrument. However, from the diffractogram of Batch A (Figure 6.29) it was possible to corroborate that the main phase was still UN, with some UO_2 also present. The pH of the water was modified in most of the samples, and this is expected by the formation of ammonia during the reaction of UN with water. The results obtained for the Cr-doped UN were always an improvement compared to the results obtained after interaction of Th-doped UN with water (Table 6.4 and Figure 6.11), where the pellet lost its integrity and almost no nitride was recovered after reaction.

*Table 6.12. Comparison the results obtained after the water exposure experiments of Cr-doped UN pellets from Batch A and B. Nitrogen and oxygen were measured only when pellet was degraded into a powder or fragmented. The n.d. indicates the value was not determined yet. * Pellet U80Cr20N-23 was heated for an additional 3 hours.*

Pellet	Reaction Temperature (°C)	Nitrogen content (wt-%)	Oxygen content (wt-%)	pH of water after interaction
UN-6	200	0.71 ± 0.04	12.9 ± 0.2	11.0
UN-4	300	0.04 ± 0.01	11.59 ± 0.04	10.4
(U80Cr20)N-2	200	3.8 ± 0.1	0.87 ± 0.45	9 - 10
(U80Cr20)N-3	300	-	-	8.0
U80Cr20N-23	300	-	-	6.9
U80Cr20N-13	300	n.d.	n.d.	9.7
U80Cr20N-23*	300	n.d.	n.d.	9.8

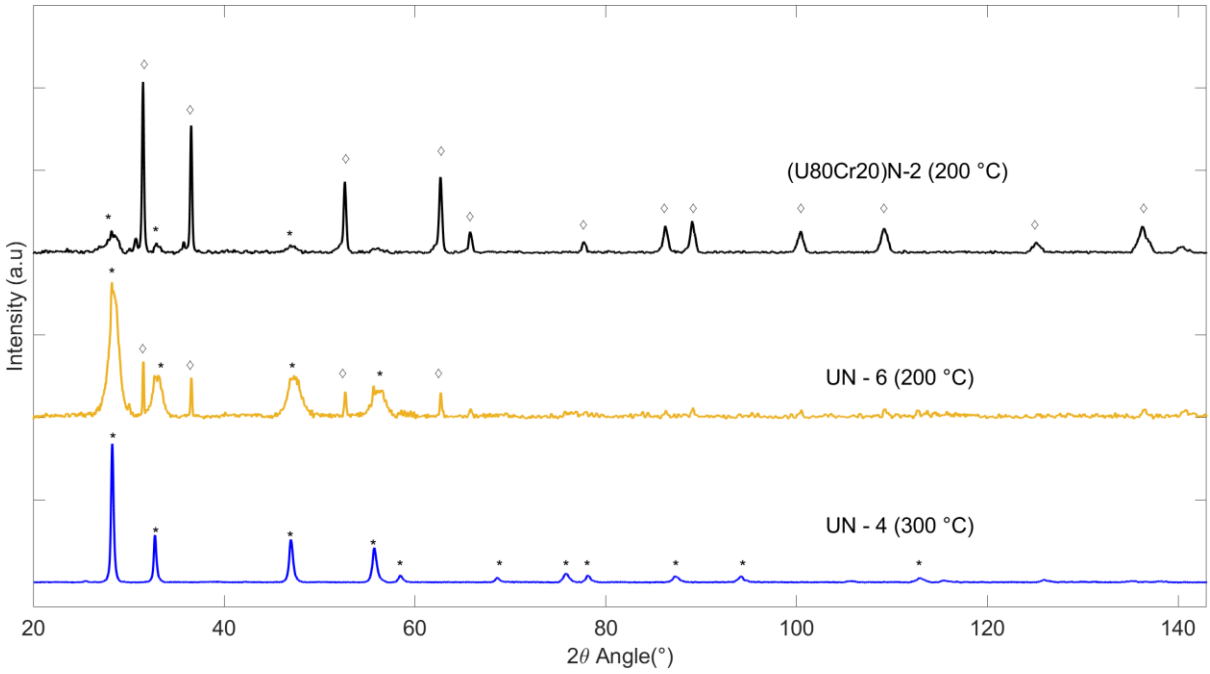

Figure 6.29. X-Ray diffractograms for powders collected after pellet disintegration in the corrosion testing of Cr-doped UN pellets, where UN(◊) and UO_2 (*) signals were identified.

6.3. Dual Cr-Al doping

Disclaimer: This work was done simultaneously with batch A of Cr-doped UN microspheres, and therefore the chromium losses, and behavior were not known at that point.

Results presented in this section are based on those published in Conference Proceedings I.

The idea of multiple additives is known in the corrosion environment. Once again, steels are the best example of materials with multiple additives. In stainless steels, C, Cr, Ni, Mo are all added to improve the mechanical and corrosion properties of iron, making it one of the most versatile materials used in different industries. In the case of UN the first dual doping idea came from the FeCrAl concept. The idea was to dope the UN with materials that show passivity and protection at different temperature ranges, as one of the elements can be protective at operating conditions, while the other can improve the corrosion resistance at accident conditions.

6.3.1. Microsphere production

For simplicity, the total amount of dopant was maintained constant, and the ratio of Cr and Al was varied. As with the previous gelation processes, the gelation parameters must be adjusted after the addition of other elements besides uranium. The heating profile A was used during the synthesis; however, the temperature was not raised to 1650 °C, in an attempt to avoid Cr evaporation, and was instead maintained at 1550 °C. It can be observed in Figure 6.30 that the spheres showed a high degree of cracking as the Cr doping levels increased. This behavior could be explained by the same reasons described previously, namely the increment in the HMTA/metal ratio. However, the reason for the small cracking of UN microspheres doped with Al compared to the Cr-doped UN must have a different origin.

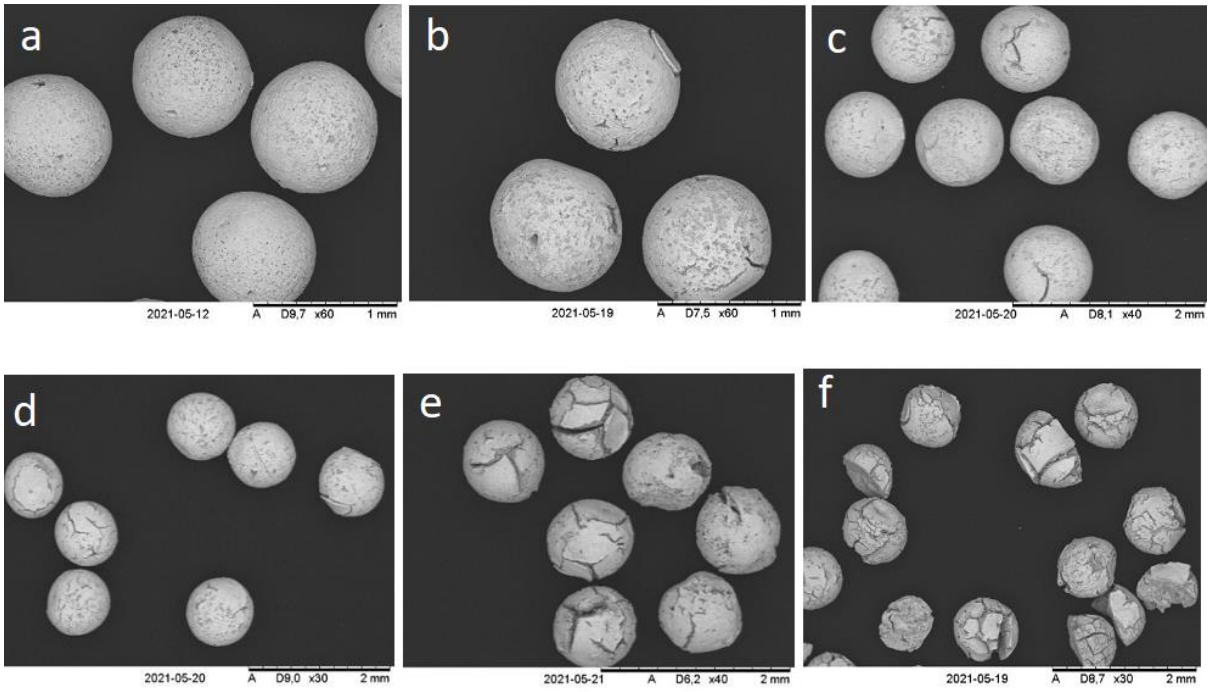

Figure 6.30. SEM images of UN samples with increasing chromium concentration. a) pure UN, b) U80Al20N, c) U80Al15Cr5N, d) U80Al10Cr10N, e) U80Al5Cr15N, f) U80Cr20N.

Closer examination at the surface, shown in Figure 6.31, revelead changes in the microstructure when aluminum was added into the mixture. Higher porosity was observed in the materials with higher Al content. This would allow the gases created during reaction to escape the bulk of the material, thus creating less damage to the sphere structure. On the contrary, materials without aluminum showed a fairly smooth surface with small porosity. It has been recently reported in the literature [79] that AlN should not be soluble in the UN crystal, and it is expected to stay in the grain boundaries. This will lead to the grains not being able to fuse together during the heating treatment. CrN on the other hand is expected to react with the UN and form complex compounds and remain in the bulk of the material. However, pebble-like precipitates were formed in the surface. They were identified as the same Cr-rich phase seen before (Figure 6.18), according to EDX. It is known now that Cr is not able to incorporate in the UN bulk if the materials are cooled in an inert atmosphere during synthesis.

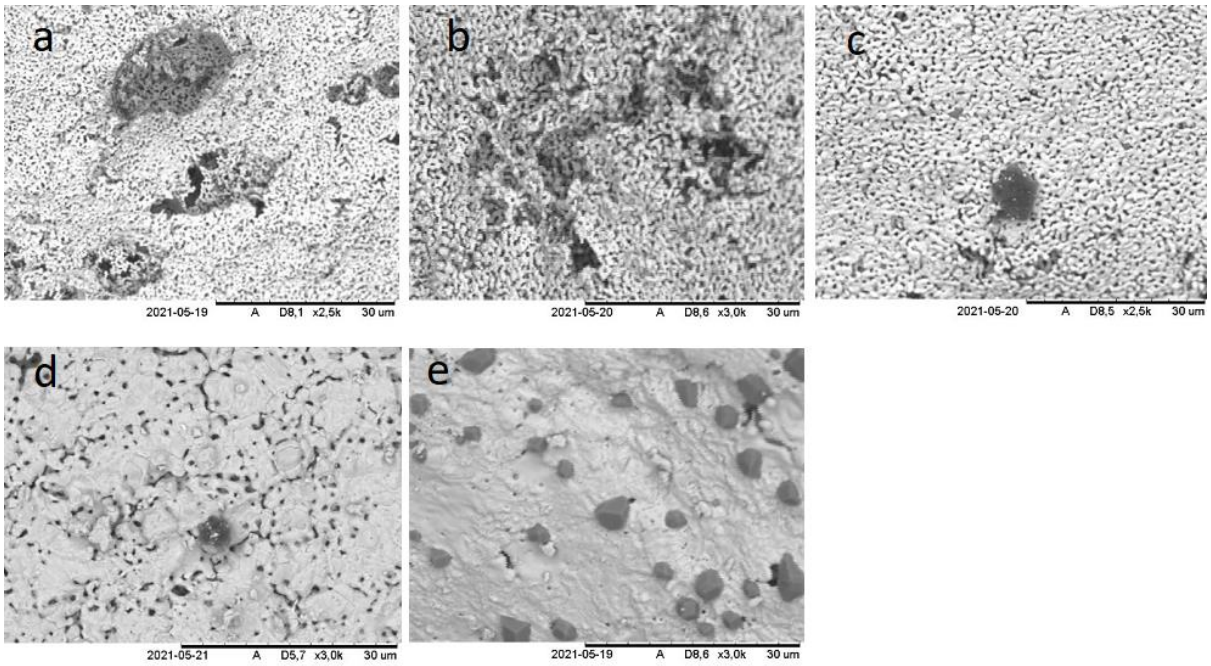

Figure 6.31. SEM images of UN samples with increasing chromium concentration. a) U80Al20N, b) U80Al15Cr5N, c) U80Al10Cr10N, d) U80Al5Cr15N, e) U80Cr20N.

Elemental analysis of doped uranium nitrides is presented in Table 6.13. All materials, regardless of the metal composition, showed a very small amount of carbon contamination, however, the oxygen content was very high compared to previous gelation products. This suggests an incomplete reduction and nitridation of the materials. It is possible that some of the carbon added was lost during washing, or that oxygen was reintroduced during transportation into the glovebox after synthesis. Additionally, as the Al content was increased the nitrogen content also increased, becoming more similar to the expected amount. This leads to the conclusion that Al is found as a nitride phase, while Cr is expected in the metallic form, which would explain the precipitates on the surface.

Table 6.13. Elemental analysis and lattice parameters of dual-doped uranium nitrides microspheres.

Sample	Carbon content (wt-%)	Oxygen content (wt-%)	Nitrogen content (wt-%)	Theoretical nitrogen content in pure compound (wt-%)	Lattice parameter (Å)
UN-D	0.021(9)	0.591(4)	5.24(3)	5.56	4.892(3)
U80Cr20N-D	0.014(4)	0.690(6)	5.099(16)	6.52	4.8837(17)
U80Cr15Al5N	0.015(7)	0.628(22)	5.40(8)	6.56	4.8888(5)
U80Cr10Al10N	0.015(5)	0.632(6)	5.8(3)	6.59	4.8897(3)
U80Cr5Al15N	0.011(8)	0.950(23)	5.97(14)	6.63	4.8899(5)
U80Al20N	0.028(8)	0.912(4)	6.18(25)	6.67	4.8899(5)

Chromium could also locate inside the UN crystal structure, either in the interstitial space or as a substituent. The lower lattice parameter measured can be attributed to minor substitution of Cr in the lattice. Additionally, it is now known that the synthesis temperature and cooling gas prevented the formation of a ternary phase in the U-Cr-N system, and therefore it is not observed in the XRD patterns in Figure 6.32. For Al-doped UN there is no change in the lattice parameter, which can be attributed to a complete separation of the UN and AlN phases. The former phase is however not observed in the XRD patterns, where only the UN and a small UO_2 phase are present. This can be attributed to the low weight percentage of AlN (less than 5%) in comparison to the UN bulk.

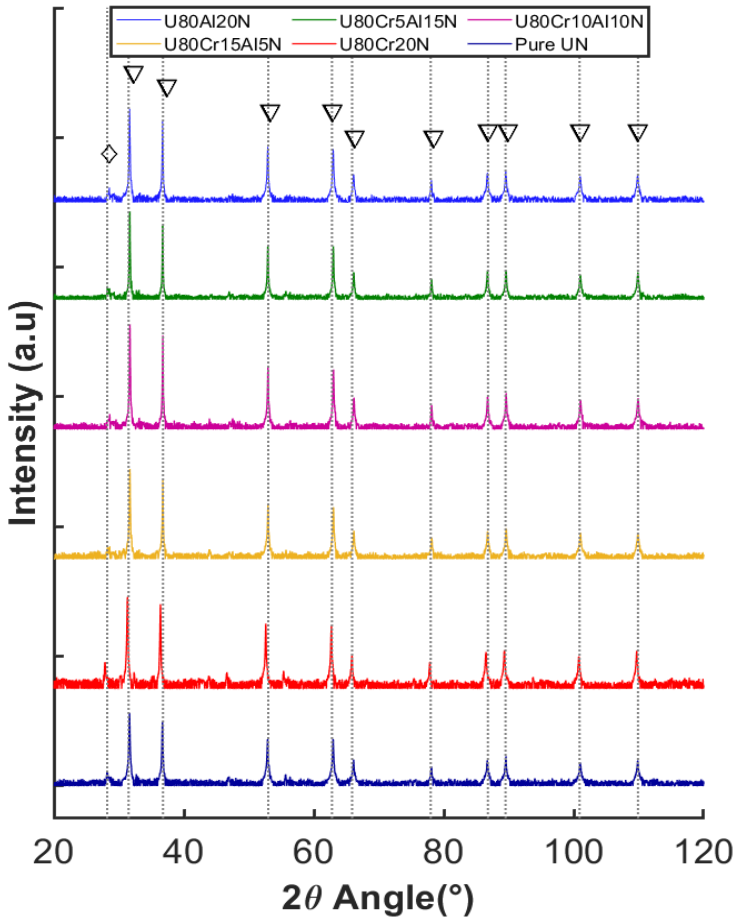

Figure 6.32. X-ray Diffractograms of UN doped with different ratios of chromium and aluminum. Phases observed were UN (∇) *and* UO_2(◊).

6.3.2. Air interaction tests

The oxidation resistance towards air of these dual doped UN microspheres was studied using TGA and the measured curves are shown in Figure 6.33. The behavior observed is similar for all the samples, where the UN oxidation occurs rapidly once the material ignites. However, there was a mass increase of the materials after 700 °C. The increase can be attributed to the oxidation of Cr or AlN phases, since it has been reported that these phases oxidize in air at temperatures higher than the UN [110]. The mass is expected to continue to increase above 900 °C, however, this is the maximal temperature available in the TGA instrument used.

The total mass gain should theoretically be higher for the doped materials. It is however seen that for the (U80Al20)N spheres, the mass gain is lower than the pure UN below 875 °C. These observations lead to the conclusion that Al is most likely completely dissociated from the UN phase, and only starts to oxidize at high temperatures. On the other hand, partial oxidation of Cr occurs simultaneously with the UN. The partial oxidation and the decrease of the lattice parameter led to the assumption that Cr might have partially reacted with the UN and might be involved in the UN crystal structure.

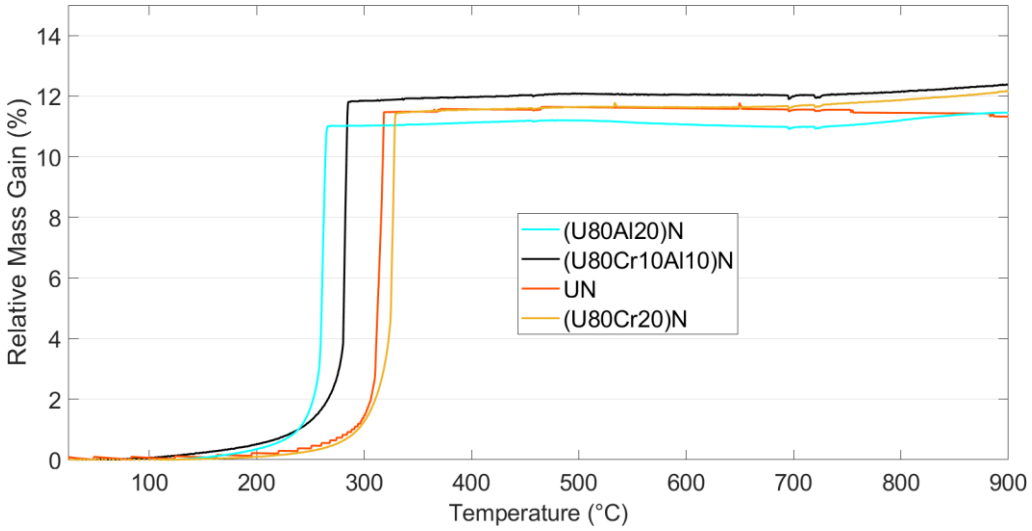

Figure 6.33. *Thermogravimetric analysis of exposure of UN microspheres doped with different ratios of Cr and Al to a synthetic air atmosphere.*

More importantly, Figure 6.33 also shows that the oxidation of Al-containing materials starts at lower temperatures than the pure UN, while the (U80Cr20)N sample had a similar oxidation temperature. The higher porosity and lack of interaction between the AlN and UN phases caused a worsening effect on the oxidation resistance of the UN. Therefore, it is possible to conclude that aluminum is not protecting the UN, as it does not oxidize with the UN to form the passive oxide layer. On the other hand, chromium is likely increasing the oxidation resistance by partial oxidation and formation of a chromia layer. Nonetheless, any increase of oxidation resistance was negatively affected by the cracking of the spheres.

7. Summary and conclusions

The work in this thesis was focused on the investigation of possible improvement to the oxidation and corrosion resistance of UN to be used as an ATF alternative. In order to achieve such enhancement, UN was doped with thorium, chromium, or aluminum. These materials were exposed to oxidizing environments, namely air, water, and steam, to determine what effect the dopants had on the oxidation and corrosion resistance of UN. The goal was to develop pellets that can provide a period of grace in case of an accident. The answer to the scientific questions raised at the beginning will be answered in this section.

The sol-gel process combined with carbothermic reduction and nitridation method were successfully used to produce doped and undoped UN microspheres. Addition of any dopants, however, had a deteriorating effect on the structure of the spheres, causing cracking due to difference in density between oxides or nitrides. Moreover, the gelation conditions required higher quantities of gelation agent (HMTA) to allow the gelation of elements with higher charge compared to the uranyl cation. Homogeneous mixtures were normally obtained before any heating processes in the furnaces.

Carbon content after nitridation varied widely, between 0.01 and 2 wt-%, while oxygen was normally between 0.1 and 0.6 wt-%. Carbon contaminations are common in carbothermic reduction processes, and the process must be optimized to reduce the carbon contaminants without causing an increase in the oxygen.

Thorium was the first dopant used, and it was shown that a complete U-Th solid solution was formed in the nitride phase, up to 20 mol-% thorium. The Th-doped microspheres were pressed into pellets using SPS, and densities were measured to be ~95% TD, which are similar to densities used in fuel pellets today. Both microspheres and pellets of Th-doped UN were exposed to heated air. Results showed that the high porosity of the spheres had a more impactful effect on the oxidation of UN in air than any protection gained by the doping with thorium. However, the onset temperatures for dense pellets of Th-doped materials were delayed by about 50 °C compared to the undoped UN.

The UN pellets were also exposed to water, and it was observed that doped and undoped pellets produced via SPS are able to survive interaction with boiling water. Once temperature was raised above 100 °C, the pellets lost their integrity and crumbled into a powder. More specifically, the oxidation reaction was almost completed at 200 °C, nonetheless, some nitrogen was still present in the powder. At 300 °C, the substrate was completely oxidized into UO_2. The Th-doped pellet heated to 200 °C in pressurized water did not show any improvement in the corrosion resistance towards water. In addition, the U-Th solid solution was lost once the material was oxidized. It was concluded then that the thoria is not protecting the UN as was intended in water environments.

The second part revolved around using chromium, which is more commonly known in corrosion protection. Chromium doping showed some similarities to the Th-doping, in that the spheres also cracked during nitridation, and carbon and oxygen contents were found in the same ranges (below 2 wt-%). However, Cr was not forming a complete solid solution with the UN, as a Cr phase was observed to precipitate on the surface of the spheres if the Cr content was 20 mol-%.

Chromium evaporation also occurred during synthesis. Therefore, measurements of Cr content were performed using two techniques: by dissolution combined with ICP-MS or XRF. These experiments led to the conclusion that the chromium phase is not completely soluble in aqua regia and therefore cannot be correctly measured in the ICP-MS.

The mechanism for the reaction of chromium and uranium during the carbothermic reduction and nitridation was investigated to determine the reason for the absence of the ternary phase (U_2CrN_3), which has been reported previously. It was demonstrated that CrN was decomposed at high temperatures and was only able to react with the uranium if enough nitrogen was present during cooling. The product of this reaction is a hyperstoichiometric uranium nitride ($UN_{1.5+x}$) combined with the ternary phase. Additional denitridation at 1200 °C into the uranium mononitride was possible without destroying the ternary phase. It was also shown that the Cr in the ternary phase was completely soluble in aqua regia, unlike the Cr phase in the materials where Cr losses were measured in ICP-MS.

The sintering in SPS of Cr-doped UN was done at first at the same conditions as for Th-doped UN, however, part of the Cr was lost during the 5 minutes of dwelling time at 1650 °C. The remaining Cr was found as metallic chromium filling the pores of the pellet. This explained the slightly higher densities (above 95% TD) measured for the Cr-doped pellets compared to the Th-doped pellets. Cr-doped UN showed a general improvement in the corrosion resistance in all the environments it was exposed to.

Onset temperatures of reaction of UN in air were increased up to 420 °C. Pellets showed that high Cr and low C contents are required for pellets to present this increment in oxidation resistance. Pellets produced with microspheres containing the ternary phase tended to start the oxidation at slightly lower temperatures than the materials that did not have the ternary phase.

Reaction of Cr-doped UN pellets with steam also had higher onset temperatures than the undoped UN. As with the interaction with air, the pellets produced with microspheres containing the ternary phase showed slightly lower onset temperatures.

Exposure of Cr-doped UN pellets to water showed the most promising results. Pellets were able to withstand 200 °C for 2 hours with minimal or no damage observed. Pellets still lost part of their integrity after reaction at 300 °C, however after 5 hours of interaction. This can provide a short time period where the fuel can be exchanged before damage to the system can occur.

The last part of the work was the selection of aluminum and chromium to study a dual doping of UN. The results showed that aluminum was relocated into the intergranular space of the UN matrix due to insolubility, which prevented the fusion of grains. This led to a higher porosity in the spheres, and the materials were oxidized at lower temperatures than undoped UN. The behavior was attributed to the formation of an AlN phase separated from the UN, which oxidizes at temperatures higher than UN. Therefore, it was concluded that Al was not able to improve the protection of the UN in the bulk.

The fuels proposed and studied in this work are a step forward in the finding of an appropriate accident tolerant fuel concept. However, further work is still necessary, as an ATF concept is required to be stable even at accident conditions, which are harsher conditions than the ones used in this work.

Future work

The aim of this work was to manufacture and test an ATF concept that can resist oxidation environments at high temperatures. Although the improvement of oxidation and corrosion was obtained up to 300 °C for Cr doping, the material still lost the integrity. The synthesis of purer nitrides needs to be properly optimized to reduce the carbon and oxygen contaminations after carbothermic reduction and nitridation, as it was observed that higher carbon residues reduced the oxidation resistance.

Water interaction experiments can be done in constant flow of water to remove the ammonia created and observe if it has any effect on the corrosion of the doped UN pellets. Composition of the water solution must also be modified to be more similar to a real BWR or PWR.

Other elements, such as Y, Zr or Ti, could also be added as additives to observe whether waterproofing can be achieved. The effect of using a mixture of additives that were not done in this work could also be interesting to study.

Finally, the interaction of the accident tolerant fuels produced with different cladding alternatives, such as Cr coated zircaloy, should also be investigated before the complete fuel concept can be implemented for irradiation tests.

Acknowledgments

This work was possible thanks to the Swedish Foundation for Strategic Research (SSF) for funding the SAFETY project (number EM16-0031).

I would like start by thanking my supervisor Teodora Retegan Vollmer, for her support and help during this process and for giving me her insights to choose my best possible future.

My co-supervisor, Marcus Hedberg, you taught me all I needed to make this work possible, helped me with your comments and corrections when I needed them the most and showed me how everything is possible with enough patience.

My examiner Christian Ekberg, for giving me the opportunity to prove myself and choose the better path for my topic.

Thanks to all the members of the SAFETY project, which were helpful during the discussions every meeting. And special mention to Yulia and Andrea for the fun in conferences and travels.

Thanks to my old friends from NC/IMR, Fredrik, Emma, Gabriele, Thea, Niklas for making this a fun and wonderful journey since day 1, I hope we will do a lake day sometime. To all the new colleagues and friends for keeping up with my crazy lunch schedules and fika activities.

Special mention has to go to my office mate Anna, I couldn't have wished for a better companion to talk and gossip. Thank you for being there by my side when we were submitting our first papers. We made the best office at work… even if some people might disagree.

And last but not least, thanks to my family and friends everywhere else, who even though they are far away, they always had my back and were happy to support me… even when it makes them sad that I live so far. Gracias!!

References.

[1] P.C. Jain, Greenhouse effect and climate change: scientific basis and overview, Renew. Energy. 3 (1993) 403–420. doi:10.1016/0960-1481(93)90108-S.

[2] Climate Watch Historical GHG Emissions, (2022). https://www.climatewatchdata.org/ghg-emissions (accessed November 3, 2022).

[3] Energy | Resource Watch, (n.d.). https://resourcewatch.org/dashboards/energy?tab=country (accessed November 3, 2022).

[4] IEA, World Energy Outlook 2022, 2022. https://www.iea.org/reports/world-energy-outlook-2022 (accessed November 3, 2022).

[5] J.D. Jenkins, Z. Zhou, R. Ponciroli, R.B. Vilim, F. Ganda, F. de Sisternes, A. Botterud, The benefits of nuclear flexibility in power system operations with renewable energy, Appl. Energy. 222 (2018) 872–884. doi:10.1016/J.APENERGY.2018.03.002.

[6] World Nuclear Association, Nuclear energy and climate change, (n.d.). https://world-nuclear.org/nuclear-essentials/how-can-nuclear-combat-climate-change.aspx (accessed December 24, 2022).

[7] World Nuclear Association, Nuclear Power Today, (2022). https://www.world-nuclear.org/information-library/current-and-future-generation/nuclear-power-in-the-world-today.aspx (accessed November 3, 2022).

[8] World Nuclear Association, The Nuclear Debate, (2022). https://www.world-nuclear.org/information-library/current-and-future-generation/the-nuclear-debate.aspx (accessed November 3, 2022).

[9] IAEA, Review of Fuel Failures in Water Cooled Reactors (2006-2015), Vienna, 2019. http://www.iaea.org/publications/index.html (accessed November 3, 2022).

[10] Y. Amano, The Fukushima Daiichi Accident Report by the Director General, Vienna, 2015.

[11] G. Choppin, J.O. Liljenzin, J. Rydberg, C. Ekberg, Radiochemistry and Nuclear Chemistry, Fourth Edition, Elsevier Inc., 2013. doi:10.1016/C2011-0-07260-5.

[12] IAEA., Nuclear Power Reactors in the World., IAEA, 2017.

[13] Su Chiang Shu Faya, A SURVEY ON FUEL PELLET CRACKING AND HEALING PHENOMENA IN REACTOR OPERATION, Sao Pablo, 1981.

[14] A. Khan, M. Rafique, N. Afzal, Z. Khaliq, R. Ahmad, Structural characterization of Zircaloy-4 subjected to helium ions irradiation of variable fluence, Nucl. Mater. Energy. 20 (2019) 100690. doi:10.1016/J.NME.2019.100690.

[15] IAEA, Japan’s Reports on Conditions at TEPCO’s Fukushima Daiichi Nuclear Power Station, 19 October 2022 | IAEA, (2022). https://www.iaea.org/newscenter/news/japans-reports-on-conditions-at-tepcos-fukushima-daiichi-nuclear-power-station-19-october-2022 (accessed December 24, 2022).

[16] N.E. Agency, State-of-the-Art Report on Light Water Reactor Accident-Tolerant Fuels, 2018. doi:https://doi.org/https://doi.org/10.1787/9789264308343-en.

[17] Shannon Bragg-Sitton, Development of advanced accident-tolerant fules for commercial LWRs, Nucl. News. 57 (2014) 83–91.

[18] K.D. Johnson, A.M. Raftery, D.A. Lopes, J. Wallenius, Fabrication and microstructural analysis of UN-U3Si2composites for accident tolerant fuel applications, J. Nucl. Mater. 477 (2016) 18–23. doi:10.1016/j.jnucmat.2016.05.004.

[19] Y.S. Kim, Uranium Intermetallic Fuels (U–Al, U–Si, U–Mo), Compr. Nucl. Mater. (2012) 391–422. doi:10.1016/B978-0-08-056033-5.00112-9.

[20] K.Y. Spencer, L. Sudderth, R.A. Brito, J.A. Evans, C.S. Hart, A. Hu, A. Jati, K. Stern, S.M. McDeavitt, Sensitivity study for accident tolerant fuels: Property comparisons and behavior simulations in a simplified PWR to enable ATF development and design, Nucl. Eng. Des. 309 (2016) 197–212. doi:10.1016/j.nucengdes.2016.09.009.

[21] R.W. Jones, J.L. Crosthwaite, Atomic Energy of Canada Limited URANIUM CARBIDE FUEL FOR ORGANIC COOLED REACTORS, 1973.

[22] F.B. Litton, The Properties and Irradiation Behaviour of Carbide Fuels: A Literature Survey, Los Alamos, 1968. doi:10.2172/4551282.

[23] S.L. Hayes, J.K. Thomas, K.L. Peddicord, Material property correlations for uranium mononitride: III. Transport properties, J. Nucl. Mater. 171 (1990) 289–299. doi:10.1016/0022-3115(90)90376-X.

[24] J.T. White, A.T. Nelson, J.T. Dunwoody, D.D. Byler, D.J. Safarik, K.J. McClellan, Thermophysical properties of U3Si2 to 1773 K, J. Nucl. Mater. 464 (2015) 275–280. doi:10.1016/J.JNUCMAT.2015.04.031.

[25] K. Johnson, High Performance Fuels for Water-Cooled Reactor Systems, 2016.

[26] P.E. Evans, T.J. Davies, Uranium nitrides, J. Nucl. Mater. 10 (1963) 43–55. doi:10.1016/0022-3115(63)90115-6.

[27] C. Ekberg, D. Ribeiro Costa, M. Hedberg, M. Jolkkonen, Nitride fuel for Gen IV nuclear power systems, J. Radioanal. Nucl. Chem. 318 (2018) 1713–1725. doi:10.1007/s10967-018-6316-0.

[28] Y.M. Gledenov, V.I. Salatski, P. V. Sedyshev, The14N(n, p)14C reaction cross section for thermal neutrons, Zeitschrift Für Phys. A Hadron. Nucl. 346 (1993) 307–308. doi:10.1007/BF01292522.

[29] A. Herman, C. Ekberg, A Uranium Nitride Doped with Chromium, Nickel or Aluminum as an Accident Tolerant Fuel, 5 (2017). doi:10.4172/2321-6212.1000196.

[30] K. Insulander Björk, A. Herman, M. Hedberg, C. Ekberg, Scoping Studies of Dopants for Stabilization of Uranium Nitride Fuel, Nucl. Sci. Eng. 193 (2019) 1255–1264. doi:10.1080/00295639.2019.1614368.

[31] H. Suwarno, Preparation of Uranium Nitride from Uranium Metal through by Hydriding and Nitriding Process, (2013). doi:10.4028/www.scientific.net/AMR.789.360.

[32] R.B. Matthews, K.M. Chidester, C.W. Hoth, R.E. Mason, R.L. Petty, FABRICATION

AND TESTING OF URANIUM NITRIDE FUEL FOR SPACE POWER REACTORS, J. Nucl. Mater. 151 (1988) 334–344.

[33] K.A. Terrani, B.C. Jolly, J.M. Harp, Uranium nitride tristructural-isotropic fuel particle, (n.d.). https://www.osti.gov/servlets/purl/1606770 (accessed December 24, 2022).

[34] Fast Reactors and Related Fuel Cycles: Challenges and Opportunities (FR09), INTERNATIONAL ATOMIC ENERGY AGENCY, Vienna, 2012. https://www.iaea.org/publications/8476/fast-reactors-and-related-fuel-cycles-challenges-and-opportunities-fr09.

[35] IAEA, Liquid Metal Coolants for Fast Reactors Cooled By Sodium, Lead, and Lead-Bismuth Eutectic, Vienna, 2012.

[36] F. Brown, H.M. Ockenden, G.A. Welch, The preparation and properties of some plutonium compounds. Part II. Plutonium nitride, J. Chem. Soc. 0 (1955) 4196–4201. doi:10.1039/jr9550004196.

[37] E.S. Wood, J.T. White, B. Jaques, D. Burkes, P. Demkowicz, Advances in fuel fabrication, Adv. Nucl. Fuel Chem. (2020) 371–418. doi:10.1016/B978-0-08-102571-0.00011-2.

[38] G.W.C. Silva, C.B. Yeamans, A.P. Sattelberger, T. Hartmann, G.S. Cerefice, K.R. Czerwinski, Reaction sequence and kinetics of uranium nitride decomposition, Inorg. Chem. 48 (2009) 10635–10642. doi:10.1021/IC901165J/ASSET/IMAGES/LARGE/IC-2009-01165J_0005.JPEG.

[39] T. Hiroaki, Phase relations and thermodynamic properties of the uranium-nitrogen system, J. Nucl. Mater. 51 (1974) 78–89. doi:10.1016/0022-3115(74)90117-2.

[40] M.W. Mallett, A.F. Gerds, Reaction of Nitrogen with Uranium, J. Electrochem. Soc. 102 (1955) 292. doi:10.1149/1.2430050.

[41] C.M. Silva, R.D. Hunt, L.L. Snead, K.A. Terrani, Synthesis of phase-pure U2N3 microspheres and its decomposition into un, Inorg. Chem. 54 (2015) 293–298. doi:10.1021/IC502457N/ASSET/IMAGES/LARGE/IC-2014-02457N_0008.JPEG.

[42] R.M. Dell, V.J. Wheeler, E.J. Mciver, Oxidation of Uranium Mononitride and Uranium Monocarbide*, 1966.

[43] G.A.R. Rao, S.K. Mukerjee, V.N. Vaidya, V. Venugopal, D.D. Sood, Oxidation and hydrolysis kinetic studies on UN, J. Nucl. Mater. 185 (1991) 231–241. doi:10.1016/0022-3115(91)90340-D.

[44] R.M. Dell, V.J. Wheeler, N.J. Bridger, Hydrolysis of uranium mononitride, Trans. Faraday Soc. 63 (1967) 1286–1294. doi:10.1039/tf9676301286.

[45] L. Lu, O. Ishiyama, Iron ore sintering, Iron Ore Mineral. Process. Environ. Sustain. (2015) 395–433. doi:10.1016/B978-1-78242-156-6.00014-9.

[46] S.J. Kang, Sintering, Elsevier Ltd, 2005. doi:10.1016/B978-0-7506-6385-4.X5000-6.

[47] A.J. Carrea, Sintering of uranium dioxide in an atmosphere of controlled hydrogen content, J. Nucl. Mater. 8 (1963) 275–277. doi:10.1016/0022-3115(63)90048-5.

[48] E.K. Papynov, O.O. Shichalin, A.Y. Mironenko, A. V. Ryakov, I. V. Manakov, P. V.

Makhrov, I.Y. Buravlev, I.G. Tananaev, V.A. Avramenko, V.I. Sergienko, Synthesis of High-Density Pellets of Uranium Dioxide by Spark Plasma Sintering in Dies of Different Types, Radiochemistry. 60 (2018) 362–370. doi:10.1134/S1066362218040045.

[49] B.J. Jaques, J. Watkins, J.R. Croteau, G.A. Alanko, B. Tyburska-Püschel, M. Meyer, P. Xu, E.J. Lahoda, D.P. Butt, Synthesis and sintering of UN-UO2fuel composites, J. Nucl. Mater. 466 (2015) 745–754. doi:10.1016/j.jnucmat.2015.06.029.

[50] V.J. TENNERY, T.G. GODFREY, R.A. POTTER, Sintering of UN as a Function of Temperature and N2 Pressure, J. Am. Ceram. Soc. 54 (1971) 327–331. doi:10.1111/j.1151-2916.1971.tb12306.x.

[51] F. Goldner, Development strategy for advanced LWR fuels with enhanced accident tolerance, Present. to Enhanc. Accid. Toler. LWR Fuels Natl. Metrics Work. Oct. (2012) l5.

[52] M. Omori, Sintering, consolidation, reaction and crystal growth by the spark plasma system (SPS), Mater. Sci. Eng. A. 287 (2000) 183–188. doi:10.1016/S0921-5093(00)00773-5.

[53] S.H. Risbud, C.-H. Shan, Fast consolidation of ceramic powders, Mater. Sci. Eng. A. 204 (1995) 146–151. doi:10.1016/0921-5093(95)09951-4.

[54] M. Eriksson, Z. Shen, G. Svensson, Policy document for National Spark Plasma Sintering (SPS) Facility About SPS Access, 2018.

[55] P. Malkki, M. Jolkkonen, T. Hollmer, J. Wallenius, Manufacture of fully dense uranium nitride pellets using hydride derived powders with spark plasma sintering, J. Nucl. Mater. 452 (2014) 548–551. doi:10.1016/J.JNUCMAT.2014.06.012.

[56] H. Muta, K. Kurosaki, M. Uno, S. Yamanaka, Thermal and mechanical properties of uranium nitride prepared by SPS technique, J. Mater. Sci. 43 (2008) 6429–6434. doi:10.1007/s10853-008-2731-x.

[57] K.D. Johnson, J. Wallenius, M. Jolkkonen, A. Claisse, Spark plasma sintering and porosity studies of uranium nitride, J. Nucl. Mater. 473 (2016) 13–17. doi:10.1016/j.jnucmat.2016.01.037.

[58] L.G. Gonzalez Fonseca, M. Hedberg, L. Huan, P. Olsson, T. Retegan Vollmer, Application of SPS in the fabrication of UN and (U,Th)N pellets from microspheres, J. Nucl. Mater. 536 (2020) 152181. doi:10.1016/j.jnucmat.2020.152181.

[59] R.F. Stratfull, K.C. Clear, C.F. Crumpton, J.E. Bukovatz, R.M. Weed, R.G. Pike, R.E. Hay, J.R. Clifton, H.F. Beeghly, R.G. Mathey, P.L. Todd, Corrosion and Corrosion Protection, Transp. Res. Rec. (2008) 291–321. doi:10.1016/B978-044452792-9.50012-9.

[60] D.A. Lopes, S. Uygur, K. Johnson, Degradation of UN and UN–U3Si2 pellets in steam environment, Http://Dx.Doi.Org/10.1080/00223131.2016.1274689. 54 (2017) 405–413. doi:10.1080/00223131.2016.1274689.

[61] K.G. Field, M.A. Snead, Y. Yamamoto, K.A. Terrani, Handbook on the Material Properties of FeCrAl Alloys for Nuclear Power Production Applications, 2017.

[62] H. Falk-Windisch, J.E. Svensson, J. Froitzheim, The effect of temperature on

chromium vaporization and oxide scale growth on interconnect steels for Solid Oxide Fuel Cells, J. Power Sources. 287 (2015) 25–35. doi:10.1016/j.jpowsour.2015.04.040.

[63] P. Aaltonen, H. Hanninen, WATER CHEMISTRY AND BEHAVIOUR OF MATERIALS IN PWRs AND BWRs, (n.d.).

[64] Potential-pH Diagrams for Ni-Cr-Fe Alloys and Pb Adsorption on Ni-Cr-Fe Alloys Surfaces in Water at 25°C and High Temperature (250-350°C), (2018). doi:10.1149/2.1291807jes.

[65] G. Heisbourg, S. Hubert, N. Dacheux, J. Purans, Kinetic and thermodynamic studies of the dissolution of thoria-urania solid solutions, J. Nucl. Mater. 335 (2004) 5–13. doi:10.1016/j.jnucmat.2004.05.017.

[66] U. Mizutani, Hume-Rothery Rules for Structurally Complex Alloy Phases:, CRC Press Inc, 2016.

[67] J.R. Rumble, Properties of the elements and inorganic compounds, in: CRC Handb. Chem. Phys., CRC Press/Taylor & Francis, Boca Raton, 2018: p. Internet Version.

[68] L. Zhou, D. Holec, M. Bartosik, F. Körmann, B. Grabowski, J. Neugebauer, P. Mayrhofer, Structural stability and thermodynamics of CrN magnetic phases from ab initio and experiment, (2014).

[69] K. Miwa, A. Fukumoto, First-principles calculation of the structural, electronic, and vibrational properties of gallium nitride and aluminum nitride, Phys. Rev. B. 48 (1993) 7897–7902. doi:10.1103/PhysRevB.48.7897.

[70] C.P. Kempter, N.H. Krikorian, J.C. Mcguire, The crystal structure of yttrium nitride, J. Phys. Chem. 61 (1957) 1237–1238. doi:10.1021/j150555a023.

[71] M. Guemmaz, A. Mosser, J.J. Grob, Ion implantation processing of sub-stoichiometric titanium nitrides and carbonitrides: Chemical structural and micromechanical investigations, Appl. Phys. A Mater. Sci. Process. 64 (1997) 407–415. doi:10.1007/s003390050497.

[72] L. Gerward, J. Staun Olsen, U. Benedict, J.P. Itié, J.C. Spirlet, The crystal structure and the equation of state of thorium nitride for pressures up to 47 GPa, J. Appl. Crystallogr. 18 (1985) 339–341. doi:10.1107/s0021889885010421.

[73] R.A. Evarestov, A.I. Panin, A. V. Bandura, M. V. Losev, Electronic structure of crystalline uranium nitrides UN, U 2N3 and UN2: LCAO calculations with the basis set optimization, in: J. Phys. Conf. Ser., Institute of Physics Publishing, 2008. doi:10.1088/1742-6596/117/1/012015.

[74] H. Holleck, E. Smailos, F. Thümmler, Zur mischphasenbildung der mononitride in den systemen U- (Y, La, Pr)-N, J. Nucl. Mater. 32 (1969) 281–289. doi:10.1016/0022-3115(69)90077-4.

[75] H. Holleck, E. Smailos, F. Thümmler, Zur mischkristallbildung von un mit den nitriden der seltenen erden CeN und NdN, J. Nucl. Mater. 28 (1968) 105–109. doi:10.1016/0022-3115(68)90061-5.

[76] H. Holleck, E. Smallos, F. Thümmler, Zur Mischkristallbildung in den quasibinären Systemen von UN und den Mononitriden der IV A-Gruppe TiN, ZrN und HfN, Monatshefte Für Chemie. 99 (1968) 985–989. doi:10.1007/BF00913744/METRICS.

[77] H. Holleck, Ternary Phase Equilibria In The Systems Actinide-Transition Metal-Carbon and Actinide-Transition Metal-Nitrogen, in: Thermodyn. Nucl. Mater., 1975. https://www.osti.gov/biblio/4177518.

[78] R. Benz, W.H. Zachariasen, Crystal structures of Th2CrN3, Th2MnN3, U2CrN3 and U2MnN3, J. Nucl. Mater. 37 (1970) 109–113. doi:10.1016/0022-3115(70)90187-X.

[79] Y. Mishchenko, K.D. Johnson, J. Wallenius, D.A. Lopes, Design and fabrication of UN composites: From first principles to pellet production, J. Nucl. Mater. 553 (2021) 153047. doi:10.1016/J.JNUCMAT.2021.153047.

[80] A. Deptuła, M. Brykala, M. Rogowski, T. Smolinski, T. Olczak, W. Łada, D. Wawszczak, A. Chmielewski, K.C. Goretta, Fabrication of uranium dioxide microspheres by classic and novel sol-gel processes, in: Mater. Res. Soc. Symp. Proc., Materials Research Society, 2014. doi:10.1557/opl.2014.672.

[81] K. Nagarajan, V.N. Vaidya, Sol-Gel Processes for Nuclear Fuel Fabrication, in: Sol-Gel Process. Conv. Altern. Energy, Springer US, Boston, MA, 2012: pp. 341–373. doi:10.1007/978-1-4614-1957-0_16.

[82] M. Streit, F. Ingold, Nitrides as a nuclear fuel option, J. Eur. Ceram. Soc. 25 (2005) 2687–2692. doi:10.1016/j.jeurceramsoc.2005.03.181.

[83] J. Collins, M. Lloyd, S. Shell, Control of Urania Crystallite Size by HMTA-Urea Reactions in the Internal Gelation Process for Preparing (U, Pu)O2Fuel Kernels, (2005). doi:10.2172/885943.

[84] A. Sajdova, ACCIDENT-TOLERANT URANIUM NITRIDE, CHALMERS UNIVERSITY OF TECHNOLOGY, 2017.

[85] B.M. Eick, J.P. Youngblood, Carbothermal reduction of metal-oxide powders by synthetic pitch to carbide and nitride ceramics, J. Mater. Sci. 44 (2009) 1159–1171. doi:10.1007/S10853-009-3249-6/TABLES/4.

[86] S.A. Chowdhury, H.S. Maiti, S. Biswas, Synthesis of spherical Al2O3 and AlN powder from C@Al2O3 composite powder, J. Mater. Sci. 41 (2006) 4699–4705. doi:10.1007/S10853-006-0039-2/FIGURES/6.

[87] R. V. Krishnarao, J. Subrahmanyam, Studies on the formation of whiskers and platelets of B4C and BN, J. Mater. Sci. 2004 3920. 39 (2004) 6263–6269. doi:10.1023/B:JMSC.0000043596.56929.11.

[88] R. V. Krishnarao, J. Subrahmanyam, M. Yadagiri, Formation of TiN whiskers through carbothermal reduction of TiO2, J. Mater. Sci. 37 (2002) 1693–1699. doi:10.1023/A:1014981722160/METRICS.

[89] M.D. Alcalá, J.M. Criado, F.J. Gotor, C. Real, β-SiALON obtained from carbothermal reduction of kaolinite employing sample controlled reaction temperature (SCRT), J. Mater. Sci. 41 (2006) 1933–1938. doi:10.1007/S10853-006-4493-7/METRICS.

[90] L.G. Gonzalez Fonseca, M. Hedberg, T.R. Vollmer, Oxidation and hydrolysis of thorium doped uranium nitride fuel for use in LWR, J. Nucl. Mater. 555 (2021) 153150. doi:10.1016/J.JNUCMAT.2021.153150.

[91] S. Zhao, Z. Zhao, Z. Yang, L.L. Ke, S. Kitipornchai, J. Yang, Functionally graded graphene reinforced composite structures: A review, Eng. Struct. 210 (2020) 110339.

doi:10.1016/J.ENGSTRUCT.2020.110339.

[92] P.A. Demkowicz, J.L. Jerden, J.C. Cunnane, N. Shibuya, R. Baney, J. Tulenko, Aqueous Dissolution of Urania-Thoria Nuclear Fuel, Nucl. Technol. 147 (2004) 157–170. doi:10.13182/NT04-A3522.

[93] A.R. Denton, N.W. Ashcroft, Vegards law, Phys. Rev. A. 43 (1991) 3161–3164. doi:10.1103/PhysRevA.43.3161.

[94] M. Hedberg, Production and Characterization of ZrN and PuN Materials for Nuclear Fuel Applications, CHALMERS UNIVERSITY OF TECHNOLOGY, 2016.

[95] S. Sugihara, S. Imoto, Hydrolysis of Thorium Nitrides and Carbonitrides, J. Nucl. Sci. Technol. 8 (1971) 630–636. doi:10.3327/jnst.8.630.

[96] M. Paljević, Z. Despotović, Oxidation of uranium mononitride, J. Nucl. Mater. 57 (1975) 253–257. doi:10.1016/0022-3115(75)90208-1.

[97] K. Johnson, V. Ström, J. Wallenius, D.A. Lopes, Oxidation of accident tolerant fuel candidates, J. Nucl. Sci. Technol. 54 (2017) 280–286. doi:10.1080/00223131.2016.1262297.

[98] S. Morita, H. Shimizu, Y. Sayama, Synthesis of Chromium Nitride Powder by Carbo-thermal Nitriding, in: 15th Int. Plansee Semin., Plansee Holding AG, 2001: pp. 139–154.

[99] T. Sand, C. Geers, Y. Cao, J.E. Svensson, L.G. Johansson, Effective Reduction of Chromium-oxy-hydroxide Evaporation from Ni-Base Alloy 690, Oxid. Met. 92 (2019) 259–279. doi:10.1007/s11085-019-09935-9.

[100] V. Peres, L. Favergeon, M. Andrieu, J.C. Palussire, J. Balland, C. Delafoy, M. Pijolat, High temperature chromium volatilization from Cr2O3 powder and Cr2O3-doped UO2 pellets in reducing atmospheres, J. Nucl. Mater. 423 (2012) 93–101. doi:10.1016/J.JNUCMAT.2012.01.001.

[101] W. Ernst, J. Neidhardt, H. Willmann, B. Sartory, P.H. Mayrhofer, C. Mitterer, Thermal decomposition routes of CrN hard coatings synthesized by reactive arc evaporation and magnetron sputtering, Thin Solid Films. 517 (2008) 568–574. doi:10.1016/J.TSF.2008.06.086.

[102] E.A. Gulbransen, K.F. Andrew, A Preliminary Study of the Oxidation and Vapor Pressure of Chromium, J. Electrochem. Soc. 99 (1952) 402.

[103] B.J. Lee, On the stability of Cr carbides, Calphad. 16 (1992) 121–149. doi:10.1016/0364-5916(92)90002-F.

[104] G.B. Reartes, P.J. Morando, M.A. Blesa, P.B. Hewlett, E. Matijevié, Reactivity of Chromium Oxide in Aqueous Solutions. 2. Acid Dissolution, Langmuir. 11 (1995) 2277–2284. doi:10.1021/LA00006A068/ASSET/LA00006A068.FP.PNG_V03.

[105] M. Seo, R. Furuichi, G. Okamoto, N. Sato, Dissolution of Hydrous Chromium Oxide in Acid Solutions, Trans. Japan Inst. Met. 16 (1975) 519–525. doi:10.2320/MATERTRANS1960.16.519.

[106] K. Yang, E. Kardoulaki, D. Zhao, B. Gong, A. Broussard, K. Metzger, J.T. White, M.R. Sivack, K.J. Mcclellan, E.J. Lahoda, J. Lian, Cr-incorporated uranium nitride

composite fuels with enhanced mechanical performance and oxidation resistance, J. Nucl. Mater. 559 (2022) 153486. doi:10.1016/J.JNUCMAT.2021.153486.

[107] A. Vorontsov, A. Filippov, N. Shamarin, E. Moskvichev, O. Novitskaya, E. Knyazhev, Y. Denisova, A. Leonov, V. Denisov, S. Tarasov, High-Temperature Oxidation of CrN/ZrN Multilayer Coatings, Metals (Basel). 12 (2022). doi:10.3390/met12101746.

[108] Y. Mishchenko, K.D. Johnson, D. Jädernäs, J. Wallenius, D.A. Lopes, Uranium nitride advanced fuel: an evaluation of the oxidation resistance of coated and doped grains, J. Nucl. Mater. 556 (2021) 153249. doi:10.1016/J.JNUCMAT.2021.153249.

[109] E.S. Sooby, B.A. Brigham, G. Robles, J.T. White, S.W. Paisner, E. Kardoulaki, B. Williams, Steam oxidation of uranium mononitride in pure and reducing steam atmospheres to 1200 °C, J. Nucl. Mater. 560 (2022) 153487. doi:10.1016/J.JNUCMAT.2021.153487.

[110] W.P. Hsieh, C.C. Wang, C.H. Lin, F.S. Shieu, Oxidation of Arc Ion-Plated CrN Coatings at Elevated Temperatures, J. Electrochem. Soc. 149 (2002) B234. doi:10.1149/1.1471545/XML.